Wide-field Ganglion Cells in Primate Retina

Kumiko A Percival

Submitted in total fulfilment of the requirements of the degree of
Doctor of Philosophy

February 2011

Department of Optometry & Vision Sciences
The University of Melbourne

(Produced on archival quality paper)

Abstract

The anatomical circuity involving distinct neuronal types within the retina, form the basis for the functional properties of ganglion cells. Such properties ultimately represent the nature of visual information carried by these cells for further processing in subsequent areas of the visual system, and are therefore crucial to our understanding of the visual system as a whole. The projects outlined in chapters 2, 3 and 4 investigate the anatomical connections of a group of ganglion cell types (wide-field ganglion cells) retrogradely labelled and photo-filled in the retina of the common marmoset (*Callithrix jacchus*). This animal model is ideal for our purposes, as ganglion cell types identified in marmoset retina to date, have closely resembled those of Old world primate species.

Chapter 1 outlines the anatomical connectivity, morphological features and physiological properties of retinal neurons.

Chapter 2 investigates the density and distribution of synaptic inputs onto the two dendritic tiers of small bistratified ganglion cells with the aim of elucidating the retinal connectivity behind their blue-ON/yellow-OFF chromatic responses. The density of presumed bipolar and amacrine cell inputs onto small bistratified cells were measured. All cells analysed showed a consistent pattern, where bipolar input to the inner tier is approximately fourfold greater than bipolar input to the outer tier. This structural asymmetry of bipolar input may help to balance the weight of cone signals from the sparse S cone array against inputs from the much denser M/L cone array.

Chapter 3 investigates the density and distribution of synaptic inputs onto two wide-field ganglion cell types with largely contrasting morphological features. Large sparse cells have sparsely branching dendritic trees that are narrowly stratified close to the ganglion cell layer. Broad thorny cells have densely branching dendritic trees broadly stratified within the center of the inner plexiform layer. The density of presumed synaptic inputs was similar for the two cell types, indicating that the larger number of synapses on broad thorny cells may be attributable to the larger membrane surface area of this cell type. Synaptic input density was comparable to previous values for midget and parasol ganglion cells, suggesting that functional differences between these cell types do not arise from variation in synaptic input densities.

Chapter 4 investigates the contribution of wide-field ganglion cells to the retinal circuity subserving foveal vision. The fovea is a region of the retina specialised for high acuity photopic vision, in which the role of the midget pathway has been implicated. The question of whether wide-field ganglion cell types and their neural partners are present within the first 1mm of the foveola was examined. Bipolar cells were immuno-labelled in vertical sections of marmoset and macaque retina. At least three types of wide-field ganglion cells previously described in peripheral retina were present at the fovea. A subset of bipolar cells likely to be involved in providing inputs onto wide-field ganglion cells at the fovea was also found, supporting the view that retinal pathways involving wide-field ganglion cells contribute to foveal vision.

Declaration

This is to certify that:

i. The thesis comprises only my original work toward the PhD except where indicated in the Preface;
ii. Due acknowledgement has been made in the text to all other material used;
iii. The thesis is less than 100,000 words in length, exclusive of tables, maps, bibliographies and appendices.

Kumiko Percival

Preface

Some of the results described in the present thesis have appeared in the following publications and abstracts:

Publications:

Percival, K.A., Martin, P.R., and Grünert, U. (2011). Synaptic inputs to two types of koniocellular pathway ganglion cells in marmoset retina. *The Journal of Comparative Neurology* In press.

Percival, K.A., Jusuf, P.R., Martin, P.R., and Grünert, U. (2009). Synaptic inputs onto small bistratified (blue-ON/yellow-OFF) ganglion cells in marmoset retina. *The Journal of Comparative Neurology* 517:655 - 699.

Published Abstracts:

Percival, K.A., Martin, P.R., and Grünert, U. (2010). Contribution of wide-field ganglion cells to central vision in primate retina. *Proceedings of the Australian Neuroscience Society*, 20, POS-MON-194.

Percival, K.A., Martin, P.R., and Grünert, U. (2009). Synaptic inputs onto large sparse and broad thorny ganglion cells in marmoset retina. *Proceedings of the Australian Neuroscience Society*, 19, ORAL-15-01.

Percival, K.A., Jusuf, P.R., Martin, P.R., and Grünert, U. (2008). Synaptic inputs onto wide-field ganglion cells in marmoset retina. *Proceedings of the Australian Neuroscience Society*, 18, ORAL-03-03.

Percival, K.A., Jusuf, P.R., Martin, P.R., and Grünert, U. (2007). Synaptic connectivity of small bistratified ganglion cells in marmoset retina. *IBRO World Congress of Neuroscience*, 118, POS-SUN-150.

Non-published Abstracts:

Percival, K.A., Martin, P.R., and Grünert, U. (2008). Synaptic inputs onto two types of wide-field ganglion cell in marmoset retina. *FASEB Summer Research Conferences - Retinal Neurobiology and Visual Processing*, POSTER # 43.

Percival, K.A., Jusuf, P.R., Martin, P.R., and Grünert, U. (2007). Synaptic inputs onto wide-field ganglion cells in marmoset retina. *Vision Down Under*, POSTER #132.

The experiments in chapter 2 were initiated during my Honours candidature and were completed during the first year of my PhD. During the course of my PhD, I also contributed to the following publications and abstracts, which involve experiments not described by this thesis:

Publications:

Eriköz, B., Jusuf, P.R., **Percival, K.A.**, and Grünert, U. (2008). Distribution of bipolar input to midget and parasol ganglion cells in marmoset retina. *Visual Neuroscience* 25:67 - 76.

Abstracts:

Abbott, C.J., **Percival, K.A.**, Martin, P.R. and Grünert, U. (2010). Bipolar and amacrine input to midget and parasol ganglion cells in marmoset retina. *Proceedings of the Australian Neuroscience Society*, 20, ORAL-15-08.

As outlined below, a small portion of the work described in chapters 2 and 3 was completed by other members of the lab, prior to my involvement with the projects. One small bistratified ganglion cell from the study described in Chapter 2 was drawn by Brett Szmajda and partially analysed by Patricia Jusuf. In the study described in Chapter 3, a single large sparse ganglion cell was analysed for its colocalisations with diffuse bipolar type 6 cells by Patricia Jusuf.

Acknowledgements

Above all I am grateful for the supervision I have received from Ulrike Grünert and Paul Martin throughout my candidature. Their expert knowledge and guidance has seen me go from a clueless undergraduate student to the budding scientist that I am today. They have poured countless hours of their time into not only teaching me the practical and analytical skills necessary for completing my work, but also in improving my written and oral communication skills. I have benefited immensely from the time I have spent with them both inside and outside of the laboratory, and would like to thank them for giving me the best possible start to what will hopefully be a fruitful career in science. I would also like to thank Algis Vingrys for stepping in as my third supervisor and keeping me on track during the final part of my PhD.

I have had the privilege of learning from many previous laboratory members including Patricia Jusuf, Brett Szmajda and Sammy Lee. I am grateful for their guidance, especially during my early years with the lab, and for their continual support and advice they have given me. I also owe a great deal to Peter Buzás for helping me with my photo-filling experiments, and Ana Lara for always maintaining an efficiently running lab.

I have enjoyed the company and support of many fellow students including Bahar Eriköz, Kenny Cheong and Ehren Terenyi. I have also had the privilege of sharing some of my work with Som Solomon, Chris Tailby, Carla Abbott, Esther Blessing and Jason Forte - their feedback and advice have contributed to significant improvements with manuscripts and presentations. I would especially like to thank Vickie Wong and Tina Tsai for their friendship and support. Thank you to Cindy Guy for her work in getting the new lab up and running and for making the relocation process as smooth as possible, and to Sander Pietersen and Arzu Demir for their company during the time I have spent in Sydney.

I thank Neville McBrien for allowing me to conduct my PhD in the Department of Optometry and Vision Sciences. I have received financial support in the form of a Melbourne Research Scholarship and several departmental reimbursements for conference travel.

Last but not least, I would like to thank my family for their encouragement and support; especially during the particularly stressful times I experienced nearing

submission. Thank you for your help with the big move, for every care package, and the many many phone calls. Thank you also to Adam for being there for me during the highs and lows, for the many visits and for putting up with being almost 900 km apart for more than a year.

Table of Contents

Chapter 1 Introduction 1

1.1 *Structure of the primate retina 1*

1.2 *Photoreceptors 3*

1.3 *Bipolar cells 8*

Midget bipolar cells 8

Rod bipolar cells 11

Diffuse bipolar cells 11

Blue cone bipolar cells 12

Other bipolar cell types 13

1.4 *Amacrine cells 13*

1.5 *Ganglion cells in primate retina 14*

Midget and parasol ganglion cells 15

Morphology 15

Physiological properties 17

Functional roles 18

1.6 *Wide-field ganglion cells 19*

Small bistratified ganglion cells 25

Large sparse ganglion cells 32

Broad thorny ganglion cells 34

1.7 *The fovea 35*

1.8 *Aims of this thesis 40*

Chapter 2 Synaptic inputs onto small bistratified (blue-ON/yellow-OFF) ganglion cells in marmoset retina 42

2.1 *Introduction 42*

2.2 *Materials and Methods 43*

Animals 43

Tracer injections and photofilling 44

Antibodies 46
Immunohistochemistry 47
2.3 *Analysis* *48*
Image acquisition 48
Ganglion cell eccentricity and quantification of dendritic parameters 48
Synaptic input 51
Cone convergence 53
2.4 *Results* *53*
Identification of small bistratified ganglion cells 53
Synaptic input to small bistratified ganglion cells: Qualitative results 57
Synaptic input to small bistratified ganglion cells: Quantitative results 62
Convergence in the blue/yellow pathway 65
2.5 *Discussion* *70*
Distribution and density of synaptic input to ganglion cells 71
Ratio of excitatory and inhibitory synaptic input 72
Functional role of the outer dendritic tier 73
Conclusion 74

Chapter 3 Synaptic inputs to two types of koniocellular pathway ganglion cells in marmoset retina 75

3.1 *Introduction* *75*
3.2 *Materials and Methods* *76*
Animals 76
Tracer injections and photofilling 77
Antibodies 78
Analysis 78
Ganglion cell eccentricity and quantification of dendritic parameters 79
Synaptic input 79
Relationship between amacrine and bipolar input 80
Cone convergence 80

DB6 overlap 80
3.3 *Results* *81*
Large sparse ganglion cells 81
Broad thorny ganglion cells 86
Quantitative comparison of morphology and cone convergence 88
Synaptic input to large sparse and broad thorny cells: Qualitative results 90
Synaptic input: Quantitative results 94
Feedforward synapses 96
Relationship between large sparse ganglion cells and DB6 cells 96
3.4 *Discussion* *100*
Differences between ganglion cell types 101
Relationship between bipolar and amacrine input 103
Feedforward synapses 104
Cell types providing input to large sparse cells 105
Bipolar types providing input to broad thorny cells 105
Conclusion 106
Chapter 4 Wide-field ganglion cells in foveal retina .. 107
4.1 *Introduction* *107*
4.2 *Materials and methods* *108*
Animals 108
Analysis of ganglion cells 109
Analysis of bipolar cells 112
4.3 *Results* *119*
Foveal/central wide-field ganglion cells 119
Bipolar cell axon terminal stratification - qualitative observations 127
Bipolar cell axon terminal stratification - quantitative results 129
4.4 *Discussion* *132*
Accounting for lateral displacement at the fovea 132
Previously identified wide-field ganglion cell types at the fovea 134

Bipolar cell types at the fovea 136
Functional implications for foveal vision 138
Conclusion 138

Chapter 5 Conclusion 139

References 141

Appendix 161

List of Figures

Figure 1.1 - Neurons of the primate retina 2
Figure 1.2 - Cone pedicle structure 7
Figure 1.3 - Bipolar cells of the primate retina 9
Figure 1.4 - Midget and parasol ganglion cells 16
Figure 1.5 - Wide-field ganglion cells in human retina 24
Figure 1.6 - Small bistratified ganglion cell circuitry 1 29
Figure 1.7 - Small bistratified ganglion cell circuitry 2 30
Figure 1.8 - The primate fovea 37
Figure 2.1 - Retrogradely labelled and photo-filled small bistratified ganglion cells 55
Figure 2.2 - Drawings of small bistratified ganglion cells 56
Figure 2.3 - Excitatory and inhibitory synaptic markers 58
Figure 2.4 - Distribution of presumed bipolar cell inputs onto small bistratified ganglion cells 60
Figure 2.5 - Distribution of presumed amacrine cell inputs onto small bistratified ganglion cells 61
Figure 2.6 - Synaptic inputs onto inner and outer dendritic tiers of small bistratified ganglion cells 63
Figure 2.7 - Cone pedicle mosaic overlying a small bistratified ganglion cell 66
Figure 2.8 - Cone pedicles overlying inner and outer dendritic tiers of small bistratified ganglion cells 67
Figure 2.9 - Cone convergence to small bistratified ganglion cells 69
Figure 3.1 - Camera lucida drawings of a large sparse and broad thorny ganglion cells 82
Figure 3.2 - Retrogradely lableled and photo-filled large sparse and broad thorny ganglion cells 83
Figure 3.3 - Drawings of retrogradely labelled large sparse ganglion cells 84
Figure 3.4 - Patterns of dendritic stratification for large sparse and broad thorny ganglion cells 85
Figure 3.5 - Drawings of retrogradely labelled broad thorny ganglion cells 87

Figure 3.6 - Dendritic field diameters of large sparse and broad thorny ganglion cells 89
Figure 3.7 - Identifying presumed synaptic input onto large sparse and broad thorny ganglion cell dendrites 91
Figure 3.8 - Distribution of presumed bipolar cell inputs onto large sparse and broad thorny ganglion cells 92
Figure 3.9 - Distribution of presumed bipolar and amacrine cell inputs onto large sparse and broad thorny ganglion cells 93
Figure 3.10 - Potential synaptic sites between DB6 axon terminal processes and large sparse ganglion cell dendrites 98
Figure 3.11 - Density of presumed bipolar inputs onto different ganglion cell types 102
Figure 4.1 - Retrogradely labelled and photofilled foveal ganglion cells 120
Figure 4.2 - Drawings of foveal wide-field ganglion cells 121
Figure 4.3 - Unclassified foveal wide-field ganglion cells 124
Figure 4.4 - Dendritic field diameters of foveal and extra foveal wide-field ganglion cells 125
Figure 4.5 - Immunohistochemical labelling of bipolar cells 128
Figure 4.6 - Bipolar cell axon terminal stratification 130

List of Tables

Table 1.1 Wide-field ganglion cells - Yamada et al. (2005) *23*
Table 2.1: Experimental parameters - Animals and anaesthesia *44*
Table 2.2: Experimental parameters - Tracer injections and photofiling *44*
Table 2.3: Experimental parameters - Immunohistochemical processing of retinal wholemounts *46*
Table 2.4: Retinal locations of small bistratified cells *49*
Table 3.1: Experimental parameters - Animals and anaesthesia *77*
Table 3.2: Experimental parameters - Tracer injections and photofiling *77*
Table 3.3: Experimental parameters - Immunohistochemical processing of retinal wholemounts *78*
Table 3.4 Synaptic input onto large sparse and broad thorny ganglion cells *95*
Table 3.5 - Presumed synaptic sites between large sparse ganglion cells and DB6 bipolar cells *99*
Table 4.1: Experimental parameters - Animals and anaesthesia for tracer injections and photofilling *109*
Table 4.2: Experimental parameters - Animals and anaesthesia for bipolar cell analysis *109*
Table 4.3: Experimental parameters - Tracer injections and photofilling *110*
Table 4.4: Experimental parameters - Immunohistochemical processing of retinal wholemounts *110*
Table 4.5 - Antibodies *114*
Table 4.6: Experimental parameters - Immunohistochemical processing of vertical sections *116*
Table 4.7: Analysis of vertical sections *119*
Table 4.8: Axon terminal stratification - Marmoset *131*
Table 4.10: Axon terminal stratification comparisons - marmoset *137*
Table 4.11: Axon terminal stratification comparisons - macaque *137*

List of Abbreviations

BSA	bovine serum albumin
CaBP	calbindin
CD15	carbohydrate epitope 15
CtBP2	c-terminal binding protein 2
DB	diffuse bipolar
DIC	differential interference contrast
FMB	flat midget bipolar
GluR4	glutamate receptor subunit 4
IgG	immunoglobulin G
IR	immunoreactive
L	long wavelength sensitive
LGN	dorsal lateral geniculate nucleus
M	medium wavelength sensitive
NHMRC	National Health and Medical Research Council
PB	phosphate buffer
PBS	phosphate buffered saline
PKCα	protein kinase Cα
S	short wavelength sensitive
vGlut-1	vesicular glutamate transporter-1

Chapter 1 Introduction

A large part of cortex is thought to be involved in the processing of visual information. All visual sensory information to be processed by these cortical areas arises from the retina, situated at the back of the eye (Figure 1.1A).

The retina is a layered structure, with each layer containing a specific group of cells which are interconnected to form distinct neuronal pathways required in the eventual experience of visual sensation. A thorough understanding of the neural connections within the retina, and the level of information processing which occurs as a result of this connectivity, is needed to help understand the distinct contributions of the subsequent downstream processes.

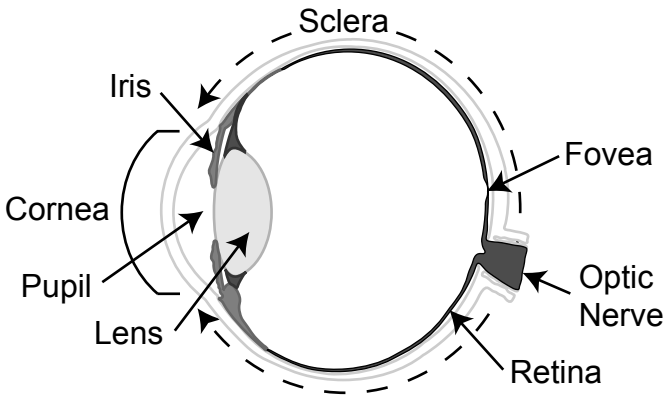
This thesis aims to uncover anatomical evidence for the connectivity underlying a collection of ganglion cell types, which as a population are the neurons that form the outputs of the retina. In this introduction, a brief summary of the general cell types within the retina will be followed by a detailed review of the literature on the types of ganglion cells examined in the studies presented in subsequent chapters. Finally, a review of the anatomical changes within a specialised region of the retina known as the fovea (Figure 1.1A) will be presented pertaining to the study presented in Chapter 4 (page 107).

1.1 *Structure of the primate retina*

Light enters the eye through the cornea at the front of the eye and travels through the pupil, which is the aperture created by the iris (Figure 1.1A). Light is then focused by the lens and ultimately falls on the photosensitive cells within the retina, near the back of the eye (Figure 1.1A).

Figure 1.1B shows a drawing from an early study of macaque retina depicting the neural cell types within the retina in vertical view (Polyak, 1935). The five main neural cells of the retina, photoreceptor, horizontal, bipolar, amacrine and ganglion cells can be divided into those involved in the vertical or horizontal pathways.

A



B

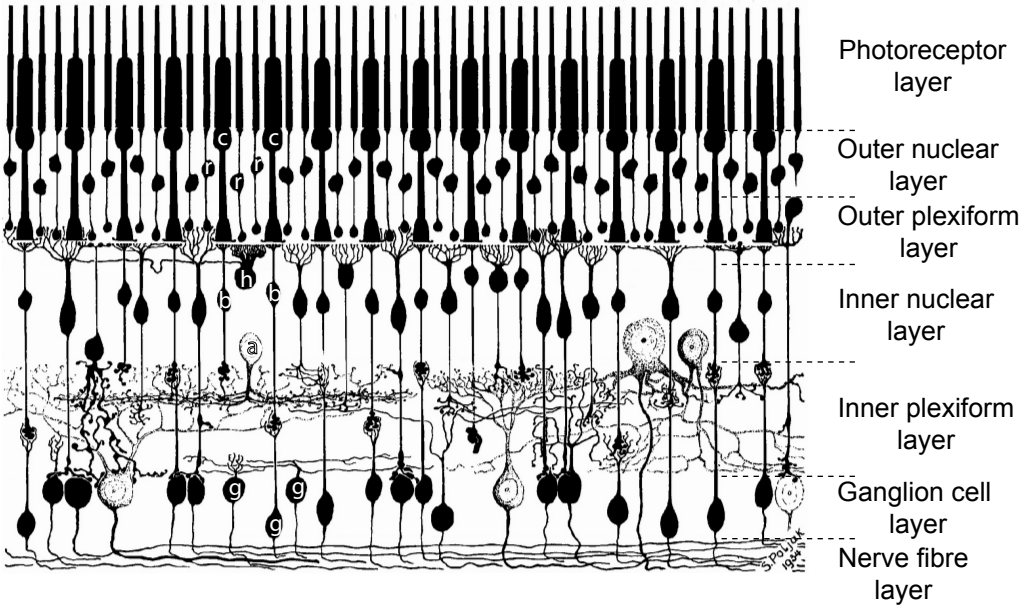


Figure 1.1 Structures of the early visual system. **A**: Schematic diagram representing a cross sectional view of the human eye. Figure modified from Rodieck, (1973). **B**: Drawing depicting the main neuronal cell types of the primate retina (as seen in vertical view) and their basic arrangement across the main retinal layers. Figure modified from Polyak, (1934). (r) rods; (c) cones; (h) horizontal cells; (b) bipolar cells; (a) amacrine cells; (g) ganglion cells.

Photoreceptors, bipolar cells, and ganglion cells of the vertical pathway are organised, in sequence, from outer to inner retina in an orientation orthogonal to the plane of the retina. The somas and processes of photoreceptors, bipolar cells and ganglion cells are usually restricted to the photoreceptor layer, inner nuclear layer and ganglion cell layer respectively. The detailed function and morphology of the neurons involved in the vertical pathway will be discussed in Sections 1.2 (page 3), 1.3 (page 8), 1.5 (page 14) and 1.6 (page 19).

The primary function of horizontal and amacrine cells, involved in the horizontal pathways of the retina, is to provide inhibitory lateral inputs onto neural cells of the vertical pathway to modulate their signals. Cell somas of the horizontal and amacrine cell types usually reside in the upper and lower portions of the inner nuclear layer, with processes extending into the outer plexiform and inner plexiform layers respectively. This thesis primarily concerns cells of the vertical pathway. As such, horizontal cells will not be discussed further, and amacrine cells will be discussed in Section 1.4 (page 13), in the context of their synaptic relationships to ganglion cells.

The axons of ganglion cells leave the retina to form the optic nerve, whose fibres project to various subcortical structures for further processing - the primary projection site being the dorsal lateral geniculate nucleus of the thalamus.

A region of increased photoreceptor density known as the fovea, allows for fine acuity central vision, and is present in the retinae of most primates. The detailed anatomical specialisations of the fovea will be outlined in Section 1.7 (page 35).

1.2 *Photoreceptors*

Photoreceptors are the main sensory neurons of the retina, conveying changes in light levels through signalling cascades initiated by conformational changes in light sensitive pigments (called opsins), upon the absorption of photons. With increases in light intensities, the signalling cascade ultimately leads to the closure of cyclic-GMP gated sodium channels, and the resultant hyperpolarisation of the photoreceptor. Under dim light levels however, sodium channels remain open leading to the depolarisation of the photoreceptor, which in turn facilitates the steady release of glutamate from the presynaptic terminal (for a review, see Baylor, 1996).

Most Old World primates, and trichomatic New World primates possess four types of photoreceptor, each with a type of opsin maximally sensitive for different wavelengths of light. In normal trichromats, the three cone photoreceptor types are each most sensitive to short (S cones), middle (M cones) and long (L cones) wavelength light. Rods, which make up the fourth photoreceptor type, mediate vision under low light levels. The photopigment contained within rods, rhodopsin, is active under scotopic conditions and saturates under photopic light conditions.

Unlike M- and L-cones, S-cones can be distinguished from other cones by the subtle differences in their morphology (Ahnelt et al., 1990; Ahnelt et al., 1987), by immunohistochemical labelling with antibodies directed against the S-cone opsin (Curcio et al., 1991; Martin and Grünert, 1999; Szél et al., 1988) or by the introduction of tissue-reactive dyes (de Monasterio et al., 1985; de Monasterio et al., 1981; McCrane et al., 1983). This has facilitated the study of the density and spatial arrangement of S-cones across the retina.

S cones are estimated to make up 7 - 10 % of the total cone population in many primate species (Curcio et al., 1991; de Monasterio et al., 1985; Marc and Sperling, 1977; Szél et al., 1988) including marmoset monkeys which are used in the studies described in chapters 2 (page 42), 3 (page 75), and 4 (page 107) (Martin and Grünert, 1999).

The pattern of S-cone distribution however, differs slightly between marmosets and other primates. An absence of S cones at the center of the foveola, where combined M and L cone densities are at their highest has been reported in macaques (de Monasterio et al., 1985; de Monasterio et al., 1981; Martin and Grünert, 1999), and humans (Curcio et al., 1991) whereas no such S cone free zone was observed in marmoset (Martin and Grünert, 1999).

In human and macaque, the S cone free area is usually surrounded by an area of highest S cone density between 0.1 and 0.3 mm from the fovea (Ahnelt et al., 1987; Curcio et al., 1991; de Monasterio et al., 1985; de Monasterio et al., 1981). The region of highest S cone density in marmoset however occurs instead, at the foveola (Martin and Grünert, 1999). Marmosets also show a higher peak S cone density than in humans and macaques (approximately 2,000 cells / mm^2 in human(Curcio et al., 1991); 6,000 cells / mm^2 in macaque and 10,000 cells / mm^2 in marmoset (Martin and Grünert, 1999). From

these regions of peak S cone density, in all three species, the proportion of S cones decreases steadily with increasing distances toward the retinal periphery (Ahnelt et al., 1987; de Monasterio et al., 1985; Martin and Grünert, 1999).

With the possible exception of the region immediately surrounding the S cone free zone, S cones in most primate species studied so far (Ahnelt et al., 1987; Curcio et al., 1991; de Monasterio et al., 1985; de Monasterio et al., 1981; Marc and Sperling, 1977; Martin and Grünert, 1999; Shapiro et al., 1985; Szél et al., 1988) form a semi-regular array. In contrast, S cones in marmoset and human retina appear to be randomly distributed across the retina (Curcio et al., 1991; Martin and Grünert, 1999; Roorda et al., 2001; Roorda and Williams, 1999).

Understanding the proportional changes of cone types, and their arrangement across the retina allows for estimation of cone convergences in later stages of the vertical pathway. Such estimates were made in the studies presented in Chapters 2 (page 42) and 3 (page 75).

At present, M and L cones cannot be distinguished by morphological or simple histochemical means (Szél et al., 1988). As such, few studies exist on the detailed topography of M and L cone types and their densities (Marc and Sperling, 1977; Mollon and Bowmaker, 1992; Packer et al., 1996).

More recently however, methods involving *in vivo* retinal imaging with the use of adaptive optics combined with retinal densitometry using wavelength controlled selective bleaching of different cone types has allowed for the estimation of M and L cone ratios and distributions from absorptance images (Hofer et al., 2005; Roorda et al., 2001; Roorda and Williams, 1999). Results from such studies show that trichromatic individuals can vary considerably in their M and L cone ratios without exhibiting phenotypic differences.

It is generally thought that M and L cone mosaics show random distributions (Marc and Sperling, 1977; Mollon and Bowmaker, 1992; Roorda et al., 2001; Roorda and Williams, 1999), however certain studies have also observed clumping of like type cones at a frequency higher than expected for a random distribution (Hofer et al., 2005; Packer et al., 1996) which may have some implications on the chromatic properties of bipolar cell types receiving non-selective inputs from all cones within their dendritic fields.

The presynaptic terminals of cones and rods are called pedicles and spherules respectively. They are located in the outer plexiform layer of the retina where they are contacted by bipolar and horizontal cell processes.

Within the terminals, vesicles containing the transmitter, glutamate, accumulate at synaptic ribbons, located on the intracellular side of invaginations within the presynaptic membrane (Figure 1.2). Synaptic ribbons are organelles, typically resembling a plate or a flat disc lying perpendicular to the presynaptic surface, which extend from the site of transmitter release unto the presynaptic cytoplasm. Vesicles are captured from the cytoplasm and tethered to the surface of ribbons by fine filaments for release at the active site. The tethering of vesicles to the ribbon is thought to provide a reserve pool of vesicles immediately available for exocytosis upon Ca^{2+} entry into the terminal. However, the exact mechanism by which the function of ribbons accelerates the exocytosis of vesicles, and allows for high rates of sustained transmitter release is unknown (for reviews, see Lagnado, 2003; Parsons and Sterling, 2003; Prescott and Zenisek, 2005; Sterling and Matthews, 2005; tom Dieck and Brandstätter, 2006).

Rod spherules typically contain one or two large crescent or horseshoe-shaped synaptic ribbons (tom Dieck and Brandstätter, 2006), whereas cone pedicles can have between 20 - 50 ribbons depending on their retinal location (Calkins et al., 1996; Chun et al., 1996). Ribbon markers are utilised in studies described in Chapters 2 (page 42) and 3 (page 75) to identify individual cone pedicles.

Contacts with processes of bipolar and horizontal cells occur within membrane invaginations opposite the ribbon. Bipolar processes directly oppose synaptic ribbons and are flanked by horizontal processes, which terminate closer to the pedicle/spherule than the bipolar terminal (Figure 1.2). The bundle of horizontal and bipolar cell processes together with the synaptic ribbon, which they oppose, is known as a triad.

Flat contacts at the pedicle base, lateral to the invagination are formed with other bipolar cells (Dowling and Boycott, 1966). Glutamate released from cone pedicles are also thought to deliver its effects onto horizontal cell processes lying further below the triad at an approximate distance of 1 - 2 μm (Haverkamp et al., 2000).

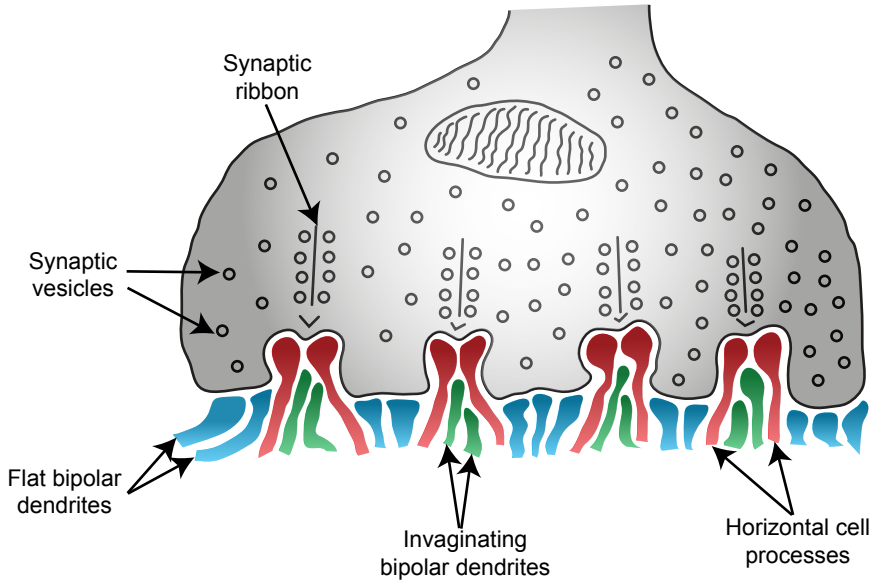


Figure 1.2 Schematic diagram of a cone pedicle as seen in cross sectional view, with four triad formations are shown. Cone pedicles make invaginating contacts with processes of bipolar (green) and horizontal cells (red) opposite their synaptic ribbons. Within the invagination, horizontal processes form the lateral elements and bipolar dendrites form the central elements. Some bipolar cells (blue) form flat contacts with the cone pedicle base. Figure modified from Haverkamp et al. (2000).

1.3 *Bipolar cells*

Bipolar cells comprise a group of retinal interneurons, receiving inputs from photoreceptors in the outer plexiform layer and synapsing onto ganglion and amacrine cells in the inner plexiform layer (Figure 1.1B). Figure 1.3 shows a schematic diagram of all bipolar cells described to date in primate, as seen in vertical view. Such bipolar types have been shown to differ primarily in the number and type of photoreceptors they contact, the extent of their dendritic fields and axon terminals, the stratification of their axon terminals, inner retinal cell types contacted, and where known, their physiological responses. The subsequent sections will briefly describe the findings from previous studies on each of the primate bipolar cells described to date. Unless stated, homologues of most of the following bipolar cell types have also been described in marmoset (Chan et al., 2001). This makes marmosets a viable animal model for studying bipolar to ganglion cell connectivity, with the ability to relate findings to Old World primates including humans.

Midget bipolar cells

Midget bipolar cells are the most numerous of cone bipolar cell types - the primary basis for their distinction being their connection to a single cone photoreceptor (although some exceptions exist in the retinal periphery; Boycott et al., 1969; Boycott and Hopkins, 1991; Chan et al., 2001; Jusuf et al., 2006b; Kolb, 1970; Kolb et al., 1992; Polyak, 1941; Telkes et al., 2008; Wässle et al., 1994).

Polyak (1941) first noted that midget bipolar cells exist in two types that differ in their pattern of axonal terminal stratification. This dichotomy was later found to correlate with the nature of the cone contacts made by each of these midget bipolar types (Boycott et al., 1969; Hopkins and Boycott, 1992).

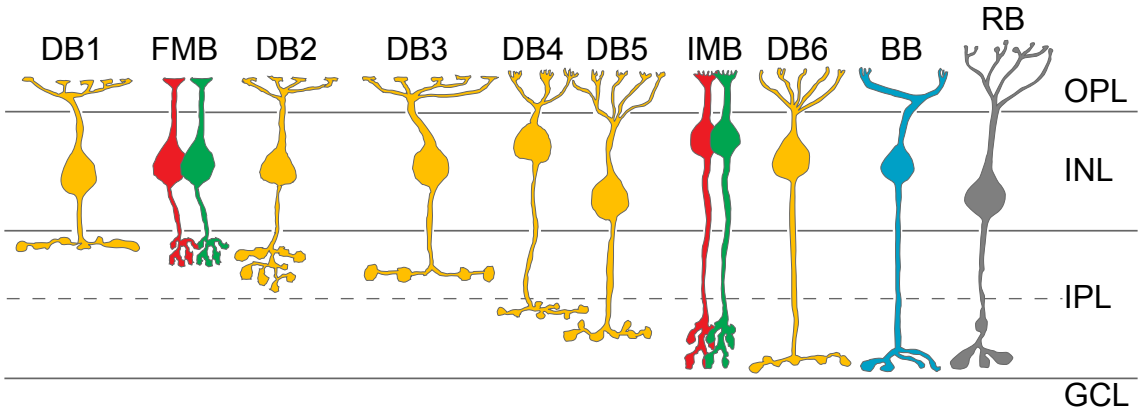


Figure 1.3 Bipolar cell types and their axonal terminal stratification in primate retina. Schematic diagrams of ten known primate bipolar cell types are shown in vertical view. Cell types are arranged according to level of axon terminal stratification. The dotted line represents the border between the ON and OFF halves of the inner plexiform layer. The colour of each bipolar cell type represents their cone input. Flat (FMB) and invaginating (IMB) midget bipolar cells receive inputs form medium- and/or long-wavelength sensitive cones. The blue cone bipolar (BB) and rod bipolar (RB) cells receive inputs from short-wavelength sensitive cones and rods respectively. Diffuse bipolar cells (DB1 - DB6) receive non-selective inputs from all cones lying within their dendritic field. (OPL) outer plexiform layer; (INL) inner nuclear layer; (IPL) inner plexiform layer; (GCL) ganglion cell layer. Modified from Boycott & Wässle (1999).

The invaginating midget bipolar type has dendritic processes that form a subset of the central invaginating elements of triads at cone pedicles, and possess axon terminals that stratify in the inner half of the inner plexiform layer (Boycott et al., 1969; Kolb, 1970). Flat midget bipolar cells, have dendritic processes which form 'flat' basal connections next to triads and whose axon terminals ramify in the outer half of the inner plexiform layer (Boycott et al., 1969; Hopkins and Boycott, 1992; Kolb, 1970). Flat and invaginating bipolar cells also differ on other morphological parameters such as the location of their somata and the number of terminal dendritic processes (Boycott et al., 1969; Kolb, 1970).

Although the level of axon terminal stratification of retinal bipolar cells and its correspondence with the ON and OFF physiological dichotomy had been shown in cat (Nelson and Kolb, 1983), the same relationship in primate was not proposed (Kolb and Dekorver, 1991), or shown directly through *in vitro* recordings from bipolar cell somas (Dacey et al., 2000; Dacey, 1999), until much later. These studies demonstrated that invaginating midget bipolar cells show ON type responses and flat midget bipolar cells displayed OFF type responses.

For all bipolar cell types discussed below, the distinction between ON and OFF types are assumed to correlate with the flat/invaginating type of contacts made with photoreceptors, and the level of axon terminal stratification. In primates, the ON and OFF division for axon terminal stratification, occurs roughly half way through the inner plexiform layer. The origin of the two different response polarities of bipolar cell types arises directly from the polarity of the cone response in the case of OFF bipolar cell types, and by signal inversion through the postsynaptic receptor on ON bipolar cells (Vardi et al., 2000).

Midget bipolar cells have been shown to preferentially contact either medium (M) or long wavelength sensitive (L) cone types over short wavelength sensitive (S) cones (Lee et al., 2005; Telkes et al., 2008). In the fovea where single-headed midget bipolar cells predominate, the single cone connection of midget bipolar cells is thought thus to provide a distinct chromatic, high acuity signal to the inner plexiform layer (Boycott et al., 1969). In the periphery individual midget bipolar cells can contact up to 4 cones in

macaque (Hopkins and Boycott, 1992; Polyak, 1941; Wässle et al., 1994) and ~ 9 in marmoset (Telkes et al., 2008).

Rod bipolar cells

Rod bipolar cells exclusively contact rod photoreceptors (Boycott et al., 1969; Kolb, 1970), which, under scotopic light conditions, then transfer the rod signal to a dedicated amacrine cell type in the inner plexiform layer (Grünert and Martin, 1991). The involvement of this amacrine cell type in the transfer of the rod signal within the inner retina will be discussed in Section 1.4 (page 13). The dendritic processes of rod bipolar cells form central elements at invaginating synapses with the rod spherule (Kolb, 1970), and their axon terminals ramify close to the border of the inner plexiform layer with the ganglion cell layer (Boycott et al., 1969; Polyak, 1941). The dendritic extent of rod bipolar cells can vary considerably, even amongst rod bipolar cells from the same eccentricity, such that, an individual rod bipolar cell may contact between 10 - 50 rods (Boycott et al., 1969).

Diffuse bipolar cells

The polysynaptic group of bipolar cells described by Polyak (1941) included the brush and flat bipolar groups; the names of which may have reflected characteristics of their dendritic processes at the level resolvable by light microscope. It is thought that the brush and flat bipolar cells correspond to the flat and invaginating diffuse bipolar cell types later described by others (Boycott et al., 1969; Kolb, 1970; Mariani, 1981), which (like the midget bipolar cells) are so named due to the nature of their contacts at the cone pedicle. In all of these studies however, the various types making up the invaginating and flat bipolar groups were not recognised.

The diffuse bipolar cell group was later further divided into 6 types (Figure 1.3), defined primarily by the shape and stratification of the axonal branches, and the number and type of cone contacts (Boycott and Wässle, 1991). The different diffuse bipolar (DB) types are denoted by numbers representing the progression of axonal stratification levels within the inner plexiform layer, starting with the DB1 type stratifying closest to the inner nuclear layer, through to the DB6 type stratifying closest to the ganglion cell layer (Boycott and Wässle, 1991). As illustrated in Figure 1.3, diffuse bipolar types 1 - 3

possess axon terminals stratifying in the outer half of the inner plexiform layer, and diffuse bipolar types 4 -6 in the inner half. Axon terminals of bipolar cells can be narrowly stratified (DB3, DB5 and DB6) or span across a few µm of the inner plexiform layer (DB1, DB2 and DB4; Boycott and Wässle, 1991).

Diffuse bipolar types 1 - 3 primarily form basal contacts with cone pedicles, and types 4 - 6 form mostly invaginating contacts. Each type shows a variation in their average dendritic field size with respect to eccentricity, with those possessing the widest of dendritic fields contacting more cone pedicles (Boycott and Wässle, 1991). Cone convergence thus differs for each diffuse bipolar cell type, ranging from 5 - 10 cones (Boycott and Wässle, 1991). In general, the number of cones contacted by a particular diffuse bipolar cell type is kept constant across the retina, where changes in photoreceptor density are accompanied by changes in the dendritic field size of bipolar cells (Boycott and Wässle, 1991; Polyak, 1941). Two examples of diffuse bipolar cells receiving non-selective inputs from all cone types within their dendritic fields have been previously reported (Boycott and Wässle, 1991; Chan et al., 2001), however another more detailed study has shown that DB4 and DB6 cells may preferentially contact M and L cones over S cones (Lee and Grünert, 2007).

Some studies have demonstrated specific connections between axonal processes of diffuse bipolar cell types and ganglion cell types (Bordt et al., 2006; Boycott and Wässle, 1991; Calkins et al., 1994; Calkins et al., 1998; Ghosh et al., 1997; Jacoby et al., 1996; Jacoby and Marshak, 2000; Jacoby et al., 2000; Marshak et al., 2002). The full connectivity of most diffuse bipolar cell types within the inner plexiform layer however, remains unknown.

Blue cone bipolar cells

Mariani (1984) described an invaginating bipolar cell type whose dendrites, when contacting two or more cones, did so with cones that were widely separated. He noted that the spacing of these cones matched the spacing of S cones at corresponding eccentricities, and thus proposed that the bipolar cell type identified selectively contacted S cones. The specificity of S cone connections to blue cone bipolar cells was later confirmed by means of electron microscopy, where it was shown that dendritic processes

of these bipolar cells form central elements opposite S cone ribbons (Herr et al., 2003; Kouyama and Marshak, 1992). Cone convergence (between 1.2 - 1.8 S cones per blue cone bipolar cell; Kouyama and Marshak, 1992; Luo et al., 1999) and divergence (1.8 blue cone bipolar cells per S cone; Kouyama and Marshak, 1992; Luo et al., 1999) for the connectivity between S cones and blue cone bipolar cells is independent of eccentricity (Boycott and Wässle, 1991).

Blue cone bipolar cells have axon terminals that stratify narrowly in the inner most stratum of the inner plexiform layer (Ghosh et al., 1997; Kouyama and Marshak, 1992; Mariani, 1984). Half of the axonal contacts of blue cone bipolar cells in the inner plexiform layer are with ganglion cells and the other half with amacrine cells (Kouyama and Marshak, 1992). The small bistratified type ganglion cell has been shown to receive inputs from blue cone bipolar cells (Calkins et al., 1998; Dacey, 1993a; Dacey and Lee, 1994; Ghosh and Grünert, 1999; Ghosh et al., 1997; Rodieck, 1991). The detailed connectivity of small bistratified ganglion cells will be discussed in Section 1.6 (page 19).

Other bipolar cell types

The rarely encountered giant bipolar cells described by Mariani (1983), Rodieck (1988) and Joo et al. (in press) in macaque retina, consist of a morphological type distinct from those described above. Giant bipolar cells are characterised by their extremely large dendritic fields, the processes of which make flat contacts with cone pedicles (Mariani, 1983; Rodieck, 1988). The equally large and sparsely branching axon terminals ramify near the center of the inner plexiform layer at the same level as DB4 axon terminals (Joo et al.). This type of bipolar cell has not yet been described in marmoset retina.

1.4 *Amacrine cells*

Most amacrine cells have somas located in the innermost part of the inner nuclear layer, with processes extending into the inner plexiform layer. Amacrine cell processes have been shown to both make and receive synapses (Dowling and Boycott, 1966), however inputs and outputs are often not segregated to particular processes emerging from opposite poles of the soma, as is the case for bipolar and ganglion cells. Twenty-six

morphologically distinct amacrine cell types have been described in macaque retina, however very little is known about the exact biochemical make up and functional roles of each (Mariani, 1990).

One example of an amacrine cell type with a known functional role is the AII amacrine cell, involved in the rod pathway of the retina. AII amacrine cells have a bistratified dendritic tree with processes present in both ON and OFF halves of the inner plexiform layer (Boycott et al., 1969; Famiglietti and Kolb, 1975; Mariani, 1990). The inner dendrites receive inputs from rod bipolar cells, which in turn, receive inputs from rod photoreceptors. This signal is then either transmitted to ON bipolar cells through gap junctions in the ON sublamina, or to OFF type bipolar cells, through output synapses of the outer dendrites of AII amacrine cells (Famiglietti and Kolb, 1975; Grünert and Martin, 1991; Grünert and Wässle, 1996).

Glycine and γ-aminobutyric acid (GABA) are two neurotransmitter types thought to be involved in the majority of inhibitory synapses in the inner plexiform layer. The amino acid glycine has been shown to be present in AII amacrine cells along with other possible primate amacrine cell types (Davanger et al., 1991; Ehinger, 1972; Frederick et al., 1984; Hendrickson et al., 1988). The inhibitory amino acid GABA is often found in displaced amacrine cell types with cell bodies residing in the ganglion cell layer, as well as others within the inner nuclear layer (Agardh et al., 1987; Davanger et al., 1991; Grünert and Wässle, 1990; Nishimura et al., 1985).

In studies described in chapters 2 (page 42) and 3 (page 75), the density of amacrine cell inputs onto ganglion cells is measured with the use of an antibody against a receptor clustering protein present at most GABA and glycinergic synapses. The presynaptic identities of the amacrine cells providing this input may include glycine or GABA containing amacrine types noted in the studies cited above.

1.5 *Ganglion cells in primate retina*

Ganglion cells are the output cells of the retina, they receive inputs from bipolar and amacrine cells in the inner plexiform layer, and their axons leave the retina to form the optic nerve. The axonal projections of retinal ganglion cells project to many subcortical

structures - the primary site of projection being the dorsal lateral geniculate nucleus (LGN) of the thalamus.

Midget and parasol ganglion cells

Midget and parasol ganglion cells make up the two major ganglion cell groups in primate retina. Midget and parasol ganglion cells respectively make up approximately 90 - 95 % and 5 - 6 % of all retinal ganglion cells in central retina (Dacey, 1993b; 1994; Grünert et al., 1993; Silveira and Perry, 1991), and play very distinct roles in the processing of visual information.

Morphology

Figure 1.4 shows drawings of midget and parasol ganglion cells representative of those found at different eccentricities across the retina (Ghosh et al., 1996). Dendritic fields of midget ganglion cells are consistently smaller than parasol ganglion cells at a given eccentricity (Dacey and Petersen, 1992; Leventhal et al., 1981; Perry and Cowey, 1981; Perry et al., 1984; Rodieck, 1988; Rodieck et al., 1985). The relationship between the field sizes of the two groups remains close to parallel across the retina with very little overlap in dendritic field sizes. The dendritic fields of both midget and parasol ganglion cells increase in size with increasing distances from the fovea (Dacey and Petersen, 1992; Perry and Cowey, 1981; Perry et al., 1984; Polyak, 1941; Rodieck, 1988; Rodieck et al., 1985; Watanabe and Rodieck, 1989) - most likely reflecting an overall decease in ganglion cell density in the periphery.

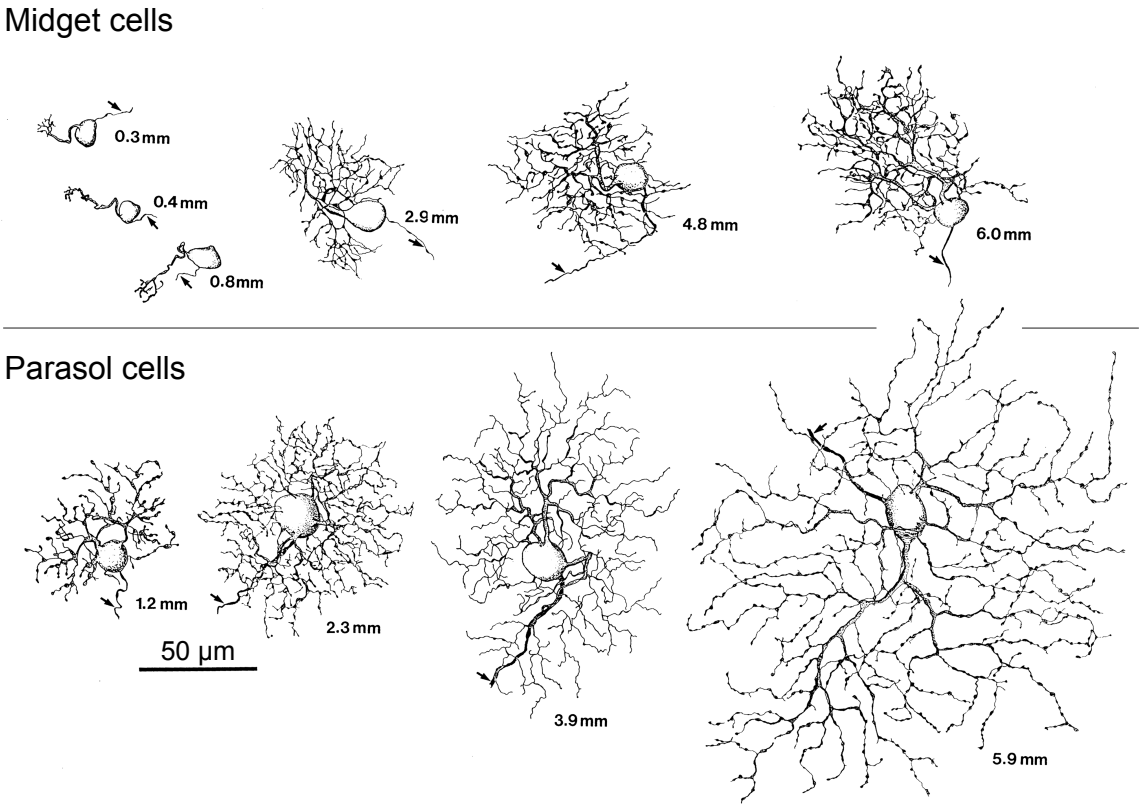


Figure 1.4 Camera lucida drawings of midget and parasol ganglion cells from different retinal eccentricities. Both midget and parasol ganglion cells show an increase in the extent of the dendritic field with increasing eccentricities. Parasol ganglion cells have larger dendritic fields than midget ganglion cells at corresponding eccentricities. Eccentricities are indicated beneath each cell. Arrows indicate axons. Modified from Ghosh et al. (1996).

The midget and parasol groups are composed of two types that differ in their dendritic stratification (Perry and Cowey, 1981; Perry et al., 1984; Polyak, 1941; Watanabe and Rodieck, 1989). For each group, there is a single type with dendrites stratifying within the inner half of the inner plexiform layer, and a second type that stratifies in the outer half. The dendrites of inner and outer stratifying parasol ganglion cells ramify closer to the middle of the inner plexiform layer; dendrites of the two midget ganglion types stratify closer to the borders of the inner plexiform layer (Watanabe and Rodieck, 1989). It was first presumed (Dacey and Petersen, 1992; Rodieck, 1988; Watanabe and Rodieck, 1989), and later shown directly (Dacey, 1999), that midget and parasol ganglion cells with ON center receptive fields correspond to the inner stratifying types and outer stratifying types possessed OFF center receptive fields.

Midget ganglion cells receive exclusive excitatory inputs from their corresponding midget bipolar cell type (ON midget ganglion cells from invaginating midget bipolar cells and OFF midget ganglion cells from flat midget bipolar cells; Dowling and Boycott, 1966; Polyak, 1941). ON and OFF type parasol ganglion cells are thought to receive inputs from a combination of either diffuse bipolar (DB) 4 and DB5 or DB2 and DB3 cells respectively (Jacoby et al., 2000; Marshak et al., 2002).

Axons of midget and parasol ganglion cells terminate in the parvocellular and magnocellular layers of the LGN respectively (Leventhal et al., 1981; Perry et al., 1984). As such, response properties observed from relay fibers in the above layers largely reflect those physiological properties observed in the respective ganglion cells (Dacey, 2000; Lee, 1996).

Physiological properties

The physiological properties of midget and parasol ganglion cells have been inferred from recordings of relay fibers in the parvocellular and magnocellular layers of the LGN and from direct recordings from the retina. For brevity, only studies where recordings were made from ganglion cell somas in the retina will be presented here.

Midget and parasol ganglion cells both show concentric, and spatially antagonistic receptive fields with an ON center and an OFF surround or vice versa (de Monasterio and Gouras, 1975; Hubel and Wiesel, 1960). Midget ganglion cells have

comparatively smaller receptive field centers than parasol ganglion cells at any given retinal location (Croner and Kaplan, 1995; de Monasterio and Gouras, 1975) - a difference which is thought to reflect the difference in the size of their dendritic fields. Despite differences in receptive field center sizes, both midget and parasol ganglion cells show similar spatial resolution limits (Crook et al., 1988; Lee, 1993). In further support of the correlation between the size of receptive field centers and dendritic fields, receptive field center sizes of midget and parasol ganglion cells have been shown to increase with increasing distances from the fovea (Croner and Kaplan, 1995; de Monasterio and Gouras, 1975; Hubel and Wiesel, 1960).

The response properties of midget and parasol ganglion cells differ in many other respects. Receptive fields of central midget ganglion cells are spectrally opponent with a single dominant cone type mediating the center and a surround of opposite spectral sensitivity (de Monasterio and Gouras, 1975; Gouras, 1968; Schiller and Malpeli, 1977). Parasol ganglion cells, on the other hand, show no spectral differences in their two receptive field components, with medium (M) and long (L) wavelength sensitive cone types contributing to both center and surround mechanisms (de Monasterio and Gouras, 1975; Gouras, 1968; Schiller and Malpeli, 1977).

Although they do not convey spectral information, parasol ganglion cells show higher contrast sensitivity than midgets (Croner and Kaplan, 1995; Kaplan and Shapley, 1986). Midget ganglion cells show sustained responses to maintained stimuli (de Monasterio and Gouras, 1975; Gouras, 1968; Schiller and Malpeli, 1977). In contrast parasol ganglion cells respond transiently to either the onset or offset of light stimuli, depending on the type (de Monasterio and Gouras, 1975; Gouras, 1968; Schiller and Malpeli, 1977). Lastly, it has been shown that axons of midget ganglion cells show longer response latencies than parasol ganglion cells, which is most likely a result of their comparatively smaller axonal diameters (Gouras, 1969; Schiller and Malpeli, 1977).

Functional roles

What can be gathered from physiological experiments described above, on the characteristics of midget and parasol ganglion cells, is that each group encodes distinct components of the visual world. The broad functional roles of these two ganglion cell

groups can also be inferred from the results of lesions to the areas of midget and parasol ganglion cell projections (Schiller et al., 1990).

Midget ganglion cells are partially involved in the encoding of colour, and are responsible for the first steps in the perception of colour along the red-green axis. They also play a role in high-resolution form vision, and high contrast stimuli.

Parasol ganglion cells are involved in the encoding of achromatic luminance levels, and are particularly important in detecting changes in luminance of low contrast stimuli. Perception of fast flicker and motion is also attributable to the response properties of parasol ganglion cells. Ultimately, the outputs of midget and parasol ganglion cells are thought to provide elementary components of the "temporal" and "parietal" pathways, which are two highly generalised streams of brain regions involved in the processing of information on form perception and movement respectively (Merigan and Maunsell, 1993).

The anatomical features, physiological responses and synaptic relationships are well established for the midget and parasol groups. On the other hand, information on wide-field ganglion cells is extremely limited due to their relatively low number.

1.6 *Wide-field ganglion cells*

Wide-field ganglion cells refer to those retinal ganglion cells that are of neither midget nor parasol types - and often possess 'wider' dendritic fields than their counterparts at corresponding retinal eccentricities. The wide-field group of ganglion cells are made up of many heterogeneous types of ganglion cells.

This section will describe the findings of previous literature examining morphological characteristics of wide-field ganglion cells. In particular, the focus will be placed on identifying those wide-field ganglion cell types or groups synonymous to two or more studies but given separate names. A summary of all known wide-field types, and their accepted names will precede an introduction to the wide-field ganglion cell types (small bistratified, large sparse and broad thorny ganglion cells) relevant to the studies presented in this thesis.

Polyak, (1941) provided the first detailed descriptions of ganglion cell types in Golgi stained macaque and chimpanzee retinas (Polyak, 1941). Methodological

limitations however, resulted in a fairly broad classification of ganglion cell groups. In his study, Polyak identified four groups of ganglion cells not including the midget and parasol types. By definition the four ganglion cell groups correspond to wide-field ganglion cells, and were appropriately classed under the 'diffuse' ganglion cell group, referring to the wide dendritic trees of these ganglion cell groups. With an exception of the 'shrub' ganglion cell type, the other three ganglion cell groups ('small diffuse', 'garland' and 'giant' ganglion cells) most likely contained a number of different morphological types. Polyak placed a heavy emphasis on the lateral extent of the dendritic field. As a result, ganglion cells were often grouped together despite large differences in their patterns of dendritic stratification. Polyak's wide-field cell groupings are, at present, no longer accepted as little focus was placed on the stratification patterns of dendrites, which is now known to be an important criterion for the functional distinction between ganglion cell types. In a later study an emphasis was placed on the stratification levels of ganglion cell dendrites (Boycott et al., 1969). Four different ganglion cell types or groups, not including midget ganglion cells, were identified with each of their names reflecting their general pattern of dendritic stratification ("diffuse", "giant", "stratified diffuse" and "unistratified"). Each of Boycott and Dowling's groups were thought to include ganglion cells belonging to Polyak's classification scheme, such that the diffuse group included Polyak's shrub ganglion cells, the giant group included Polyak's giant group, the stratified diffuse group included Polyak's parasol type and the unistratified group included Polyak's small diffuse and garland cells.

With the advent of retrograde tracing methods, the identification of ganglion cell projection sites was made possible. Wide-field ganglion cells projecting to the pretectum and superior colliculus were identified in macaque retina (Leventhal et al., 1981; Perry and Cowey, 1984). Leventhal et al. (1981) divided their wide-field ganglion cells into two groups (C and D) labelled after injections into the superior colliculus and pretectum respectively, both were characterised by very large, sparsely branching dendritic fields, and differed primarily in soma size. A subsequent study also found that features common to most pretectum and superior colliculus projecting ganglion cells were their large dendritic trees made up of sparsely branching thin dendrites, some of which have small somas and others larger somas (Pγ and Pε cells respectively) (Perry and Cowey, 1984).

In a large scale Golgi stain study of neurons of the human retina wide-field ganglion cells were classified based on their similarities with cat and rabbit ganglion cells (Kolb et al., 1992). Sixteen different types (G3a, G3b, G4, G5, G7, G8, G10, G11, G12, G16, G17, G19, G20, G21, G22, and G23) were identified and named according to previous schema adopted in cat retina.

Ganglion cells described included types with sparsely branching (G3a, G3b, G4, G10, G17, G20, G21, G22) or relatively densely branching dendritic trees (G5, G7, G8, G11, G12, G16, G19, G23). A wide range of dendritic stratification patterns were reported including those with dendrites spanning all depths of the inner plexiform layer (G4, G5, G22), those with a relatively narrow plane of stratification (G3a, G3b, G8, G12, G16, G19, G20, G21, G23) and those with bistratified dendritic trees (G7, G10, G11, G17). The authors suggest correspondences between previously described types in monkey retina and their reported types. G5 cells were thought to correspond to Polyak's small diffuse group, and both G8 and G16 to include Polyak's garland cells. G11 cells were thought to be the equivalent of Boycott and Dowling's diffuse cells and G10 and G16 to be examples of Boycott and Dowling's unistratified group.

A downside to the retrograde tracer methods from Leventhal et al. (1981) and Perry and Cowey (1984) was that dendritic labelling was often incomplete, making it difficult to morphologically distinguish certain ganglion cell types. To overcome the poor labelling experienced by previous retrograde tracer studies, Rodieck and Watanabe (1993) combined tracer injections with subsequent intracellular injections of dye into retrogradedly labelled ganglion cells. In this way it was possible to ensure complete dendritic filling and to correlate definitively morphological types of ganglion cells with their projection sites. Subcortical structures targeted for tracer injections were the superior colliculus, pretectum and the parvocellular layers of the dorsal lateral geniculate nucleus (LGN). Ganglion cells projecting to the pretectal region were found to have the largest dendritic fields of the three projections studied, and were characterised by sparsely branching dendritic trees - thus named PT-sparse cells. Ganglion cells projecting to the superior colliculus were classified into three groups, S, M and T. Both S and T groups consisted of bistratified and unistratified varieties, with those of the S group having relatively sparsely branching dendritic trees and T group cells having densely

branching dendritic trees. M group cells were thought to make up a single morphological type, with monostratified dendritic trees whose processes were spread evenly across the dendritic field and rarely overlapped. In addition to midget ganglion cells, a bistratified ganglion cell type (parvicellular bistratified) and a large ganglion cell with sparsely branching dendrites (parvicellular giant) were thought to project to parvocellular layers of the LGN.

In all aforementioned studies, observations were made in retinas of Old World primates. Homologous types of ganglion cells were later identified in marmoset and capuchin monkey, including those resembling the parvicellular bistratified type, the parvicellular giant type, and T group cells from Rodieck and Watanabe (1993), and the P_{γ} or P_{ε} from Perry and Cowey (1984) (Ghosh et al., 1996; Yamada et al., 1996).

In two subsequent studies, Peterson and Dacey (1999, 2000) gave detailed descriptions of wide-field ganglion cell types with monostratified, bistratified and diffusely branching dendritic trees from intracellular injections in human retina (Figure 1.5). Their large sample size encompassing a wide range of eccentricities allowed for the distinction of ganglion cell types based on clusters within scatter plots showing measurements of retinal eccentricity, dendritic field diameter and dendritic branch point number. This allowed for a classification scheme, which did not rely heavily on subjective judgements in grouping different ganglion cell types. As shown in Figure 1.5, six different groups of wide-field ganglion cells with monostratified dendritic trees were found (giant very sparse, large very sparse, large dense, large sparse, large moderate and thorny), three of which (giant very sparse, large very sparse and large dense) were thought to be made up of inner and outer stratifying types (Peterson and Dacey, 1999). Two groups of wide-field ganglion cell with bistratified dendritic trees were identified, differing primarily in the number of dendritic branch points, pattern of branching, thickness of dendrites and the presence/absence of dendritic spines. These were not given separate names, but an example of each morphological form is shown in Figure 1.5. Wide-field ganglion cells within the diffuse group possessed dendritic trees that stratified across both inner and outer portions of the inner plexiform layer. As shown in Figure 1.5, this group was most likely made up of at least two morphologically distinct types, one with a relatively sparsely branching dendritic tree, and a second with densely branching

dendritic trees and many thorny twig-like processes along their dendrites (Peterson and Dacey, 2000).

Dacey et al. (2003) described a novel method for the identification of ganglion cell morphology and projection, without the need for targeted intracellular injections after tracer uptake in the retina. This new method allowed for the complete labelling of a large number of ganglion cells *in vitro*, thereby revealing those wide-field types that are present in small numbers. Findings using this new method of retrograde photodynamics highlighted the diversity of wide-field ganglion cell types projecting to the LGN. The previously unknown primary projections of eight types of wide-field ganglion cells (inner and outer stratifying types of large sparse, giant sparse and narrow thorny groups, plus the broad thorny, and large bistratified types) were identified as the LGN.

Recently, Yamada et al. (2005) presented a more extensive catergorisation of the different wide-field ganglion cell types, as revealed by intracellular injections in macaque retina. The primary basis for this new scheme of classification was the pattern of dendritic stratification within the inner plexiform layer. As summarised in Table 1.1, wide-field groups were broadly divided into four groups consisting of narrowly unistratified, broadly stratified, bistratified and diffuse types.

Table 1.1 Wide-field ganglion cells - Yamada et al. (2005)

Group	Type	Dendritic stratification
Narrowly unistratified	Narrow thorny	S3 or S5
	Large sparse	S4
	Large moderate	S4
	Large dense	S2
	Large radiate	S2 or S4
	Narrow wavy	S1
	Large very sparse	S4
	Fine very sparse	S5
Broadly stratified	Broad thorny	S2 - S4
	Multi-tufted	S2 - S4
	Borad wavy	S2 - S4
	Parvocellular giant	S2 - S4
Bistratified	Small bistratified	S2 & S4 - S5
	Large bistratified	S2 & S4 - S5
Diffuse	Diffuse thorny	S1 - S5
	Diffuse smooth	S1 - S5

Sublamina 1 - 5 within inner plexiform layer (S1 - 5)

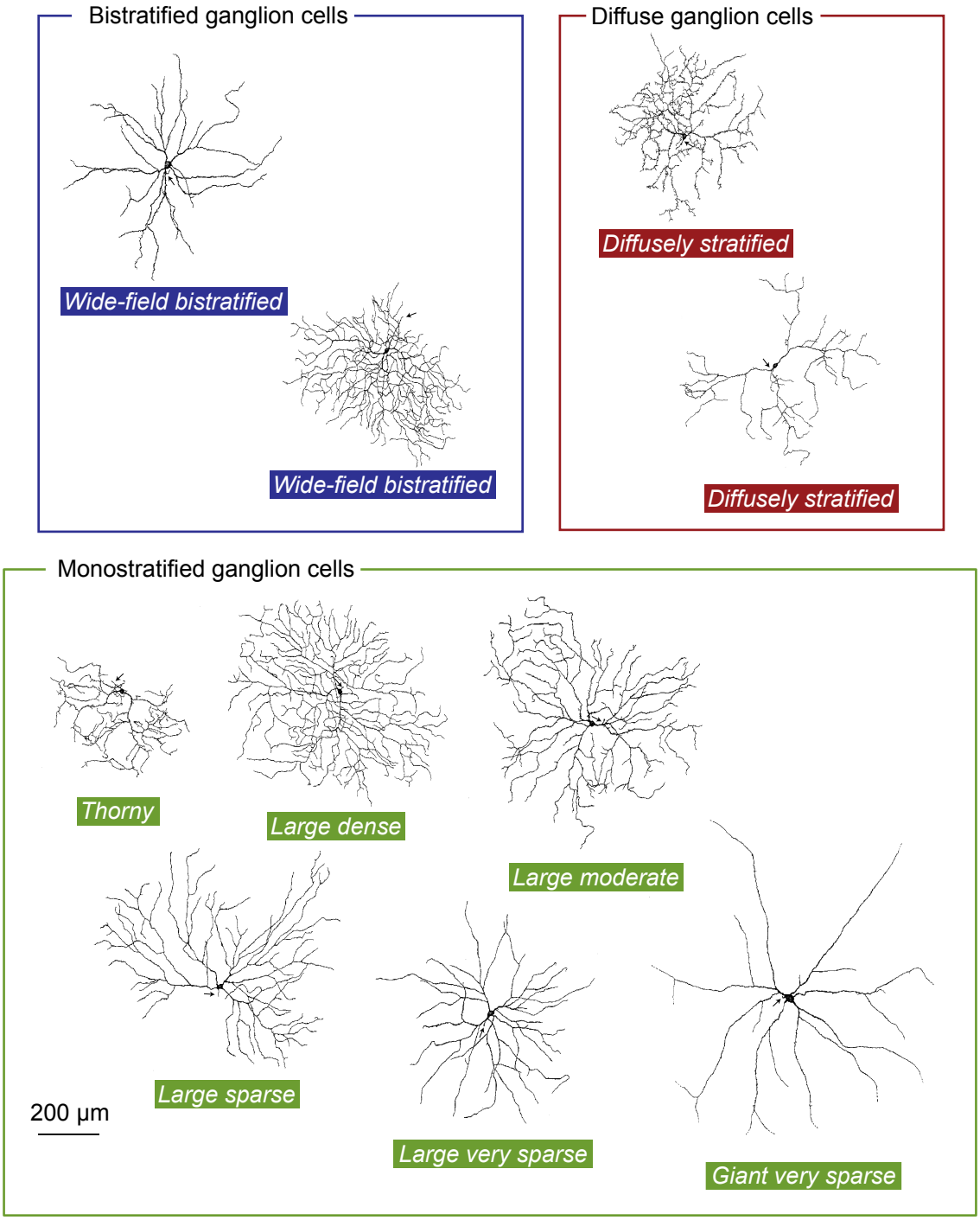


Figure 1.5 Camera lucida drawings of bistratified, diffusely stratified and monostratified ganglion cells, from Peterson & Dacey (1999, 2000). Relative dendritic field sizes are not directly comparable as cells vary in eccentricity. Eccentricities of ganglion cells shown range from 6.4 - 18.8 mm. Arrows indicate axons. Scale bar shown applies to all cells. Figure modified from Peterson & Dacey (2000).

Ten types of ganglion cells belonging to the narrowly unistratified group were identified (the narrow thorny and large radiate groups containing both inner and outer stratifying types), all with dendrities which were restricted to one stratum of the inner plexiform layer. The broadly stratified group, which were grouped together as their dendrities spanned 3 adjoining strata (S2 - S4) of the inner plexiform layer, consisted of four different types (broad thorny, broad wavy, multi-tufted and parvocellular giant). The bistratified group consisted of two previously identified bistratified types - the large and small bistratified ganglion cells. Two types (diffuse thorny and smooth diffuse) belonging to the diffuse group possessed dendrites that ramified throughout all strata of the inner plexiform layer. In total, Yamada and colleagues described 18 morphologically distinct wide-field types, including a subset of previously defined types.

A review of the main morphological features, and physiological properties of the small bistratified, large sparse and broad thorny types of wide-field ganglion cells (concerned in the studies of this thesis) are presented in chapters 2 (page 42) and 3 (page 75). A brief overview of the literature including the earlier accounts of these wide-field types in primate retina will be presented below. Tables 1.1, 1.2 and 1.3 in Appendix A summarise the primary findings of studies concerning small bistratified, large sparse and broad thorny ganglion cells in chronological order.

Small bistratified ganglion cells

Polyak's (1941) description of "shrub ganglion cells", include features common to the wide-field ganglion cell type now commonly known as small bistratified ganglion cells. Polyak noted the presence of "hook shaped shoots and buds" along the dendrites of these cells whose dendritic terminals were found mainly in the upper and lower layers of the inner plexiform layer. In a later study, Boycott et al. (1969) listed their "diffuse" ganglion cell type as a correlate of Polyak's (1941) shrub type. A physiological study of blue sensitive ganglion cells was reported at around the same time (Gouras, 1968), which included recordings from blue-ON cells showing sustained excitatory responses to blue light. In subsequent studies, it was shown that S-cone sensitive mechanisms of such blue sensitive ganglion cells are opposed by the combination of both medium (M) and long (L) wavelength sensitive cone inputs (de Monasterio and Gouras, 1975; de Monasterio et

al., 1975). In the same set of studies, the receptive field structure of a subset of blue-ON/yellow-OFF ganglion cells were shown to be non-concentric, as the two spectrally opposing components overlapped one another (de Monasterio et al., 1975). In a purely physiological study that followed, Zrenner and Gouras (1981) further characterised the receptive fields of blue-ON type ganglion cells, noting their poor temporal and spatial resolution (Zrenner and Gouras, 1981).

de Monasterio (1979) intracellularly labelled ganglion cells which were physiologically characterised as blue-ON ganglion cells, potentially allowing for the identification of a morphological correlate to this functionally distinct type. The morphological characteristics described by de Monasterio (1979) however, were thought to correspond to OFF parasol ganglion cells, and therefore did not correspond well with those of the small bistratified type (de Monasterio, 1979).

In his review article concerning physiological properties of colour opponent cells in the retina and LGN, Rodieck (1991) raises the possibility of bistratified ganglion cells being the morphological correlate of blue-ON ganglion cells (Rodieck, 1991). This suggestion was primarily based on similarities between receptive field center sizes of blue-ON ganglion cells, with dendritic field sizes of morphologically identified bistratified ganglion cells. Further, he proposed that the two dendritic tiers of bistratified cells, each lying in the ON and OFF sublaminae of the inner plexiform layer, may provide the basis for the spatially co-extensive receptive fields of blue-ON ganglion cells.

Kolb et al. (1992) presented an extensive study of Golgi stained neurons of the human retina, with the goal of drawing correspondences with previously identified ganglion cell types in cat or rabbit retina. The authors describe a bistratified type, which they name G11, due to its similarities with the previously described cat G11 ganglion cell (Kolb et al., 1992). The authors also note morphological similarities between the human G11 cell and the ON-OFF direction selective ganglion cell type described previously in rabbit retina (Amthor et al., 1984; Amthor et al., 1989).

In a study of small-field bistratified ganglion cells in macaque and human retina, it was shown that detailed morphological characteristics of these ganglion cells are shared by the two species (Dacey, 1993a). It was also estimated that these small-field bistratified

ganglion cells made up ~1 % of the total ganglion cell population in central retina, and between 6 - 10 % in peripheral retina.

As described in the earlier section on wide-field ganglion cells, Rodieck and Watanabe (1993) identified sites of ganglion cell projections by making injections of retrograde tracers into subcortical structures followed by intracellular injections of labelled ganglion cells. In their study they showed a ganglion cell type with bistratified dendritic trees to project to the parvocellular layers of the LGN (Rodieck and Watanabe, 1993). While the authors note that the injection site was confined to parvocellular laminae, a point to note here is that this may have included the intercalating koniocellular layers of the LGN.

Three years after it was first proposed by Rodieck (1991), Dacey and Lee (1994) showed a direct link between blue-ON ganglion cells and the small bistratified ganglion cell type. Based on this new evidence, the authors suggested a model for the anatomical circuity underlying the chromatic responses of small bistratified cells. In this model, the blue-ON component of the physiological response was thought to arise from blue cone bipolar cell input onto the inner dendrites, and the yellow-OFF response from OFF diffuse bipolar input onto the outer dendrites of small bistratified ganglion cells (Dacey and Lee, 1994).

In two subsequent studies, homologues of the small bistratified ganglion cell type were described in marmoset (Ghosh et al., 1996; Ghosh et al., 1997) and capuchin (Yamada et al., 1996) monkeys. The same animal models were then used to show that the inner dendrites of small bistratified ganglion cells co-stratify with axon terminal processes of blue cone bipolar cells (Ghosh et al., 1997; see Figure 1.6A) and that the chromatic responses of small bistratified ganglion cells in capuchin are similar to what has been shown previously in macaque (Silveira et al., 1999).

At around the same time, an electron microscopy study on foveal blue/yellow ganglion cells from macaque retina, showed inner tier dendrites receive exclusive input from blue cone bipolar cells and outer tier dendrites receive combined input from both diffuse bipolar (DB) 2 and DB3 cells, as depicted in Figure 1.7A (Calkins et al., 1998). The authors also showed for one foveal small bistratified cell that bipolar cell inputs (70 %) far outnumber amacrine cells inputs (30 %). This is in contrast with the findings of

Ghosh and Grünert (1999) who found that amacrine cells provide the majority (over 85 %) of synaptic inputs onto small bistratified ganglion cells from peripheral marmoset retina (Ghosh and Grünert, 1999). The study described in Chapter 2 (page 42) builds on the results of these studies by quantifying the proportion of bipolar and amacrine cell inputs across a larger sample of small bistratified cells from different eccentricities, in order to establish whether there is a eccentricity related change in the proportion of bipolar and amacrine cell inputs onto small bistratified cells.

Chichilnisky and Baylor (1999) used a microelectrode array to record from *in vitro* preparations of retina, in order to understand the microstructure of small bistratified cell receptive fields. This study demonstrated that blue-ON responses of peripheral small bistratified ganglion cells arise from pooled inputs of multiple S-cones within their dendritic fields (Chichilnisky and Baylor, 1999).

In 2003, Dacey and colleagues replicated the findings of Rodieck and Watanabe (1993) in showing that small bistratified ganglion cells are labelled from retrograde tracer injections into the LGN. The authors theorise that small bistratified ganglion cells specifically project to the koniocellular layers of the LGN. This was later shown to be the case in a combined physiological and anatomical study in marmoset (Szmajda et al., 2008).

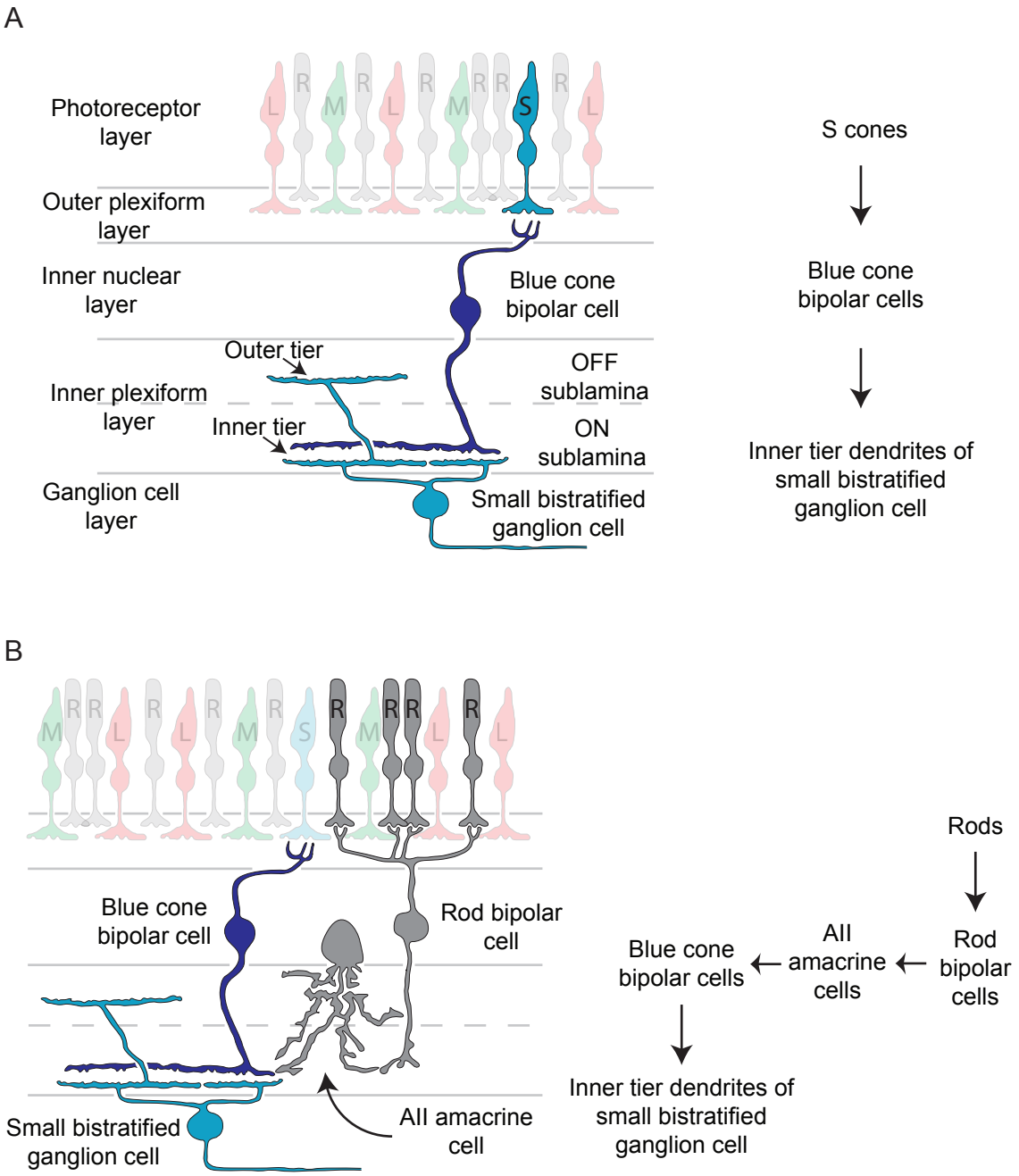


Figure 1.6 Small bistratified ganglion cell circuitry. **A**: Schematic diagram outlining retinal circuitry underlying blue ON responses of small bistratified ganglion cells (Ghosh et al., 1997; Calkins et al., 1999). **B**: Schematic diagram showing proposed retinal circuitry underlying scotopic responses in small bistratified ganglion cells (Crook et al., 2009; Field et al., 2009). Diagrams adapted from Martin (1998).

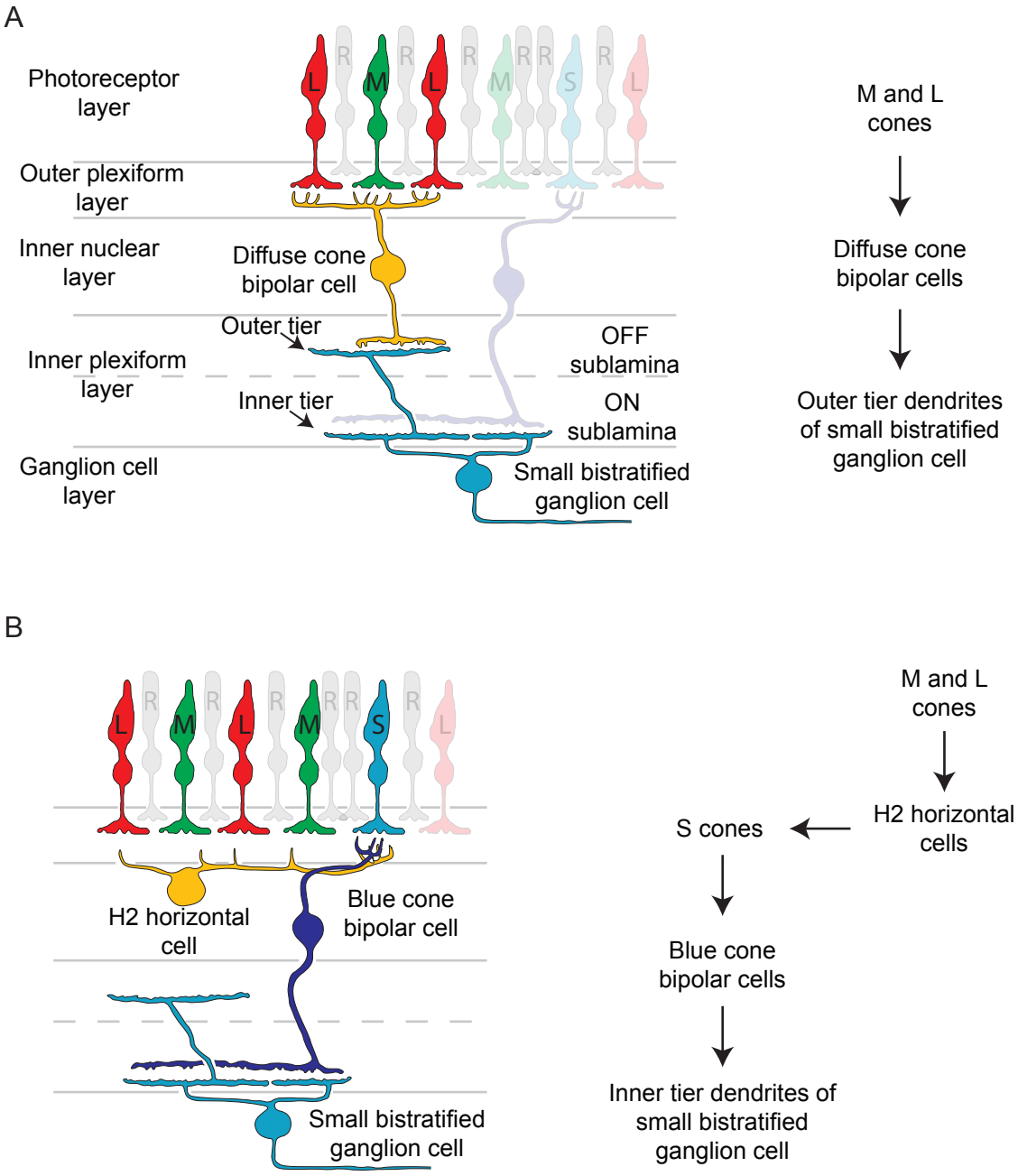


Figure 1.7 Small bistratified ganglion cell circuitry. **A**: Schematic diagram showing possible retinal circuitry underlying yellow OFF response of small bistratified ganglion cells via diffuse bipolar cells as suggested by Crook et al. (2009). **B**: Schematic diagram outlining retinal circuitry underlying yellow OFF responses of small bistratified ganglion cells via H2 horizontal cells as proposed by Field et al. (2007). Diagrams adapted from Martin (1998).

More recent studies focus primarily on uncovering the retinal circuitry underlying the responses of small bistratified ganglion cells, through inferences based on physiological recordings or direct anatomical observations.

Field et al. (2007) showed small bistratified ganglion cells to have spatially concentric receptive fields with chromatically opponent center-surround organisation, as opposed to the spatially overlapping organisation found in previous studies (Dacey and Lee, 1994; de Monasterio and Gouras, 1975). When the response kinetics of small bistratified ganglion cells were measured, the yellow-OFF component was found to be slower in comparison to the blue-ON response (Field et al., 2007). The authors also tested the responses of small bistratified ganglion cells under the application of $_{L}$(+)-2-amino-4-phosphonobutyric acid ($_{L}$-AP-4; a metabotropic glutamate receptor agonist thought to block transmission between cones and ON-type bipolar cells), which attenuated both the blue-ON and yellow-OFF response components. The authors write that such findings can be explained by a model, whereby yellow-OFF surround responses are conferred onto individual S-cones via horizontal cell (H1 cell) feedback from M and L cones, as shown in Figure 1.7B.

The findings of Field et al. (2007) were challenged by Crook et al. (2009), who maintained that small bistratified ganglion cells show spatially coextensive blue-ON/yellow-OFF components in their receptive fields. The authors show that, under their experimental conditions, the yellow-OFF component of the response was spared under the application of $_{L}$-AP-4 (Crook et al., 2009). Further examination of the yellow-OFF component revealed the presence of a blue-ON surround mechanism, consistent with the proposed receptive field structure of diffuse bipolar cells. Accordingly, the authors suggest the origin of the yellow-OFF component to small bistratified ganglion cells to be from OFF diffuse bipolar cells. The possibility of inner retinal inhibition from amacrine cells as a source of the yellow-OFF response was also ruled out through a series of tests with pharmacological antagonists to GABA and glycine receptors, in which the yellow-OFF component was spared. The study described in Chapter 2 (page 42) investigates the density of bipolar and amacrine inputs onto the inner and outer dendritic tiers of small bistratified cells in order to further understand the anatomical basis for the chromatic responses of these cells.

One other significant finding from Crook et al. (2009) included the identification of rod input onto small bistratified cells, which was also identified in a study published at the same time from Field and colleagues (2009). In both studies it was found that under low light levels, below the threshold for cone-mediated responses, non-chromatically selective, sustained ON responses could be recorded from small bistratified ganglion cells. These achromatic responses were slower in comparison to cone mediated responses under photopic light conditions - a delay which may be due to the additional steps involved in the rod pathway. Under the application of $_{L}$-AP-4, achromatic responses were abolished, consistent with the rod response arising from the rod pathway (Crook et al., 2009; Field et al., 2009). Anatomical findings from (Field et al., 2009) suggest the presence of gap junctions between AII amacrine cells and blue cone bipolar cells. Given the presence of such gap junctions, the proposed retinal circuitry giving rise to rod mediated responses in small bistratified ganglion cells is complete. As shown in Figure 1.6B, the rod input is thus thought to arrive from rod bipolar cells via AII amacrine cells electrically coupled to blue cone bipolar cells, which in turn contact the inner dendrites of small bistratified ganglion cells.

Large sparse ganglion cells

Large sparse ganglion cells have been recognised in recent studies as a distinct ganglion cell type with sparsely branching dendrites ramifying near the border of the inner plexiform layer and ganglion cell layer (Peterson and Dacey, 1999; Szmajda et al., 2008; Yamada et al., 2005). The following section provides a summary of previous studies describing ganglion cells that most likely correspond to the large sparse type. In some of the studies described below, it is not clear whether authors have made the distinction between giant sparse / melanopsin containing cells and the large sparse type. It is now known that dendrites of some giant sparse / melanopsin containing wide-field ganglion cells stratify within the sublamina of the inner plexiform layer closest to the ganglion cell layer (Dacey et al., 2005; Jusuf et al., 2007). These ganglion cells also possess sparsely branching dendrites that are relatively thin and free of spines. Both of these characteristics are also common to large sparse ganglion cells. The main distinguishing feature between giant sparse / melanopsin containing ganglion cells and the large sparse

type is that the dendritic fields of the former type are almost 1.4 times larger than the latter (Peterson and Dacey, 1999). It is therefore important to note that in some of the studies mentioned below cell types listed as being possible homologues of large sparse cells may, in some cases, be examples of giant sparse / melanopsin containing ganglion cells.

Polyak (1941) described a group of ganglion cells, which may have included examples of large sparse ganglion cells. The "small diffuse" group had small somas and sparsely branching dendrites. Another consistent feature of this group were their relatively thin and smooth dendrites with almost no instances of spines. Ganglion cells belonging to the small diffuse group may have included a distinct type with dendrites which stratified in the portion of the inner plexiform layer lying closest to the ganglion cell layer. The same type of ganglion cell was most likely included in the group of unistratified ganglion cells from Boycott et al. (1969).

In two subsequent studies ganglion cells with similarly sparsely branching, thin dendrites were labelled from tracer injections into the superior colliculus ("C cells" Leventhal et al., 1981); "Pγ cells"(Perry and Cowey, 1984) and pretectum (Leventhal et al., 1981). Perry and Cowey (1984) note that dendrites of C group cells lay at distinct planes within the inner plexiform layer, and as such these groups most likely consisted of many morphological types. As mentioned in the preceding sections, ganglion cells from these two studies were often incompletely labelled, and as a result the authors were unable to report accurate measures of dendritic field sizes.

Yamada et al. (1996) report the presence of Perry and Cowey's (1984) Pγ-like cells in capuchin, owl and marmoset monkey retinas. Unlike the current large sparse type, however, the authors note the presence of both ON and OFF type Pγ-like cells (Yamada et al., 1996).

The first clear distinction between large sparse ganglion cells and the giant sparse / melanopsin group is made by Peterson and Dacey (1999). The large sparse cells differed from what they call the "giant very sparse" group in overall dendritic field sizes and number of branch points (Peterson and Dacey, 1999). The authors also note that the giant very sparse group consisted of ON and OFF types whereas all large sparse cells were of the ON variety.

In three subsequent publications it was shown that large sparse ganglion cells are labelled from injections of retrograde tracers into the LGN (Dacey and Packer, 2003; Dacey et al., 2003; Dacey et al., 2002). Preliminary recordings from such dorsal lateral geniculate projecting large sparse cells showed blue-OFF/yellow-ON responses (Dacey and Packer, 2003; Dacey et al., 2002). The fact that dendrites of large sparse ganglion cells stratify at the same depth of the inner plexiform layer as blue cone bipolar cells fits well with the newly uncovered physiological response. The only inconsistency being, the difference in polarity between blue cone bipolar cell and the blue component of the large sparse ganglion cell response. It seems most certain that the blue cone bipolar cell does provide inputs onto large sparse ganglion cells, as the application of $_{L}$-AP-4 abolished both chromatic components of the large sparse cell's response. The exact mechanism by which the blue-OFF component arises in large sparse cells however still remains unknown.

While the morphological characteristics of large sparse cells are relatively well established, very little is currently known about the connectivity of large sparse cells underlying its proposed chromatic response. The study described in Chapter 3 (page 75) aims to further build on our understanding of large sparse cells by investigating the pattern of synaptic inputs onto large sparse cells and whether this forms a basis for the physiological properties of this cell type, and also looks at the possibility of DB6 bipolar cells as being a presynaptic partner to large sparse cells.

Broad thorny ganglion cells

A possible correlate to the wide-field ganglion cell type now named broad thorny (Dacey, 2004; Dacey et al., 2003; Yamada et al., 2005) was probably included in Polyak's (1941) "garland" group, which included ganglion cells possessing dendrites "thickly covered with countless minute contorted branchlets and thorny or hook-shaped appendages". The dendritic expanse was thought to cover the outer two-thirds of the inner plexiform layer. As in the large sparse ganglion cells, the broad thorny type was most likely included in the unistratified group from Boycott et al. (1969). In their study of retinal projections to the superior colliculus and pretectum, Leventhal et al. (1981) briefly note the presence of

ganglion cells resembling those of Polyak's (1941) garland variety (Leventhal et al., 1981).

Rodieck and Watanabe (1993) present drawings of cells resembling the broad thorny type in amongst their "group T" cells labelled from tracer injections into the superior colliculus (Rodieck and Watanabe, 1993). One slight discrepancy being that T group cells usually formed bistratified dendritic trees, instead of the broad stratification pattern seen in broad thorny cells.

In their study of ganglion cells in marmoset retina, Ghosh et al. (1996) describe a type of cell, which they call the "hedge" type. The authors state that cells of this type formed a large and densely branching dendritic tree, which was broadly stratified within the inner plexiform layer (Ghosh et al., 1996). Similar ganglion cells were subsequently described in human retina by Peterson and Dacey (2000), which these authors name as the "thorny diffuse" type (Peterson and Dacey, 2000).

The first instance of the name "broad thorny" arises in a study by Dacey et al. (2003) where it was established that these cells are labelled from injections of retrograde tracer into the LGN (Dacey et al., 2003). In his review, Dacey (2004) states that initial recordings from broad thorny ganglion cells revealed a transient ON-OFF response in these cells consistent with their pattern of dendritic stratification encompassing both ON and OFF portions of the inner plexiform layer (Dacey, 2004).

As described, very little is known about the broad thorny ganglion cells apart from its general morphological characteristics. The study described in Chapter 3 (page 75) compares the pattern of synaptic inputs onto broad thorny and large sparse ganglion cells to elucidate any differences that may arise from their contrasting pattern of dendritic branching and stratification.

1.7 *The fovea*

The fovea is a specialised region of the retina involved in the transmission of high spatial visual information. The improved spatial sampling of the visual world is achieved through the increased density cone photoreceptors at the fovea that are in one-to-one connection with midget bipolar and midget ganglion cells. The sections to follow will outline morphological features of the fovea that assist in its primary function and, where

known, the developmental processes thought to be involved in such structural specialisations. The more detailed anatomical circuitry of the fovea will be discussed in the introduction to the study presented in chapter 4 (page 107).

Amongst mammals, the presence of a fovea is unique to the retinae of most diurnal primates (for a review, see Slonaker, 1897; Woollard, 1927), including the marmoset and macaque monkeys. Depending on the primate species, the fovea is located between 2 - 4 mm temporal to the optic disc (Andrade da Costa and Hokoç, 2000; Curcio et al., 1990; Packer et al., 1989; Polyak, 1941; Slonaker, 1897; Troilo et al., 1993) and is primarily characterised by a local increase in photoreceptor density, and the presence of a foveal pit, formed as a result of the lateral displacement of cells and cellular components lying vitread to the inner segments of the photoreceptors (Ahnelt and Pflug, 1986; Perry and Cowey, 1988; Polyak, 1941; Schein, 1988; Sjöstrand et al., 1999b; Yamada, 1969).

The center of the fovea, or the foveola, corresponds with the region of highest cone photoreceptor density (Figure 1.8A). In topographical studies of photoreceptor distribution over the last 30 years, average peak cone densities have been reported in a number of primate species including human (115,000 - 196,248 cones / mm^2;(Curcio et al., 1990; Hirsch and Curcio, 1989; Jonas et al., 1992; Sjöstrand et al., 1994; Yuodelis and Hendrickson, 1986), macaque (140,000 - 250,000 cones / mm^2;(Borwein et al., 1980; Krebs and Krebs, 1989; Packer et al., 1989; Perry and Cowey, 1985; Schein, 1988; Wässle et al., 1989; 1990; Wikler et al., 1990), marmoset (132,813 - 211,724 cones / mm^2;(Finlay et al., 2008; Franco et al., 2000; Troilo et al., 1993; Wilder et al., 1996) and other diurnal species (Andrade da Costa and Hokoç, 2000; Finlay et al., 2008; Franco et al., 2000). The large variability between peak cone density measures from studies of the same species is considered to be a reflection of inter-individual differences (Curcio et al., 1990; Jonas et al., 1992; Packer et al., 1989; Wikler et al., 1990), methodological limitations or differences in the measuring procedures (Curcio et al., 1990; Packer et al., 1989; Perry and Cowey, 1985; 1988; Yuodelis and Hendrickson, 1986). Differences in measures of peak cone density between studies of different species may be due to differences in eye size between species (Franco et al., 2000; Rolls and Cowey, 1970). Nonetheless in all studies, cone density is highest at the foveola and decreases dramatically outside of this region.

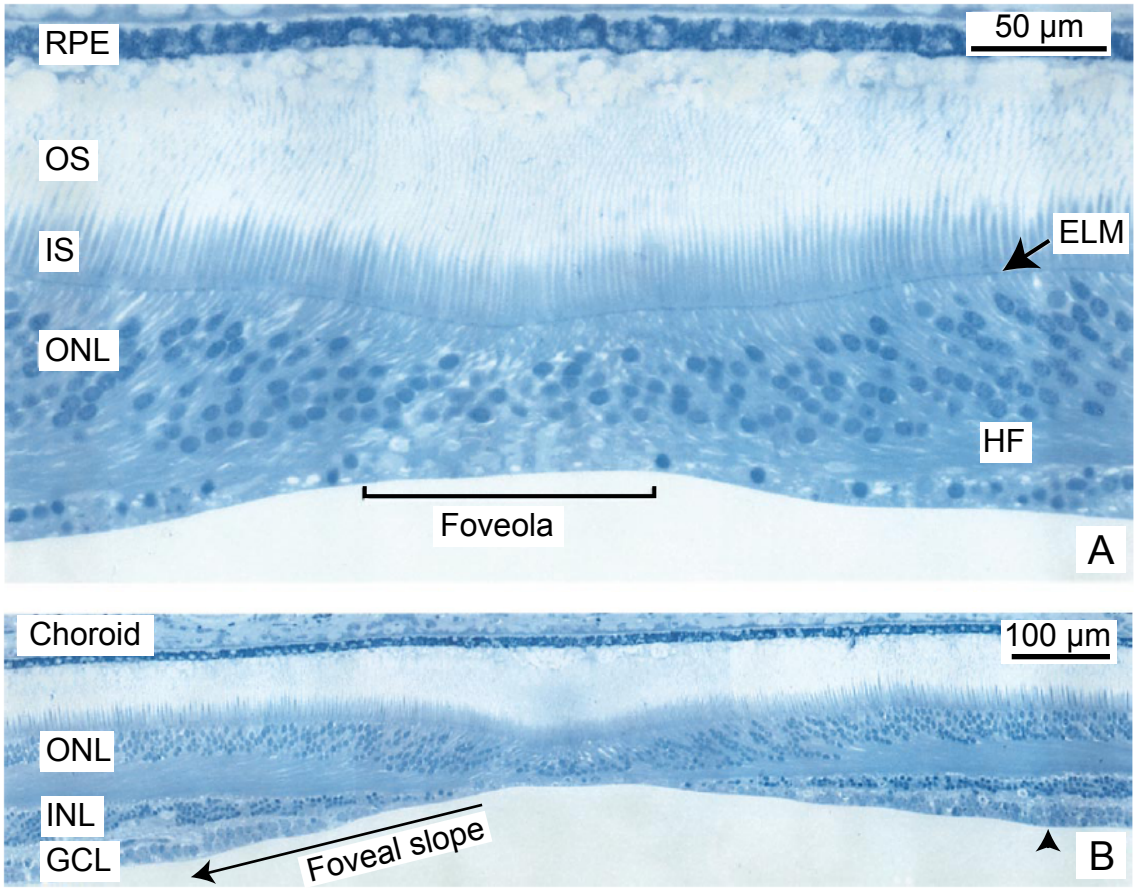


Figure 1.8 Radial sections through the fovea of human retina from Provis et al. (1998) **A**: The bracket indicates the extent of the foveola, where cone outer segment density is at its highest. The lateral shift of neural components lying vitread to the external limiting membrane can be appreciated. **B**: Micrograph showing the foveal slopes extending out from either side of the foveola. It can be seen that the inner nuclear and ganglion cell layers gradually increase in the thickness as you move away from the foveola. The arrowhead indicates the temporal boarder of the fovea, where the ganglion cell layer reaches it maximum thickness. Outer nuclear layer (ONL); inner nuclear layer (INL); ganglion cell layer (GCL); retinal pigment epithelium (RPE); cone outer segments (OS); cone inner segments (IS); external limiting membrane (ELM); Henle fibers (HF). Modified from Provis et al. (1998).

The developmental process leading to the accumulation of cones at the fovea is thought to arise from the centripetal movement of cones toward the center of the fovea, during the foetal stage (Hendrickson and Kupfer, 1976);(for reviews see, Provis et al., 1998; Yuodelis and Hendrickson, 1986). Anatomical measurements of cones at the foveola show that they are often longer and thinner than cones located outside of the foveola (Andrade da Costa and Hokoç, 2000; Borwein et al., 1980; Curcio et al., 1990; Dowling, 1965; Packer et al., 1989; Polyak, 1941; Yamada, 1969). During the development of the foveola, the centripetal migration of cones is most likely combined with the morphological thinning to allow for the maximal packing of cones within the region.

Reported sizes of the foveola region, corresponding to the center of the fovea (see Figure 1.8A) where cone density is highest, ranges from 300 - 450 μm in diameter depending on the species (Polyak, 1941; Stone and Johnston, 1981). The rod free area of the fovea usually extends slightly beyond the foveola, with diameters ranging from 350 - 750 μm in human retina (Curcio et al., 1990; Polyak, 1941; Yamada, 1969; Yuodelis and Hendrickson, 1986) and 40 - 200 μm in macaque retina (Hendrickson and Kupfer, 1976; Packer et al., 1989; Polyak, 1941; Wikler et al., 1990). The exact developmental process involved in the selective exclusion of rods from the foveola is not known (for a review see Provis et al., 1998).

Another prominent anatomical feature of the fovea is the 'foveal pit' (Polyak, 1941), the slopes of which extend from the outer edges of the foveola to the border of the fovea, where the ganglion cell layer is at its thickest (see Figure 1.8B). The total extent of the fovea, including the foveola region, ranges from 1000 - 1500 μm in diameter (Polyak, 1941). The foveal slope is formed as the result of the eccentric displacement of retinal components vitread to cone inner segments, during the early stages of retinal development (Hendrickson and Kupfer, 1976);(for reviews see, Provis et al., 1998; Yuodelis and Hendrickson, 1986). This occurs such that in the mature retina cone pedicles are absent from the first 100 - 350 μm from the center of the fovea (100 - 350 μm for human,(Ahnelt and Pflug, 1986; Missotten, 1974; Yuodelis and Hendrickson, 1986); 150 - 200 μm for macaque,(Perry and Cowey, 1988; Schein, 1988; Yamada, 1969); 130 μm for marmoset,(Wilder et al., 1996), the outer nuclear layer however

remains as a continuous layer. The elongation of Henle fibers connecting cone somas to their pedicles permits for the lateral shift within cones. Henle fibers measuring up to 350 - 600 μm have been reported in human (Missotten, 1974; Polyak, 1941; Sjöstrand et al., 1999b; Yuodelis and Hendrickson, 1986) and 300 - 400 μm macaque retina (Perry and Cowey, 1988; Polyak, 1941; Schein, 1988; Wässle et al., 1989; 1990) which result in lateral shifts between cone inner segments and their pedicles of a maximum of 300 - 400 μm in macaque (Martin and Grünert, 1992; Perry and Cowey, 1988; Schein, 1988).

The radial displacement between cone inner segments and their pedicles are thought to account for the majority of the eccentric displacement of neurons at the fovea (Perry and Cowey, 1988; Schein, 1988), however slight shifts are also observed within inner retinal neurons. The elongations of Henle fibers away from the center of the fovea, in conjunction with the lateral shifts within foveal bipolar cells mean bipolar cells are absent from the central 100 μm of the retina (Martin and Grünert, 1992). Closest to the fovea, the maximum radial displacement of bipolar axon terminals from their dendrites is 66 μm (Perry and Cowey, 1988). Ganglion cells lying closest to the center of the fovea have been found along the foveal slope within eccentricities of 60 - 300 μm (Curcio and Allen, 1990; Leventhal et al., 1993; Perry and Cowey, 1984; 1985; 1988; Schein, 1988; Sjöstrand et al., 1994; Stone and Johnston, 1981; Wässle et al., 1989; 1990). There is some lateral displacement of ganglion cell bodies with relation to their dendritic trees (Schein, 1988). Due to the overall shift of postreceptoral elements, peak ganglion cell density is usually reached between 500 and 1000 μm from the foveal center of approximately 26,000 - 57,500 cells / mm^2 for human (Conradi and Sjöstrand, 1993; Curcio and Allen, 1990; Missotten, 1974; Sjöstrand et al., 1994; Sjöstrand et al., 1999a), 10,000 - 65,000 cells / mm^2 for macaque (Ahmad et al., 2003; Martin and Grünert, 1992; Perry and Cowey, 1984; Rolls and Cowey, 1970) and 55,000 cells / mm^2 for marmoset retina (Wilder et al., 1996).

Many studies have described functions for determining the overall shift between cone outer segments and the ganglion cells to which they connect (Schein, 1988; Sjöstrand et al., 1994; Sjöstrand et al., 1999b; Wilder et al., 1996). Such studies have shown that total radial displacement can reach maximal values of approximately 300 - 350 μm for cones located 300 - 400 μm from the foveal center in macaque and human

retina (Curcio and Allen, 1990; Perry and Cowey, 1988; Schein, 1988). Careful consideration of lateral shifts is crucial to studies of retinal connectivity such as that presented in chapter 4 (page 107).

Another prominent anatomical feature of the fovea is the absence of inner retinal blood vessels (Stone and Johnston, 1981). These blood vessels have been shown to curl around the fovea, following a similar course to retinal axons travelling between the optic disc and regions lying temporal to the fovea (Polyak, 1941). It is thought that the avascular nature of the foveal region may improve acuity and lessen light scatter introduced by presence of blood vessels in other regions of the retina (Weale, 1966). As this thesis mainly concerns the neural elements of the retina and the pattern of retinal vasculature at the fovea will not be discussed any further.

As outlined, the fovea is characterised by gross structural specialisations that contribute to improved spatial acuity at the fovea. Comparatively little is known about the specialisations that occur at the neuronal level within the fovea. The significance of the one to one connectivity between cones and inner retinal neurons of the midget pathway has been well studied (Boycott et al., 1969; Calkins et al., 1994; Kolb and Dekorver, 1991; Polyak, 1941). The contributions, if any, of non-midget pathways to vision at the fovea however remain relatively unexplored. The study described in Chapter 4 (page 107) considers the anatomical evidence for the involvement of wide-field ganglion cells to foveal vision.

1.8 *Aims of this thesis*

The three projects described in this thesis aim to investigate the retinal connectivity of small bistratified ganglion cells through the analysis of synaptic inputs to inner and outer dendritic tiers; to understand the basis of synaptic distribution and the source of bipolar inputs for two ganglion cell types with contrasting dendritic morphology; and to uncover contributions of wide-field ganglion cell types to the retinal circuitry sampling information from foveal cones. The focus of all three chapters is in building on what little is currently known on non-midget, non-parasol pathways of the retina.

With the exception of some of the results presented in Chapter 4 (page 107), the main animal model used in the studies described here, is a New World monkey with an

X-linked polymorphism for genes encoding medium (M) and long (L) wavelength sensitive cone opsins. As a result, all male and homozygous female marmoset monkeys present as dichromats, while heterozygous females are trichromatic. Experiments described in this thesis combine results from both dichromatic and trichromatic marmosets as no major differences have been reported in the types and properties of ganglion cells between the two phenotypes so far (Ghosh et al., 1996; Jusuf et al., 2006b; Szmajda et al., 2005).

The three experimental chapters address the following questions:

- **Chapter 2**: Does the density of synaptic inputs differ between inner and outer tiers of small bistratified ganglion cells and what can this tell us about their retinal circuitry?
- **Chapter 3**: How does the density and distribution of synaptic inputs differ between two wide-field ganglion cell types with contrasting morphological characteristics?
- **Chapter 4**: Are the neural components involved in non-midget, non-parasol retinal pathways present in foveal retina, thus making them capable of contributing to foveal vision?

Chapter 2 Synaptic inputs onto small bistratified (blue-ON/yellow-OFF) ganglion cells in marmoset retina

2.1 *Introduction*

The experiments described in this chapter explore the anatomical basis of convergence of ON- and OFF-type signals to small bistratified ganglion cells in the retina of marmoset monkeys, with a further aim of understanding the retinal circuitry behind the colour responses of these cells.

In the blue/yellow channel of color vision, signals from short wavelength sensitive (S) cones are compared to those of medium (M) and long (L) wavelength sensitive cones. As outlined in section 1.6 (page 19), the small bistratified ganglion cell type exhibits blue-ON/yellow-OFF responses (Dacey and Lee, 1994), making it an important component in the processing of colour in primate retina. Small bistratified cells are characterised by an extensive (inner) dendritic tier, which stratifies in the ON sublamina, and a sparse (outer) dendritic tier, which stratifies in the OFF sublamina of the inner plexiform layer (Dacey, 1993a; Ghosh et al., 1997; Rodieck, 1991; Rodieck and Watanabe, 1993; Silveira et al., 1999).

It is generally agreed that the inner dendritic tier receives blue-ON input from S cones *via* blue cone bipolar cells (Calkins, 2001; Calkins et al., 1998; Dacey, 1999; Dacey and Lee, 1994; Ghosh et al., 1997) but the origin of the yellow-OFF input is still a matter of debate. One possibility is that blue/yellow opponency originates in the S-cones *via* inhibitory feedback from H2 horizontal cells (see Figure 1.7BDacey, 2000; Field et al., 2007; Herr et al., 2003; Packer et al., 2007; Schein et al., 2004). Alternatively, it has been suggested that diffuse bipolar cells, which receive mixed input from medium (M) and long (L) wavelength sensitive cones, provide the yellow-OFF input to the outer dendritic tier of small bistratified cells (see Figure 1.7ACalkins, 2001; Calkins et al., 1998; Crook et al., 2009; Dacey and Lee, 1994).

To date, the micro-circuitry of small bistratified cells has only been investigated in a small number of cells in two electron microscopic studies that report different results. Calkins et al. (1998) found, for two completely reconstructed small bistratified ganglion cells in macaque fovea that the outer dendritic tier receives input from diffuse bipolar cells. For one of the two cells, both bipolar and amacrine inputs were quantified and found that bipolar inputs (70 %) outnumber amacrine input (30 %). They showed that the density of the bipolar input to the outer tier is consistent with the functional weight of yellow-OFF responses measured in blue-ON/yellow-OFF ganglion cells in a previous study of macaque retina (Zrenner, 1983). In contrast, Ghosh and Grünert (1999) found very little bipolar input to the outer tiers of two (partially reconstructed) small bistratified cells in peripheral marmoset retina, instead the large majority (over 85 %) of the input was derived from amacrine cells. Currently, the applicability of the model advanced by Calkins et al. (1998) across all retinal eccentricities, and across different primate species, remains largely unexplored.

The present study aimed to establish whether there is a consistent pattern of synaptic input to small bistratified cells across the retina, and whether this helps to explain the possible circuitry behind the yellow-OFF component of the response. Retrograde labelling, immunohistochemistry and high-resolution light microscopy were used to quantitatively analyse synaptic input, and its variation with eccentricity, in a sample of small bistratified cells from marmoset retina.

2.2 *Materials and Methods*

Animals

Experiments were carried out on five adult marrmosets (*Callithrix jacchus*), obtained from the Australian National Health and Medical Research Council (NHMRC) combined breeding facility (see Table 2.1). All procedures were carried out according to the provisions of the NHMRC code of practice for the care and use of animals and were approved by the University of Melbourne ethics committee.

Table 2.1: Experimental parameters - Animals and anaesthesia

Animal number	Sex	Weight (g)	Anaesthesia for surgery
My113	Male	436	Ketamine / Zylazine
My115	Female	496	Ketamine / Zylazine
My124	Male	460	Ketamine / Zylazine
My127	Female	356	Ketamine / Zylazine
My131	Female	386	Alfaxalone

Tracer injections and photofilling

Dye injections and photofilling were carried out as described in detail previously (Dacey et al., 2003; Jusuf et al., 2006a; Jusuf et al., 2006b; Percival et al., 2009; Szmajda et al., 2005; 2008). In brief, animals were anaesthetised with isoflurane (Forthane, Abbott, Sydney, Australia; ICI, 1-2%), intramuscular ketamine (30 mg/kg) and xylazine hydrochloride (Rompun, Bayer Animal Health Australia, Pymble, NSW, Australia; 2-4 μg/kg), in the case of one animal ketamine was replaced with alfaxalone (Alfaxan, Jurox, Rutherford, NSW, Australia). Anesthesia was maintained using sufentanil citrate (Sufenta-Forte, Janssen-Cilag, Beerse, Belgium; 4-8 μg/kg) in dextrose ringer solution (Baxter, Sydney, NSW, Australia).

Animals were prepared for electrophysiological recordings from the dorsal lateral geniculate nucleus (LGN) using standard methods (Blessing et al., 2004). The LGN was located using a multi-unit recording electrode. Once the koniocellular layer was located, the recording electrode was withdrawn and replaced with a micropipette (20-70 μm tip (see Table 2.2); drawn from a glass capillary tube with an inner diameter of 0.86 mm and an outer diameter of 1.5 mm, SDR Clinical Technology, Sydney, Australia).

Table 2.2: Experimental parameters - Tracer injections and photofiling

Animal number	Injection tip size (μm)	Microruby concentration (%)	Duration of injection (min)	Transport time for injection (hours)
My113	30	5	45	61.6
My115	20 - 25	5	50	88.0
My124	70	5	120	66.0
My127	50	5	125	58.3
My131	50	5	120	88.5

As outlined in Table 2.2, the micropipette was filled with 5 % dextran, tetramethylrhodamine and biotin ("microruby", D7162; Invitrogen, Mount Waverley, Vic, Australia) in 0.9% NaCl. Injections were made by iontophoresis using a positive current (7 μA x 6s, positive pulse, period 12s) for durations listed in Table 2.2. Retrograde transport of the tracer was allowed to take place over 58 - 88 hours (see Table 2.2) following injections, during which single cell recordings were made from the contralateral LGN for unrelated experiments.

At the end of the experiments, animals were overdosed with sodium pentobarbitone (80 - 150 mg/kg, i.v; Nembutal, Rhone Merieux Pro Vet, Pinkenba, Queensland, Australia). The eyes were removed and the posterior eyecup placed into carboxygenated (95 % O_2 / 5 % CO_2) Ames' tissue culture medium (Sigma, St. Louis, MO). The retina was dissected and mounted onto Millipore filter paper (either AABG02500, 0.8 μm pore size, or SSWP02500, 3.0 μm pore size, Millipore, Bedford, MA) and placed into a superfusion chamber (Warner Instruments, Hamden, CT) on a fixed stage microscope (Axioskop 2, Zeiss). The chamber was superfused with carboxygenated Ames medium at a rate close to 2 ml/minute, and the chamber temperature maintained close to 37.5ºC. Cells were photofilled by illumination with a dual-band Lucifer Yellow/Rhodamine filter (Chroma filter set 51016). Retinal pieces were viewed through either a x10 and/or x40 water immersion objective. Subsequent to photofilling, retinal pieces were removed from the superfusion chamber and fixed in 4% paraformaldehyde in 0.1M phosphate buffer (PB, pH7.4) for 30 or 60 minutes (see Table 2.3) at 4°C. Pieces were then rinsed with 0.1M PB before processing for immunohistochemistry.

Table 2.3: Experimental parameters - Immunohistochemical processing of retinal wholemounts

Retinal piece	Concentration / duration of immersion fix	Primary antibodies used	Duration of primary antibody incubation (days)	Secondary antibodies used
My113R1	4 % PFA / 60 min	CtBP2 (ms)	14	g ∝ ms Alexa 488
My115R1	4 % PFA / 30 min	CtBP2 (ms)	7	g ∝ ms Alexa 488
My115L1	4 % PFA / 60 min	CtBP2 (ms)	7	g ∝ ms Alexa 488
My124R1	4 % PFA / 30 min	Gephyrin (ms) / GluR4 (rb)	9	g ∝ ms Cy5 / g ∝ rb Alexa 488
My127R1	4 % PFA / 30 min	Gephyrin (ms) / GluR4 (rb)	9	g ∝ ms Alexa 488 / g ∝ rb Cy5
My131R1	4 % PFA / 30 min	Gephyrin (ms) / GluR4 (rb)	4	g ∝ ms Alexa 488 / g ∝ rb Cy5

Paraformaldehyde (PFA), mouse (ms), rabbit (rb), goat (g)

Antibodies

Primary antibodies used on each retinal piece are listed in Table 2.3. A mouse monoclonal antibody against the C-terminal binding protein 2 (CtBP2) domain of the ribbon protein RIBEYE (BD Biosciences, Heidelberg, Germany, no.612044) was used at a dilution of 1:10,000. This antibody is raised against the C-terminal amino acids 361 – 445 of mouse CtBP2 (BD Biosciences, technical information). It has been characterised by Western blot analysis of mouse retina which recognises two bands of 110-kDa and 120-kDa representing the RIBEYE B-domain, and a single band of 50-kDa representing CtBP1 (tom Dieck et al., 2005). This antibody has been shown to label synaptic ribbons in mammalian retinas including primate (Hendrickson et al., 2009; Jusuf et al., 2006a; Schmitz et al., 2000; tom Dieck et al., 2005).

A mouse monoclonal antibody against the 93kD protein gephyrin was used at a dilution of 1:200 (mAb7a; provided by H. Betz, Max Planck Institute for Brain Research, Frankfurt, Germany). This antibody is directed against a 93-kDa polypeptide derived from rat spinal cord and has been characterised by Western blots of rat spinal cord, where it stains a 93 kDa band (Pfeiffer et al., 1984). Antibody binding is specific to the 93-kDa polypeptide found within postsynaptic glycine receptor complexes (Schmitt et al., 1987).

Gephyrin has been shown to be involved in the clustering of receptor channels at the majority of inhibitory postsynaptic sites (Kneussel and Betz, 2000). In gephyrin null mice, mAb7a labelling was abolished (Fischer et al., 2000). Immunoreactivity to this antibody has been localised to postsynaptic sites of amacrine and ganglion cell processes in retinas of mammals including primates (Grünert and Wässle, 1993; Pourcho and Owczarzak, 1991).

A polyclonal rabbit antiserum against the C-terminus of rat glutamate receptor 4 (GluR4) subunit (RQSSGLAVIASDLP; AB1508, Chemicon, Temecula, CA) conjugated to bovine serum albumin (BSA) with glutaraldehyde was used at a dilution of 1:400. This antiserum has been characterised by Western blots of rat brain by the manufacturer and shows a single band co-migrating with GluR4 expressed in transfected cells (Chemicon, technical information). Furthermore, in a recent study a band between 105 - 108kD was labelled in Western blots of solubilised homogenates of adult vestibular nuclear complex from rats where it recognises a band between 105 and 108-kDa (Tse et al., 2008). Immuoreactivity to this antiserum has been found at postsynaptic locations in mammalian retinas including primate (Grünert et al., 2002; Haverkamp et al., 2001; Haverkamp et al., 2000).

Immunohistochemistry

Retinal pieces containing retrogradely labelled ganglion cells were separated from the filter paper, immersed into 30% sucrose in PB overnight and subsequently freeze-cracked with liquid nitrogen. Pieces were then rinsed in 0.1M PB for 10 minutes and subsequently preincubated in phosphate buffered saline (PBS, pH 7.4) containing 5 % BSA and 0.5 % Triton X-100 for 60 minutes. Four preparations used for the analysis of synaptic input were incubated in either one (CtBP2) or a combination of two primary antibodies (GluR4 and gephyrin) for 4 to 14 days (see Table 2.3). Primary antibodies were diluted in PBS containing 1 % BSA, 0.5 % Triton X-100, and 0.05 % sodium azide. Pieces were then rinsed in PBS and incubated in secondary antibodies overnight. Secondary antibodies used for each retinal piece are shown in Table 2.3. Secondary antibodies used were goat anti-mouse immunoglobulin G (IgG) coupled to Alexa 488 (Invitrogen), at a dilution of 1:500, alone or in combination with goat anti-rabbit Cy5 (Jackson ImmunoResearch,

Westgrove, PA) at a dilution of 1:100. For a single retinal preparation secondary antibodies used were goat anti-rabbit IgG coupled to Alexa 488 (Invitrogen) at a dilution of 1:500 together with goat anti-mouse Cy5 (Jackson ImmunoResearch, Westgrove, PA) at a dilution of 1:100. Secondary antibodies were diluted in PBS containing 1 % BSA and 0.5 % Triton X-100. Following immunostaining, pieces were mounted and coverslipped in Mowiol (Hoechst, Sydney, Australia) containing 10 % 1,4-diazobicyclo-[2.2.2]-octane (Harlow and Lane, 1988).

2.3 *Analysis*

Image acquisition

High-resolution micrographs of labelled ganglion cells together with the synaptic markers were taken under oil immersion using a digital camera (Axiocam; Zeiss) mounted onto a Zeiss Axioplan 2 microscope with a x40 or x63 objective. Stacks of approximately 30 to 80 digital images at 0.2 μm, 0.275 μm or 0.3 μm spacing were acquired under the appropriate filter sets: Cy3 (# 43, Zeiss), FITC (# 10, Zeiss), Cy5 (#26, Zeiss) or filter set 10, Ex BP450-490 wedge free (Zeiss); filter set Texas Red, 4040B, zero pixel shift, Ex562/40 BS 600 Em 624/40 (Semrock, Coherent Scientific, Hilton, SA, Australia); filter set CY5 4040A, zero pixel shift, Ex628/40 BS 669 Em 692/40 (Semrock). Images of preparations were also taken under bright field illumination using differential interference contrast (DIC) optics. The brightness and contrast of the images were adjusted in Axiovision software (Zeiss) or Adobe Photoshop (7 or CS4).

Ganglion cell eccentricity and quantification of dendritic parameters

As in previous studies (Troilo et al., 1993; Wilder et al., 1996) the term “foveal retina” is used here to mean the part of the retina which deals with the first degree (radius) of visual angle from the fovea. The term “central retina” refers to the first 12 degrees of visual angle (up to 1.5 mm in marmoset), mid-peripheral retina refers to eccentricities of 12 to 31 degrees of visual angle (> 1.5 mm to 4 mm in marmoset), and “far peripheral retina” refers to eccentricities above 31 degrees of visual angle (> 4 mm in marmoset).

Only ganglion cells labelled in their entirety, as judged by consistently bright labelling at distal dendritic tips were included in the analysis. By excluding cells where labelling faded in the peripheral parts of the dendritic field, it was likely that all analyses included the entire dendritic tree.

In order to determine retinal eccentricities of labelled ganglion cells, micrographs of entire retinal pieces were taken using a Zeiss Axiocam MRm digital camera mounted onto a Zeiss SteREO Lumar stereomicroscope at a magnification of x12 or a Zeiss Axiocam HRc digital camera mounted on a Zeiss Axioplan 2 microscope using the x2.5 objective. Micrographs were also taken of the patch of labelled ganglion cell bodies at higher resolution, i.e. between x40 and x80 on the Stereo Lumar or using the x10 objective at the Axioplan 2. The locations of the fovea, optic disc and labelled cell bodies were mapped onto an outline of the retinal piece, which was drawn using a drawing tablet. From these maps, the retinal quadrants, eccentricities and polar angles of individual ganglion cells were determined (Table 2.4).

Table 2.4: Retinal locations of small bistratified cells

Cell ID	Eccentricity (mm)	Retinal quadrant*	Polar angle of the cell (deg)**
My131R1-26	0.68	Nasal	216.5
My131R1-02	0.68	Superior	123.5
My131R1-25	0.75	Nasal	222.0
My131R1-08	1.18	Nasal	143.5
My124R1-07	1.50	Nasal	201.0
My124R1-06	1.52	Nasal	202.0
My113R1-04	1.60	Inferior	270.0
My113R1-F02	1.66	Inferior	265.0
My127R1-02	1.85	Nasal	223.5
My113R1-F01	2.59	Inferior	258.0
My115R1A-02	2.78	Nasal	211.0
My115R1-F02	2.89	Nasal	202.0
My115R1-F05	3.45	Inferior	232.5
My115L1-F02	3.80	Nasal	208.0

*Temporal retina 315 - 45°, superior retina 45 - 135°, nasal retina 135 - 225°, inferior retina 225 - 315°.
**The angle of a line joining the cell to the fovea, relative to a line between the fovea and optic disc.

Small bistratified ganglion cells were distinguished from other labelled ganglion cell types according to their dendritic field size, stratification within the inner plexiform layer, branch density and general morphology.

The steps involved in the quantification of these dendritic parameters have been described previously (Percival et al., 2009; Szmajda et al., 2008). In brief, image stacks were imported into custom software written in MatLAB (image processing toolbox, Mathworks, Natick, MA) where the area of a convex polygon, created by connecting the outer most dendritic tips of dendrites making up the inner tier of small bistratified cells was determined. An average of the major and minor axis of an ellipse of the same area and orientation as the polygon was used as an estimate for the dendritic field diameter of the inner tier.

Because of its small size, measurements of the outer tier were made from a collection of convex polygons outlining connected branches of the outer tier. For each cell, the areas of these polygons were summed and expressed as the diameter of a circle with the same area. In some instances polygons were constructed with concave vertices to avoid overlap between two adjacent polygons.

The depth and breadth of dendritic stratification was also quantified using the same custom software. A sampling circle roughly corresponding to 75 % of the minor axis of the ellipse obtained in the dendritic field diameter measurement was placed onto image stacks. The z-stack position at which each dendrite intercepting the sample circle came into focus was measured. At eight approximately equidistant points along the sampling circle, z-stack positions of the borders of the inner plexiform with the ganglion cell layer and inner nuclear layer, as judged from DIC images, were also determined. The locations of these points were then used to calculate the stratification depth within the inner plexiform layer for each dendritic crossing. An estimate of the stratification breadth was taken as the range of stratification values which included the majority of dendritic crossings, as judged by the user. The average stratification depth was then taken as the middle of this range of stratification values. Dendritic branch density was expressed as the number of dendritic crossings / μm of the sampling circles circumference.

Tracings of the dendritic tree and soma of all small bistratified cells were made onto acetate sheets, from photomicrographs displayed on a liquid crystal display monitor.

Acetate sheets were then scanned on a flatbed scanner and either redrawn using a drawing tablet or automatically (auto-trace function) reproduced as vector graphics using Adobe Illustrator graphics program.

Synaptic input

The density of excitatory and/or inhibitory input was quantified with relation to dendritic surface area using semi-automated custom software written in MatLAB as described previously (Eriköz et al., 2008; Grünert et al., 2003; Percival et al., 2009). In short, image stacks of ganglion cell dendrites and synaptic markers were divided into smaller regions (approximately 40 µm by 40 µm) and processed using Axiovision deconvolution software. Images were then imported into MatLAB where the (X, Y) position and the (Z) focal plane of each immunoreactive (IR) punctum in the z-stack of images were determined by finding local intensity maxima in the three-dimensional (image voxel) space. Using the image stacks of the dendritic processes, outlines of the dendritic regions in focus at each optical level were defined by the user, from a pixel intensity contour map. A lateral displacement of up to 1 pixel for postsynaptic markers (antibodies against gephyrin and GluR4) and 2 pixels for presynaptic markers (antibody against CtBP2) was allowed between the (X, Y, Z) centre position of IR puncta and the (X, Y, Z) coordinates of dendritic processes outlined. This displacement is equivalent to 0.084 µm (1 pixel) and 0.169 µm (2 pixels) for images taken at x40, and 0.053 µm (1 pixel) and 0.107 µm (2 pixels) for images taken at x63. Estimates of colocalised puncta density were then made automatically by Boolean logic operations on these data. Dendrities belonging to separate tiers were analysed separately, so as to obtain separate density values for the inner and outer tiers. Synaptic densities for each cell were obtained from averages of all sample regions analysed from the cell. The reliability of this procedure was verified for at least two locations in each sampled cell by carefully focusing through the image stack, and confirming that almost all identified colocalisations corresponded to the judgment of a trained human observer. The locations of colocalised IR puncta were plotted onto reconstructions of the ganglion cell dendritic tree described above, in order to determine the overall distribution of presumed synaptic input onto the dendritic trees of ganglion cells.

One cell was analysed manually as the label in the dendrites was too weak to proceed with the semi-automated analysis. The number of colocalised puncta found for this cell was in the same range as determined for the other cells, consistent with our previous finding that results obtained manually are comparable to those obtained with the semi-automated method (Jusuf et al., 2007).

It must be noted that results may exclude small portions of dendrite where processes were either obscured by somas of other labelled ganglion cells, or obscured by the bright labelling from the soma of the cell under analysis. At times, small portions of dendrites could not be outlined from intensity contour maps without overestimation of the dendritic area, and, as such were excluded from the analysis.

To assess the specificity of colocalisation, previous studies have used procedures whereby one image channel is rotated, or flipped around the vertical axis, following which pseudo-random colocalisations are determined (Grünert et al., 2002; Jusuf et al., 2006a; Mills et al., 2001; Zhang et al., 2002). Such procedures are informative where an entire target population of neurons is labelled by immunohistochemistry, but are of less value where an individual member of the target population is labelled. This is because the proportion of IR puncta associated with *unlabelled* members of the target population is, perforce, unknown. Furthermore, if IR puncta are present at high density (as is the case in the present study) the flip procedure yields high numbers of impossible colocalisations (for example, IR puncta in the centre of a ganglion cell dendrite, or in the dark interstices occupied by Müller cell processes). Consistently, in the present study only a small average reduction (~15%) of colocalisation in the flipped *vs.* veridical image conditions were found. This reduction was significant ($p < 0.05$, Wilcoxon rank-sum test) for preparations immunoreacted with CtBP2 or gephyrin antibodies, but non-significant ($p = 0.67$) for preparations immunoreacted with GluR4. The non-significant differences for the GluR4 immunoreactivity can probably be explained by the comparatively low sample size for this antibody (only five cells were analysed, and they were all from foveal or central retina and thus have small dendritic trees). For reasons of the difficulties of interpretation outlined above, a more sophisticated analysis of colocalisation was not attempted (Jusuf et al., 2006a; Mills et al., 2001) but relied on the judgment of

experienced observers, and the consistency between manual and semi-automated approaches to quantify the pattern of colocalisation.

Cone convergence

The number of cones located in the dendritic field of small bistratified cells was estimated in two different ways. In some preparations the superimposed cone pedicles could be distinguished as they were labelled with the ribbon marker CtBP2 or the antibody against GluR4, which in the outer plexiform layer can be used to identify glutamate receptor clusters opposite cone pedicles (Haverkamp et al., 2001). In these preparations, the number of cones within the dendritic field was determined by counting the number of cone pedicles overlying the outline of the dendritic field used earlier in the quantification of the dendritic field size of that cell. Pedicles were counted as being within the outline, if the 'centre of gravity' of the pedicle lay within the outline of the dendritic field.

In cases where cone pedicles could not be counted directly, the number of cones within the inner dendritic field was estimated by multiplying the dendritic field area (mm^2) by the estimated cone density (cone pedicles / mm^2) from published data (Wilder et al., 1996), at the same eccentricity as the labelled small bistratified cell. For cells located within 2 mm of the fovea, the spatial displacement due to Henle fibers was taken into account when estimating local cone density (for details, seeWilder et al., 1996). The number of short wavelength sensitive (S) cones encompassed by the dendritic field was estimated by multiplying the total number of cones in the dendritic field (determined as described above) by the proportion of S cones at the same eccentricity. The S cone proportion was determined from published data on S cone densities and S cone proportions across marmoset retina (Martin and Grünert, 1999).

2.4 *Results*

Identification of small bistratified ganglion cells

These results are based on a total of fourteen retrogradely labelled small bistratified ganglion cells. The dendritic morphology of seven of these cells have been described in a previous study showing their projections to the koniocellular layers of the dorsal lateral

geniculate nucleus (LGN; Szmajda et al., 2008). The central most cell was located at 0.68 mm eccentricity and the most peripheral cell from 3.8 mm eccentricity. This corresponds to an eccentricity range of approximately 5 to 30 degree visual angle, as calculated from the function described by Wilder et al. (1996).

All cells described here are comparable in terms of their general morphology, dendritic field size and stratification levels, to small bistratified cells described in previous studies of marmoset and macaque retinae (Dacey, 1993a; Ghosh and Grünert, 1999; Ghosh et al., 1997; Silveira et al., 1999; Szmajda et al., 2008). Examples of retrogradely labelled small bistratified cells are shown in Figures 2.1 and 2.2. They have fine dendrites sometimes displaying hook-like structures (Figure 1E, F). The exact function of such hooks and spines is currently unknown. The smaller outer dendritic tier stratifies in the OFF sublamina and the more extensive inner tier stratifies in the ON sublamina of the inner plexiform layer. Dendritic field diameters ranged from 49 to 224 μm for the inner dendritic tier. This is below the range reported for large bistratified / G17 cells in macaque and human retina, even when differences in eye size (difference in retinal magnification) are taken in to account (Dacey et al., 2003; Kolb et al., 1992; Peterson and Dacey, 2000; Yamada et al., 2005).

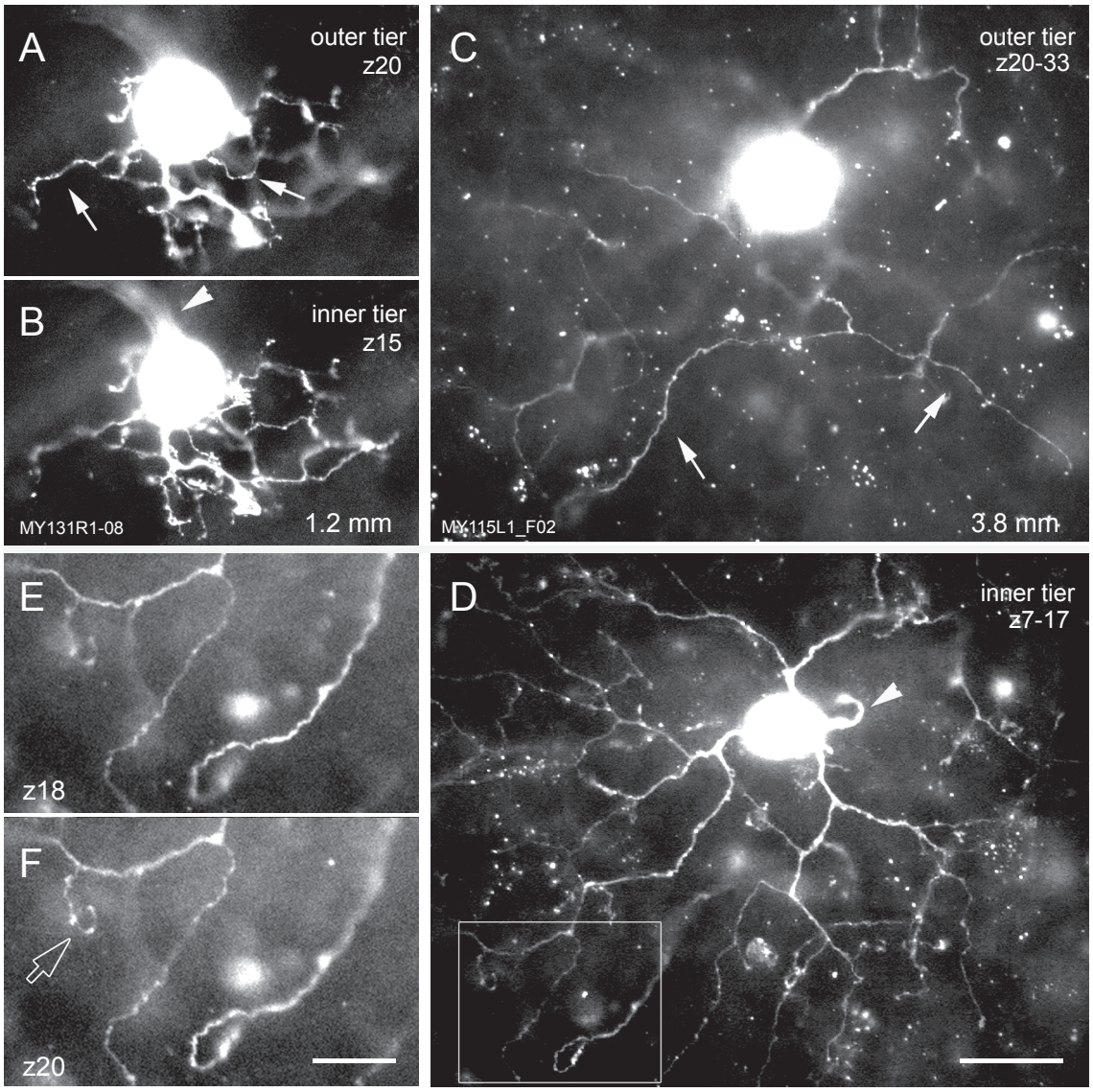


Figure 2.1 Micrographs of two retrogradely labeled and photo-filled small bistratified cells. **A, B**: Single images from different z-planes are showing a large proportion of outer and inner tier dendrites respectively. **C, D**: Collapsed images (14 images in C; 11 images in D) from stacks of images through the outer and inner tier. **E, F**: Single images at different z-planes showing hook-like dendrites. Eccentricities are indicated beneath each cell in B and C. Arrows in A and C point to branches of outer dendritic tiers. Arrow-heads in B and D indicate axons. The box in D indicates the region shown at higher resolution in E and F. For drawings of the cells shown in A-D see Figure 2.4C, D and Figure 2.5A, B. Scale bar shown in D = 20 µm (applies to both A and D). Scale bar shown in F = 10 µm (applies to both E and F).

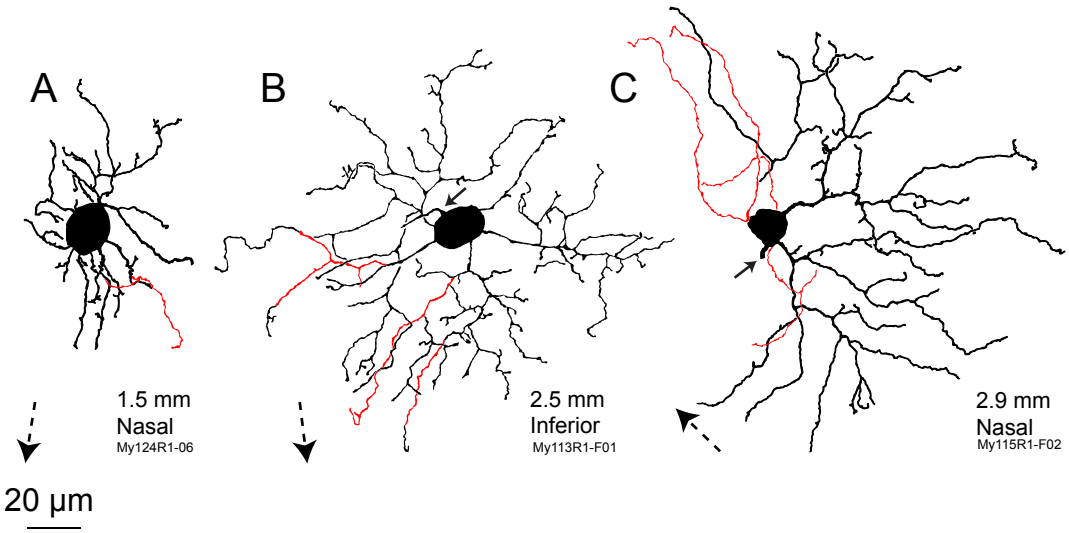


Figure 2.2 A - C: Drawings of small bistratified ganglion cells. The outer dendritic tier is shown in red, and the inner dendritic tier in black. Eccentricities and retinal quadrants are indicated beneath each cell. Arrows indicate axons. The axon for the cell on the left is not drawn. Dotted arrows indicate the direction of the fovea.

Synaptic input to small bistratified ganglion cells: Qualitative results

Presumed bipolar input was estimated by counting immunoreactive (IR) puncta (obtained with antibodies against the C-terminal binding protein, CtBP2) that were colocalised with the dendrites of retrogradely labelled cells. As described previously, antibodies against CtBP2 can be used to identify presynaptic ribbons in primate retina (Jusuf et al., 2006a). Figure 2.3A and B show examples of colocalised CtBP2 IR puncta (arrows) on outer and inner dendrites of small bistratified cells.

Presumed amacrine input onto dendrites of small bistratified cells were identified with antibodies against the receptor anchoring protein gephyrin. Gephyrin is expressed at postsynaptic sites on amacrine and ganglion cell processes together with glycine and $GABA_A$ receptors, and serves the function of linking the receptor to the cytoskeleton (Fischer et al., 2000; Kneussel and Betz, 2000; Sassoè-Pognetto et al., 1995). Gephyrin is most likely present at the large majority of inhibitory synapses in the retina. Figure 2.3F shows gephyrin IR puncta (arrow) which were colocalised with dendrites from the inner tier of a small bistratified cell.

In some preparations, excitatory input was directly compared to inhibitory input by combining the antibody against the glutamate receptor subunit 4 (GluR4) of the AMPA receptor with the antibody against gephyrin. Immunoreactivity for GluR4 is usually localized to one of the two postsynaptic elements of bipolar dyads (Grünert et al., 2002; Qin and Pourcho, 1999), and the large majority of GluR4 IR puncta have been shown to colocalise with CtBP2 IR puncta (Jusuf et al., 2006a). It is therefore probable that GluR4 IR puncta are present at a large majority of bipolar input synapses. Figure 2.3C-K show images from a triple labelled preparation. Both gephyrin IR and GluR4 IR puncta can be found colocalised with the dendrites of the small bistratified cell. There is practically no overlap between GluR4 and gephyrin IR puncta, consistent with the idea that the two markers are localised at distinct synaptic locations.

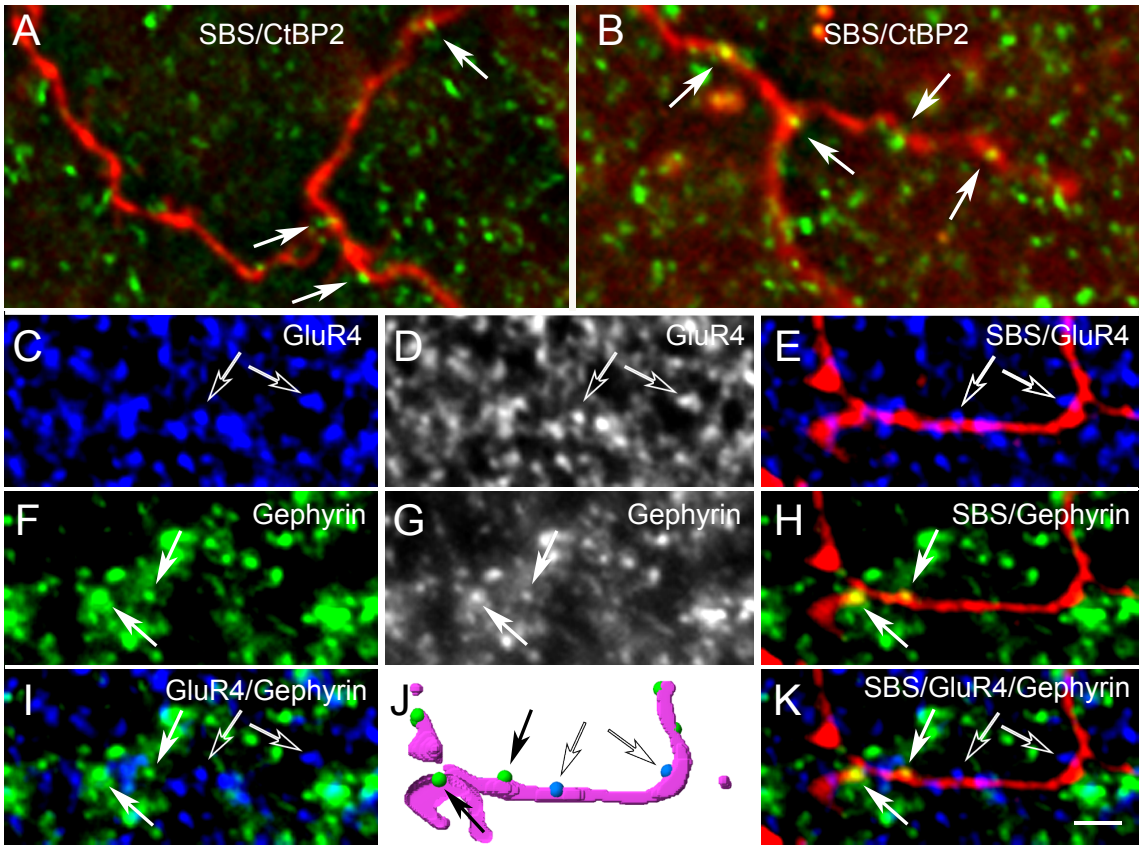


Figure 2.3 Micrographs of retinal preparations containing retrogradely labelled small bistratified cells. Only images representing a single plane of focus are shown. **A**, **B**: Micrographs from a double labelled preparation showing dendritic processes (red) together with synaptic ribbons or presumed bipolar input (green) as labelled using an antibody against the C-terminal binding protein 2 (CtBP2). Arrows point to colocalised immunoreactive puncta. Dendritic processes in A are from the outer tier, and in B are from the inner tier. **C**-**K**: Micrographs from a triple labelled preparation showing dendritc processes (red, E, H, J, K), presumed amacrine input as labelled using an antibody against gephyrin (green, F, G) and presumed bipolar input as labeled using an antibody against the AMPA receptor subunit glutamate receptor subunit 4 (GluR4; blue, C, D). Filled arrows point to colocalised gephyrin immunoreactive puncta and open arrows point to colocalised GluR4 immunoreactive puncta. I: shows there is no overlap between gephyrin and GluR4 immunoreactive puncta within the same region. J: shows a computer reconstruction of the dendritic processes and colocalised immunoreactive puntcta for the area shown in micrographs. Scale bar = 2 µm.

Figure 2.4A-D show the distribution of CtBP2 IR puncta on inner and outer dendrites of two cells, from central (1.6 mm) and mid-peripheral (3.8 mm) retina. Both cells receive presumed bipolar input to outer (Figure 2.4A, C) and inner dendritic tiers (Figure 2.4B, D). IR puncta are relatively evenly distributed across outer and inner tiers, however regions devoid of bipolar input are also observed.

The question of whether the distribution of CtBP2 IR puncta on the inner tier is consistent with convergent synaptic input from blue cone bipolar cells was investigated. For the cell from 3.8 mm shown in Figure 2.4C, D, the drawing of the inner dendritic field was superimposed with a simulated blue cone bipolar axon terminal mosaic, based on a DiI labelled blue cone bipolar cell located at similar eccentricity (Chan et al., 2001). Assuming a blue cone bipolar density of approximately 400 cells per mm^2 (Luo et al., 1999) this small bistratified cell may be contacted by eleven blue cone bipolar cells and with 70 areas of potential contact (dendrite/axon crossings). The number of colocalised CtPB2 puncta (n=195) is almost threefold higher than the number of potential contact areas (n=70), consistent with the idea that each contact area most likely contains several synaptic ribbons (Calkins et al., 1998; Ghosh and Grünert, 1999). The density of bipolar input to the inner tier of this cell therefore shows there is dominant input from blue cone bipolar cells.

Figure 2.5 shows the distribution of gephyrin IR puncta (open circles) on the inner and outer dendritic tiers of three cells from central retina. Both the outer tier (Figure 2.5A, C, E) and inner tiers (Figure 2.5B, D, F) receive presumed amacrine input. For one cell the bipolar input is also shown (filled circles, Figure 2.5A, B).

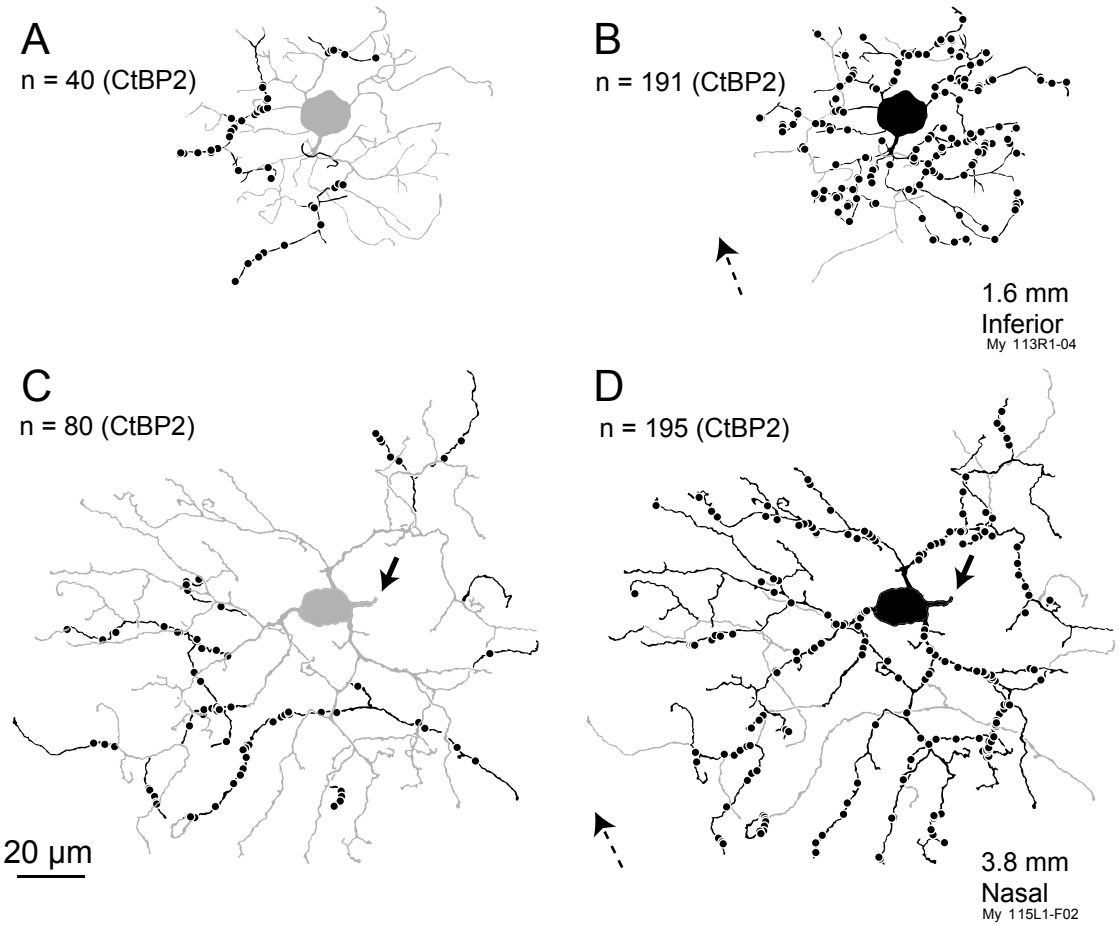


Figure 2.4 Drawings of two small bistratified cells together with colocalised C-terminal binding protein (CtBP2) immunoreactive puncta (filled circles). **A, C**: Show colocalised immunoreactive puncta on outer dendrites (black), inner dendrites are shown in grey. **B, D**: Show colocalised immunoreactive puncta on inner dendrites (black), outer dendrites are shown in grey. Immunoreactive puncta are enlarged for the purposes of this figure and are not drawn to scale. n indicates the number of colocalised immunoreactive puncta. Eccentricities and retinal quadrants are indicated beneath each cell. Arrows indicate axons. Dotted arrows indicate the direction of the fovea.

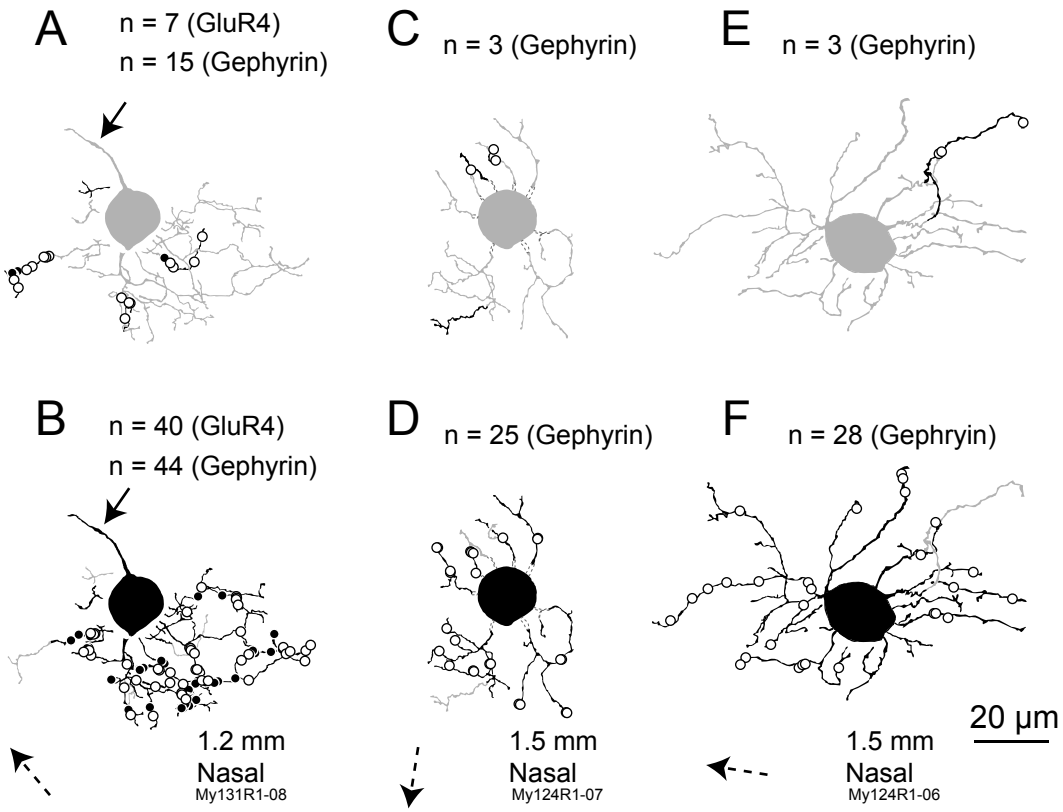


Figure 2.5 Drawings of three small bistratified cells together with colocalised gephyrin (open circles; presumed amacrine input) and/or GluR4 (closed circles; presumed bipolar input) immunoreactive puncta. **A, C, E**: Show colocalised immunoreactive puncta on outer dendrites shown in black; inner dendrites are shown in grey. **B, D, F**: Show colocalised immunoreactive puncta on inner dendrites shown in black; outer dendrites are shown in grey. Immunoreactive puncta are enlarged for the purposes of this figure and are not drawn to scale. n indicates the number of colocalised immunoreactive puncta. Eccentricities and retinal quadrants are indicated beneath each cell. Arrows indicate axons. Dotted arrows indicate the direction of the fovea.

Synaptic input to small bistratified ganglion cells: Quantitative results

Bipolar input

Presumed bipolar input was determined for twelve cells (n = 7 cells for CtBP2 IR puncta; n = 5 cells for GluR4 IR puncta). The total number of colocalised CtBP2 puncta ranged from 29 - 80 for the outer tier and 127 - 225 for the inner tier. The total number of colocalised GluR4 IR puncta per cell (outer tier: 1 to 7; inner tier: 7 to 76) was lower than the number of colocalised CtBP2 IR puncta. However, the density of colocalised puncta did not differ substantially for the two markers, consistent with the assumption that both markers can be used to identify the bipolar input to small bistratified cells (see above). For this reason, in the sections that follows, data for CtBP2 and GluR4 are presented together. The difference in the total numbers is likely to be due to the fact that all cells from preparations processed with GluR4 were from foveal or central retina, possessing smaller dendritic trees.

Graphs in Figure 2.6A, B plot presumed bipolar input for the two tiers with respect to eccentricity. While total presumed input to the outer tier is smaller than the inner tier, the average density is close to 4 puncta per 100 μm^2 for both tiers. The lower total number of puncta on outer tiers can be explained by the sparse morphology of the outer dendritic tree compared to the inner tier. The error bars in Figure 2.6B show standard error of the mean (s.e.m.) for the multiple samples taken from each cell. Most of these error bars show substantial overlap, consistent with approximately matched excitatory synaptic input density to both tiers.

In summary, the total number of presumed bipolar synapses is higher for the inner tier than for the outer tier (Figure 2.6A), but densities are comparable for the two tiers (Figure 2.6B). No clear eccentricity related difference with respect to the density of presumed bipolar input could be detected (Figure 2.6B).

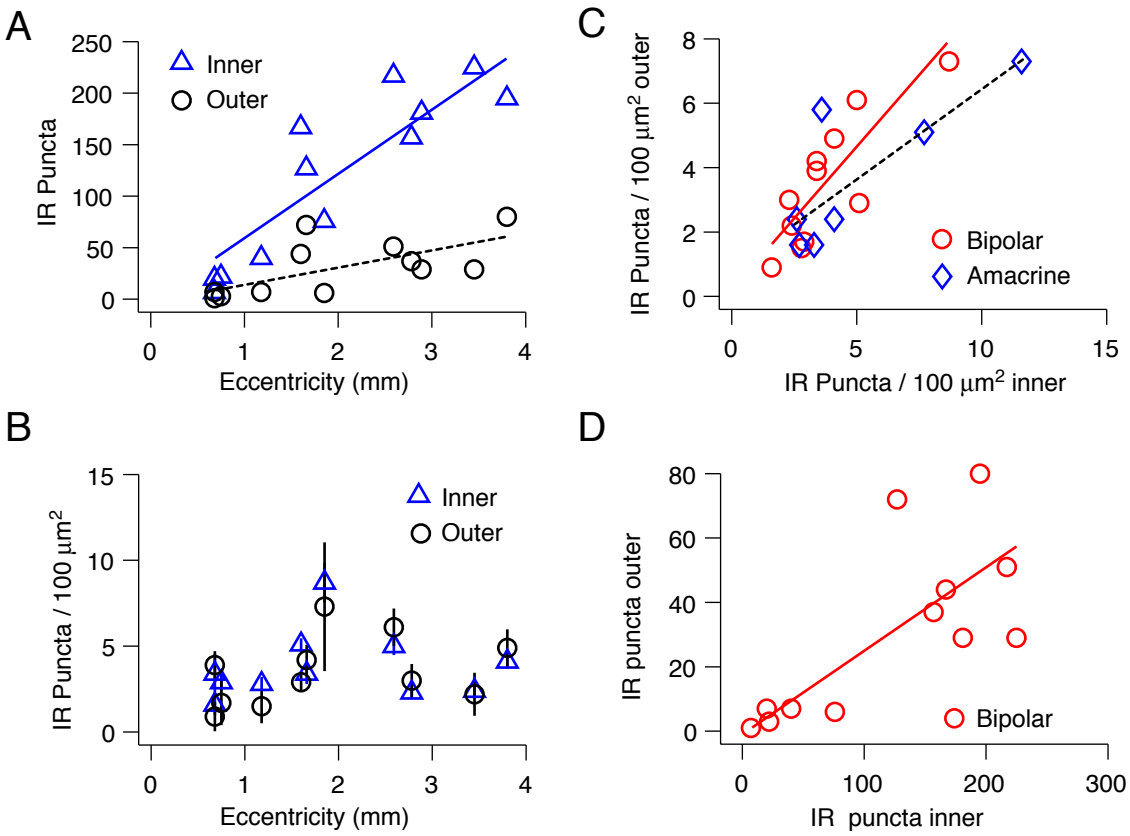


Figure 2.6 Presumed synaptic input to small bistratified cells determined in retinal preparations processed with antibodies against C-terminal binding protein 2, glutamate receptor subunit GluR4, or gephyrin. **A**: Bipolar input: Total number of immunoreactive (IR) puncta colocalised to outer and inner dendritic tiers. Solid line shows linear regression for inner tier (slope, 67.31; y-intercept, -14.6; r^2 0.80; $P < 0.01$). Dashed line shows linear regression for outer tier (slope, 16.06; y-intercept, -1.5; r^2 0.41, $P = 0.03$). **B**: Bipolar input: Density of colocalised IR puncta per 100 µm² dendritic membrane. Error bars show standard error of mean. **C**: Bipolar and amacrine input: Comparison of the density of colocalised IR puncta between the two tiers. Solid line shows linear regression for presumed bipolar input (slope, 0.855; y-intercept, 0.26; r^2 0.70; $P < 0.01$). Dashed line shows linear regression for presumed amacrine input (slope, 0.552; y-intercept, 0.93; r^2 0.65; $P = 0.03$). **D**: Correlation of IR puncta numbers on inner and outer dendritic tiers. Solid line shows linear regression for presumed bipolar input (regression slope 0.24, y-intercept 1.55, $r^2 = 0.53$, $p < 0.01$, $n = 11$ cells). Note that one of the seven CtBP2 cells was analysed manually and thus is not included in the data for panels B and C; one of the 5 GluR4 cells was only partially analysed and thus is not included in the data for panel A.

An estimate of the average ratio of bipolar inputs to inner and outer tiers across the population of small bistratified cells was obtained, by pooling the data shown in Figure 2.6A across the eccentricity range studied (~0.7 mm – 4 mm). This procedure is justified because the density of synaptic inputs does not show strong variation with eccentricity (Figure 2.6B), and the density of inputs to inner and outer tiers is correlated on a cell-by-cell basis (Figure 2.6C). The result (Figure 2.6D) shows that there are approximately four times more bipolar synapses on the inner tier than on the outer tier (solid line, Figure 2.6D). It was concluded that the outer tiers of small bistratified cells show consistent evidence for synaptic input from OFF bipolar cells, at a level that would predict excitatory synaptic weight of 25% relative to the inner tier.

Amacrine input

Presumed amacrine input was determined for seven cells from foveal and central retina using antibodies against gephyrin. These cells had an average of 5.5 ± 4.7 IR puncta on outer tier dendrites and an average of 28.7 ± 7.7 IR puncta on inner tier dendrites. Differences in the total number of colocalised gephyrin IR puncta between outer and inner tier are correlated with the differences in the size of the two tiers as average densities of colocalised puncta are similar for the two tiers. For the outer tier the average was 3.5 ± 3.0 IR puncta per 100 μm^2 and for the inner tier was 5.0 ± 3.9 puncta per 100 μm^2.

Comparison of amacrine and bipolar input

For five cells the density of presumed synaptic input with respect to dendritic length in the inner tier was determined using the "walk analysis" (Lin et al., 2000), which also gave rise to similar densities of both presumed bipolar and amacrine input. The average number of colocalised IR puncta was 25.8 ± 10.0 puncta per 100 µm dendritic length for CtBP2 (n = 3 cells, from 1.6 mm, 2.89 mm, and 3.8 mm eccentricity), and 19.8 puncta per 100 µm dendritic length for GluR4 (one cell from 1.18 mm eccentricity). Accordingly, there is, on average one bipolar synapse for every 4 to 5 µm of dendrite. The value for presumed amacrine input (one cell from 1.5 mm) was 20.3 puncta per 100 µm or one presumed amacrine synapse every 5 µm.

Presumed bipolar and amacrine input was compared directly for five cells in foveal and central retina (eccentricity range 0.68 to 1.85 mm). These cells had an average ratio of presumed bipolar to amacrine input of approximately 1:1.5 for the outer tier and 1:1.3 for the inner tier. A single example is shown in Figure 2.5. For this cell, approximately 11% (5 of 44) of colocalised gephyrin IR puncta on inner tier dendrites were located close to colocalised GluR4 IR puncta. This is consistent with results from electron microscopy, where presynaptic amacrine processes providing input to inner dendrites of small bistratified cells were frequently found in the vicinity of ribbon synapses onto the same dendrites (Ghosh and Grünert, 1999).

Relative densities of presumed amacrine and bipolar inputs are summarised in Figure 2.6C. Across the sample of cells there is a strong correlation between the densities for both inhibitory and excitatory inputs (bipolar input, correlation coefficient 0.84; amacrine input, correlation coefficient 0.81) onto inner and outer tiers. Consistently, linear regression for bipolar input to inner and outer dendrites (solid line, Figure 2.6C) yields a slope close to unity (0.86, y-intercept 0.27, $r^2 = 0.70$, n=11). The slope of the regression line for amacrine input (dashed line, Figure 2.6C) is slightly lower (0.55, y-intercept 0.94, $r^2 = 0.65$, n=7). This suggests a bias towards a higher density of amacrine input onto inner tiers, however the effect is relatively small.

Convergence in the blue/yellow pathway

In order to estimate how many cones provide input to the two dendritic tiers of small bistratified cells, the number of cones located in the inner and outer dendritic fields were counted (see methods). For six cells the number of cones within the dendritic field was identified directly by counting cone pedicles immunoreactive to CtBP2 or GluR4 (see Figures 2.7 and 2.8). For eight other cells, the number of cones in the dendritic field was estimated using previously published cone densities from corresponding eccentricities (see methods). The percentage of short wavelength sensitive (S) cones, which in primates make up less than 10% of the cone population (Curcio et al., 1991; Martin and Grünert, 1999; Wikler and Rakic, 1990), was also determined from published data.

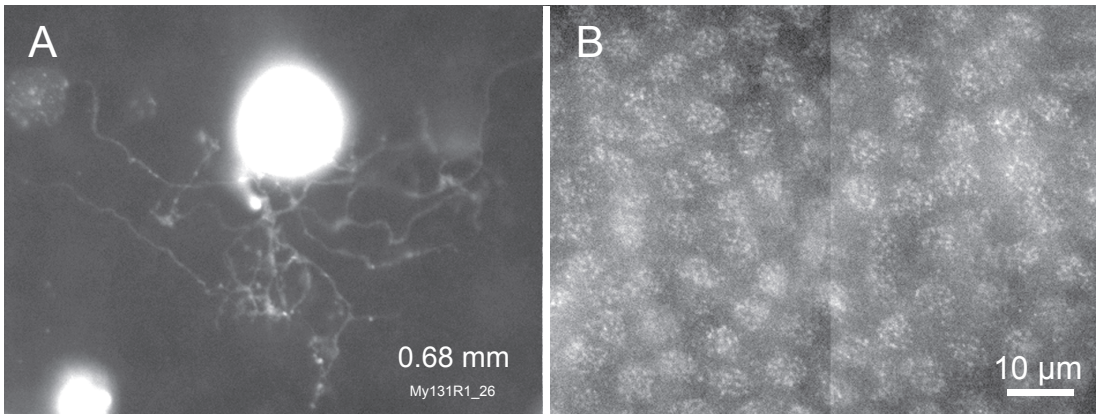


Figure 2.7 Micrographs of a small bistratified cell together with the overlying cone pedicle mosaic labeled for GluR4 immunoreactivity. **A**: A single image representing a single plane of focus is shown. **B**: A montage of two images, each representing a single plane of focus.

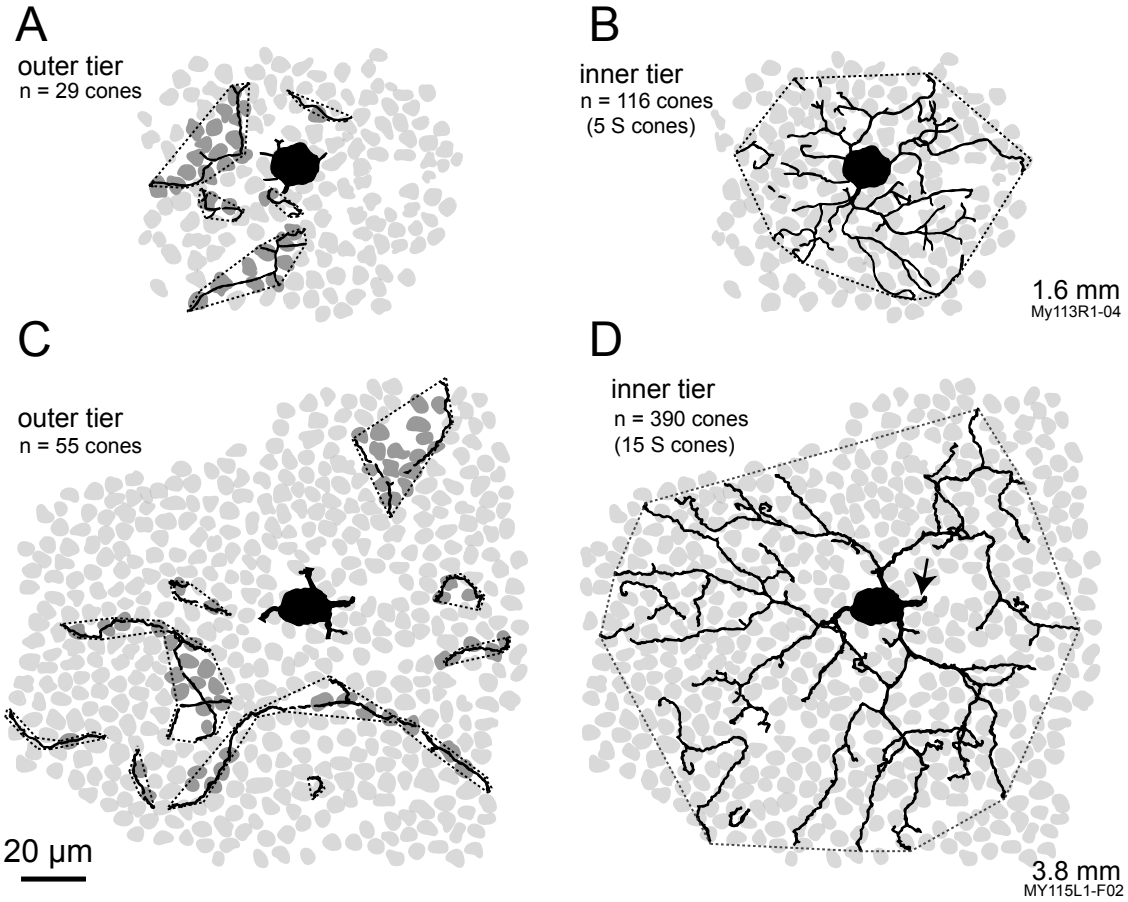


Figure 2.8 Drawings of the outer and inner dendritic fields (stippled outline) of the two small bistratified cells shown in Figure 2.4 together with the cone pedicle mosaic (light grey) determined from C-terminal binding protein 2 labeling. **A, C**: Cone pedicles in the outer dendritic field are indicated in dark gray. The number of cones in the dendritic field was determined as described in the methods. The cell at 1.6 mm eccentricity (A) has 29 cones, and the cell at 3.8 mm eccentricity (C) has 55 cones in its outer dendritic field. **B, D**: Cones located in the inner dendritic field are outlined by the dotted line. The cell at 1.6 mm eccentricity has 116 cones in its inner dendritic field, 5 of which are presumed S cones. The cell at 3.8 mm eccentricity has 390 cones in its inner dendritic field, 15 of which are presumed S cones. Eccentricities are indicated beneath each cell. Arrows indicate axons.

For the two cells shown in Figure 2.8 the number of cones within the inner tier is 116 and 390, respectively. Cone input to the inner tier presumably derives exclusively from S cones (Calkins et al., 1998; Dacey and Lee, 1994), therefore, these two cells may only receive input from 5 and 15 S cones, respectively.

The number of cones encompassed by the outer tier of the two cells shown in Figure 2.8 is 29 and 55, respectively. Presumed bipolar input to the outer tier is presumably provided by two types of diffuse bipolar cell (Calkins et al., 1998; Ghosh et al., 1997) which, depending on eccentricity, contact between 7 and 20 cones (including S, medium (M) and long (L) wavelength sensitive cones; Boycott and Wässle, 1991; Chan et al., 2001).

Figure 2.9A, B summarise the data obtained for all cells analysed for cone convergence. The number of S cones overlying the inner tier increases with eccentricity (Figure 2.9A; correlation coefficient 0.79). The number of cones encompassed by the outer tier also rises (Figure 2.9B, correlation coefficient 0.83). Cone convergence increases with increasing eccentricity, because the increase in dendritic field area of both inner and outer tiers outweighs the decrease in cone density. In Figure 2.9C the cone convergence for inner and outer dendritic tiers are compared. It was found that although the dendritic area occupied by the outer tier on average makes up only 10% of the area occupied by the inner tier, the total number of cones encompassed by the outer dendritic field is always greater than the number of S cones encompassed by the inner dendritic field (solid line, Figure 2.9C, regression slope 2.50).

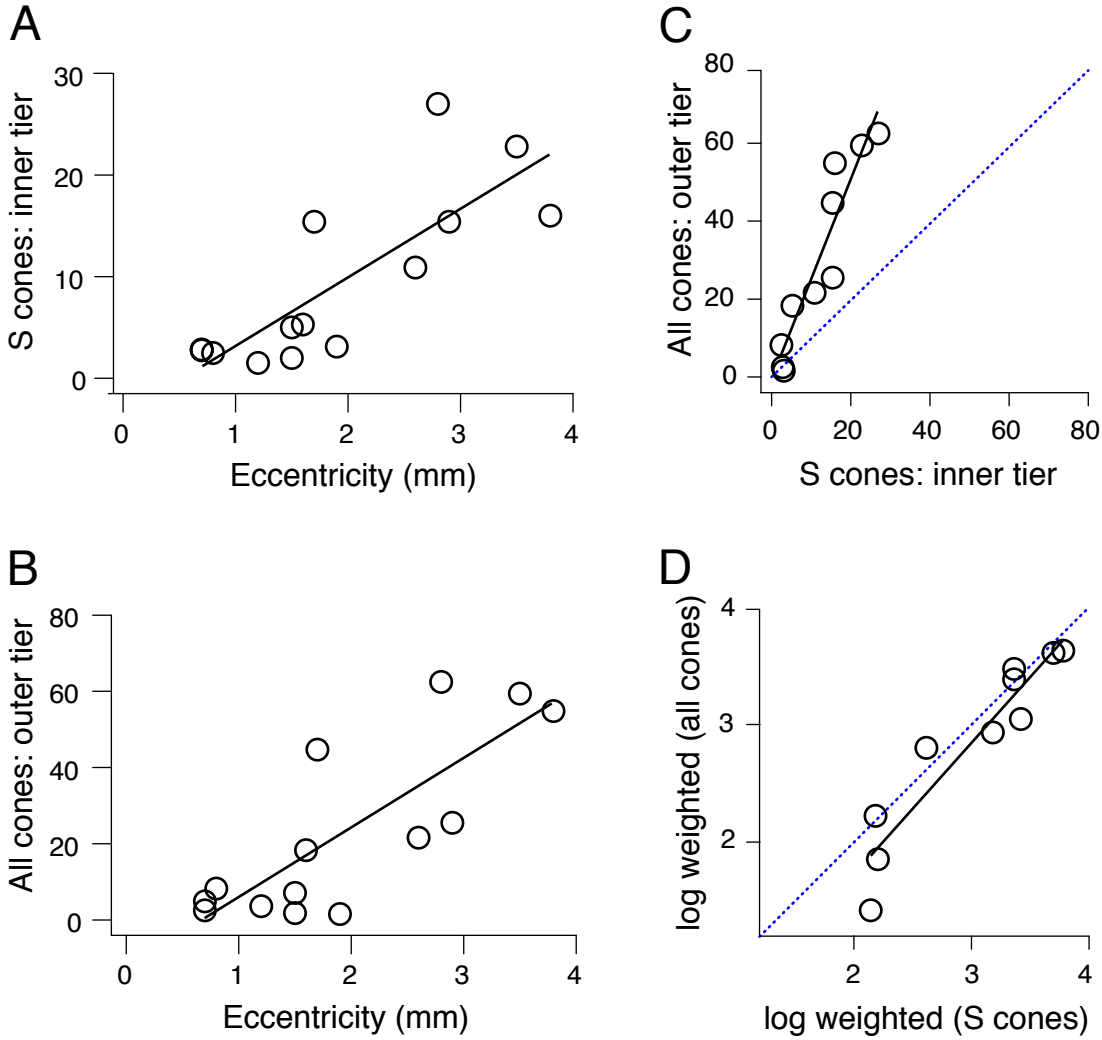


Figure 2.9 Cone convergence to small bistratified cells. Convergence was estimated directly by counting the cone pedicles in the dendritic field or by multiplying the dendritic field area by the local cone density estimated from published data (Martin and Grünert, 1999). **A**: S cone convergence to the inner tier with respect to eccentricity. Dashed line shows linear regression (slope, 6.57; y-intercept, –3.38; r^2 , 0.63; correlation, 0.79; $P < 0.01$). **B**: Cone convergence to the outer tier with respect to eccentricity. Dashed line shows linear regression (slope, 24.74; y-intercept, –22.02; r^2 , 0.68; correlation, 0.98; $P < 0.01$). **C**: Scatterplot showing number of S cones encompassed by the inner dendritic field vs. the total number of cones encompassed by the outer dendritic field. Dashed line shows 1:1 ratio. Solid line shows linear regression (slope, 2.50; y-intercept, 0.02; r^2 , 0.89; correlation, 0.94; $P < 0.01$). **D**: Scatterplot showing an estimate of synaptic weight from the log-transformed product of puncta number and cone convergence. Dashed line shows unity ratio. Solid line shows linear regression (slope, 1.12; y-intercept, -0.52; r^2 , 0.88; correlation, 0.94; $P < 0.01$). This shows that over two orders of magnitude the integrated weights of inputs from S cones (to the inner tier) and ML cones (to the outer tier) are approximately matched.

Even though the cone connectivity of the bipolar types providing inputs to the two tiers was not directly investigated, the known connectivity of bipolar cells indicates that the number of contacts made between S cones and blue cone bipolar cells (between 20 and 30 in macaque Herr et al., 2003; Kouyama and Marshak, 1992) is similar to the average number of contacts made between M/L cones and the two OFF bipolar types diffuse bipolar (DB) 2 and DB3 cells (between 14 and 24 Calkins, 1999; Hopkins and Boycott, 1997). It is therefore reasonable to assume that each cone contributes with equal synaptic weight to the bipolar array. The presumed synaptic input (number of colocalised puncta) was next compared with the cone convergence for the two tiers. Figure 2.9D plots on a logarithmic scale, for each cell, the product of colocalised IR puncta number (as shown in Figure 2.6A) and cone convergence for inner (S cones, Figure 2.9A) and outer dendritic tiers (all cones, Figure 2.9B). There is strong positive correlation between the values for inner and outer tier (correlation coefficient 0.94), and the regression slope of the log transformed product is close to unity (slope, 1.12, y-intercept 0.00, $r^2 = 0.89$, $p < 0.01$, n=10). These data are consistent with the hypothesis that the functional weight of S cone inputs to small bistratified cells is amplified, because the inner dendritic field collects more bipolar synapses than does the outer dendritic field (Calkins et al., 1998). In other words, small bistratified cells collect inputs from the sparse S cone array over a large (inner) dendritic field, and inputs from the dense M/L cone array over a small (outer) dendritic field.

2.5 *Discussion*

The results from the current study support and extend previous electron microscopic studies showing amacrine and bipolar input to both dendritic tiers of small bistratified ganglion cells in macaque and marmoset retinae (Calkins et al., 1998; Ghosh and Grünert, 1999). The data show correlated presumed bipolar input densities for inner and outer dendritic tiers across the range of eccentricities studied. In the discussion to follow, the results from the current study are compared to other studies of synaptic input to ganglion cells, following which; the functional implications of the anatomical results obtained here are considered.

Simlarities between small bistratified cells in marmoset and macaque retina are well documented (Dacey, 1993a; Dacey and Lee, 1994; Ghosh et al., 1997; Rodieck, 1991; Rodieck and Watanabe, 1993; Silveira et al., 1999; Szmajda et al., 2008; Yamada et al., 1996). Likewise, the majority of blue-ON/yellow-OFF receptive fields in the retina and LGN of these species show stereotyped properties consistent with small bistratified cells (de Monasterio and Gouras, 1975; Derrington et al., 1984; Hashemi-Nezhad et al., 2008; Martin et al., 1997; Schiller and Malpeli, 1978; Solomon et al., 2005; Tailby et al., 2008a; Tailby et al., 2008b; White et al., 1998; Wiesel and Hubel, 1966; Yeh et al., 1995a). This makes it likely that conclusions drawn from studies of marmoset retina are applicable to macaque monkeys and other diurnal primates.

Distribution and density of synaptic input to ganglion cells

The method used here, of identifying synaptic input by light microscopy is supported by two recent studies showing the spatial pattern of synaptic input to ganglion cells in rabbit and mouse retinae transfected with fluorescent postsynaptic proteins (Jakobs et al., 2008; Morgan et al., 2008). These studies show that there is good coincidence between presynaptic ribbon markers and postsynaptic proteins. It is possible however, that the number of colocalised immunoreactive (IR) puncta determined with the antibodies against the glutamate receptor subunit 4 (GluR4) and gephyrin represent underestimates of the number of actual bipolar and amacrine inputs as small bistratified cells may express glutamate receptors not containing the GluR4 subunit. Likewise the possibility that some amacrine input to small bistratified cells is mediated by $GABA_A$ or glycine receptors that are not labelled with the antibody against gephyrin cannot be excluded (Sassoe-Pognetto and Fritschy, 2000; Sassoè-Pognetto et al., 1995; Sassoè-Pognetto et al., 1994).

For all cells analysed in the present study, colocalised IR puncta were distributed throughout the dendritic tree suggesting, small bistratified ganglion cells, like other ganglion cells types in mammalian retinae, receive synaptic input throughout the entire dendritic tree (Calkins et al., 1994; Famiglietti, 2005; Freed and Sterling, 1988; Jacoby et al., 1996; Jakobs et al., 2008; Jeon et al., 2002; Jusuf et al., 2007; Kolb and Dekorver,

1991; Lin et al., 2000; Macri et al., 2000; McGuire et al., 1986; Morgan et al., 2008; Owczarzak and Pourcho, 1999; Xu et al., 2008).

Densities of presumed bipolar and amacrine synapses found here for small bistratified cells are in the same order of magnitude as those found for midget and parasol cells in marmoset and macaque retinae (Bordt et al., 2006; Eriköz et al., 2008; Lin et al., 2002). Results are also comparable to values reported for various ganglion cell types in the retinae of other mammals including cat, guinea pig, rabbit and mouse (Freed and Sterling, 1988; Jakobs et al., 2008; Jeon et al., 2002; Kier et al., 1995; Morgan et al., 2008; Owczarzak and Pourcho, 1999; Xu et al., 2008). Data from this study are thus in agreement with the suggestion that the distinct properties of different ganglion cell types are not determined by the density of their synaptic input, but depend more on the properties of postsynaptic receptors and presynaptic neurons (DeVries et al., 2006; Jakobs et al., 2008; Xu et al., 2008).

Ratio of excitatory and inhibitory synaptic input

The number of bipolar and amacrine cell inputs for the sample of five cells from foveal and central retina of marmosets were about equal. A similar ratio (70% bipolar and 30% amacrine input) was found for a single foveal small bistratified cell in macaque retina (Calkins et al., 1998). In contrast, an EM study of two partially reconstructed small bistratified ganglion cells from far peripheral retina in marmoset found a low ratio of bipolar input (less than 20%) for both dendritic tiers (Ghosh and Grünert, 1999). Similarly, in macaque retina, a large proportion of amacrine input has been observed for OFF parasol ganglion cells from peripheral retina (73%; Bordt et al., 2006) compared to those from central retina (42%; Calkins and Sterling, 2007). An eccentricity related increase in the ratio of amacrine to bipolar input has also been suggested for midget ganglion cells (Kolb and Marshak, 2003). In the present study, the density of bipolar and amacrine input to small bistratified cells in mid or far peripheral retina were not directly compared, as cells labelled with both markers at these eccentricities were not obtained. It was found however that the absolute density of bipolar input over the eccentricity range studied remained rather uniform (Figure 2.6B). This suggests that changes in the bipolar:amacrine input ratio may be due to changes in amacrine synapse density. In

summary, there may be a common pattern, whereby central ganglion cells receive relatively more inputs from bipolar cells compared to peripheral cells, but a direct test of this hypothesis has not been carried out.

Functional role of the outer dendritic tier

The current data support the model in which diffuse OFF bipolar cells receiving their main input from medium (M)/long (L) wavelength sensitive cones (Boycott and Wässle, 1991) form the anatomical basis for the yellow-OFF response in small bistratified ganglion cells (Calkins et al., 1998; Crook et al., 2009; Dacey and Lee, 1994). These OFF-signals balance ON-type signals, which are drawn from a sparsely distributed receptor pool of short wavelength sensitive (S) cones to supply the more extensive inner dendritic tier. Because the ON and OFF inputs derive from distinct cone classes, this arrangement produces a spectrally opponent, blue-ON/yellow-OFF receptive field. Lines of evidence which support this hypothesis are the consistent presence of bipolar synapse markers on the outer tier of all cells in the sample analysed, consistent density of synaptic input across eccentricities studied, covariance of punctal density between inner and outer tiers (Figure 2.6), and the correlation between S cone convergence to the inner tier and total cone convergence to the outer tier (Figure 2.9).

The role of OFF diffuse bipolar cells in providing the yellow-OFF response has been challenged by results from electrophysiological experiments. Field et al. (2007) found that application of the metabotropic glutamate receptor agonist L (+)-2-amino-4-phosphonobutyric acid (L-APB) eliminated both blue-ON and yellow-OFF responses in simultaneous extracellular recordings from an array of blue-ON/yellow-OFF cells. The authors suggest that the yellow-OFF response does not pass through the outer tier but is carried together with the blue-ON input by the blue cone bipolar cell (see also Packer et al., 2007). On the other hand, recordings made *in vivo* from blue-ON/yellow-OFF cells in macaque retina have demonstrated that the OFF response does not show the temporal delay expected from horizontal cell inputs *via* inhibitory synapses (Yeh et al., 1995a). Responses of small bistratified ganglion cells to cone selective gratings in a recent study using an *in vitro* preparation of macaque retina provide further support for dominant OFF-excitatory input from M/L cones passing through the outer tier of small bistratified

cells *via* diffuse bipolar cells, and the presence of a suppressive M/L surround (presumably mediated by horizontal cells) that is unmasked by the application of L-APB (Crook et al., 2009).

Conclusion

In conclusion, results from this study are consistent with convergence of ON and OFF inputs as a source of chromatic opponency in small bistratified cells. Nevertheless it is important to note that ON-OFF convergence is not a prerequisite for cone opponency. For example, synaptic circuitry involving amacrine cell connections may underlie cone opponent inputs to monostratified blue-OFF/yellow-ON cells (Dacey and Packer, 2003). Likewise, recent experiments in guinea pig retina (Yin et al., 2009) revealed a very rare type of S+/M- opponent cell that is monostratified in the ON sublamina. Finally, responses in the great majority of red-green opponent cells in the midget-parvocellular pathway in trichromatic primates (Buzás et al., 2006; Dacey and Lee, 1994; Derrington et al., 1984; Yeh et al., 1995a; Yeh et al., 1995b) are consistent with horizontal and/or amacrine cell-mediated inhibition as a source of cone-opponent interactions.

Chapter 3 Synaptic inputs to two types of koniocellular pathway ganglion cells in marmoset retina

3.1 *Introduction*

This chapter investigates two types of wide-field cells with distinct and largely contrasting morphologies: the large sparse and the broad thorny cell types. As outlined in the discussion of large sparse cells in section 1.6 (page 19), examples of ganglion cells with sparsely branched dendrites and large dendritic fields have previously been identified using various techniques, but they have not been systematically studied. Examples of these cells were detected in Golgi-impregnated human retina (also named G20 by Kolb et al., 1992), by intracellular injection in human (Peterson and Dacey, 1999), macaque (Yamada et al., 2005) and marmoset retinas (Ghosh et al., 1996), and in retrogradely labelled macaque (Dacey et al., 2003; Leventhal et al., 1981; Perry and Cowey, 1984; Rodieck and Watanabe, 1993) and marmoset (Szmajda et al., 2008) retinas. The retrograde injection experiments showed that sparse cells project to the dorsal lateral geniculate nucleus (LGN) in both macaque (Dacey et al., 2003) and marmoset (Szmajda et al., 2008). Sparse cells can be further distinguished into large sparse and giant sparse cells, where the latter type is identical with the melanopsin-containing ganglion cell type (Dacey et al., 2005; Jusuf et al., 2007). Recordings from one large sparse cell in macaque retina showed blue-OFF response characteristics (Dacey and Packer, 2003) consistent with the idea that blue-OFF receptive fields recorded in the LGN may derive from large sparse cells (Szmajda et al., 2006; Tailby et al., 2008b; Valberg et al., 1986). The synaptic connectivity of large sparse cells however, remains unknown.

Broad thorny cells fall into the group of broadly stratified ganglion cell types that have previously been described in Golgi-impregnated retinas of various Old World primates (also named diffusely stratified by Boycott et al., 1969; Kolb and Dekorver, 1991; Polyak, 1941). They were also found using intracellular injections in human (Peterson and Dacey, 1999), macaque (Yamada et al., 2005) and marmoset retinas

(named hedge cells by Ghosh et al., 1996), and by retrograde labelling in macaque (included in T-group cells by Dacey et al., 2003; Rodieck and Watanabe, 1993) and marmoset (Szmajda et al., 2008). They have densely branching dendrites that stratify broadly across most of the ON and OFF halves of the inner plexiform layer. Retrograde tracer injections in macaque showed that these cells project to the superior colliculus (Rodieck and Watanabe, 1993) and the dorsal lateral geniculate nucleus (LGN; Dacey et al., 2003). The functional properties and synaptic connectivity of broad thorny cells are not yet known.

Targeted tracer injections into the LGN in marmoset indicate that both large sparse cells and broad thorny cells project to the koniocellular layers (Szmajda et al., 2008). The object of the present study is to establish whether these to two types of koniocellular projecting ganglion cells show similar or a distinct pattern of synaptic input to that previously shown for midget-parvocellular and parasol-magnocellular ganglion cells (Eriköz et al., 2008). The density of synaptic input to retrogradely labelled and photofilled large sparse and broad thorny cells was analysed using immunohistochemistry and high-resolution light microscopy.

3.2 *Materials and Methods*

Animals

Experiments were carried out on six adult marrmosets (*Callithrix jacchus*), obtained from the Australian National Health and Medical Research Council (NHMRC) combined breeding facility (see Table 3.1). All procedures were carried out according to the provisions of the NHMRC code of practice for the care and use of animals and were approved by the University of Melbourne ethics committee.

Table 3.1: Experimental parameters - Animals and anaesthesia

Animal number	Sex	Weight (g)	Anaesthesia for surgery
My103	Male	443	Ketamine / Zylazine
My104	Female	340	Ketamine / Zylazine
My109	Female	348	Ketamine / Zylazine
My115	Female	496	Ketamine / Zylazine
My124	Male	460	Ketamine / Zylazine
My131	Female	386	Alfaxalone

Tracer injections and photofilling

Dye injections, photofilling and immunohistochemical processing of retinal pieces were carried out as described in Section 2.2 (page 43) using the following experimental parameters shown in Table 3.2 and 3.3.

Table 3.2: Experimental parameters - Tracer injections and photofiling

Animal number	Injection tip size (µm)	Microruby concentration (%)	Duration of injection (min)	Transport time for injection (hours)
My103	25	10	70	88.8
My104	100	10	75	54.2
My109	80	10	120	89.8
My115	20 - 25	5	50	88.0
My124	70	5	120	66.0
My131	50	5	120	88.5

Table 3.3: Experimental parameters - Immunohistochemical processing of retinal wholemounts

Retinal piece	Concentration / duration of immersion fix	Primary antibodies used	Duration of primary antibody incubation (days)	Secondary antibodies used
My103L1	4 % PFA / 120 min	CD15 (ms)	?	g ∝ ms Alexa 488
My104L2	4 % PFA / 120 min	CD15 (ms)	16	g ∝ ms Alexa 488
My109L2	4 % PFA / 120 min	CD15 (ms)	14	g ∝ ms Alexa 488
My115R1	4 % PFA / 30 min	CtBP2 (ms)	7	g ∝ ms Alexa 488
My115L1	4 % PFA / 60 min	CtBP2 (ms)	7	g ∝ ms Alexa 488
My124R1	4 % PFA / 30 min	Gephyrin (ms) / GluR4 (rb)	9	g ∝ ms Cy5 / g ∝ rb Alexa 488
My131R1	4 % PFA / 30 min	Gephyrin (ms) / GluR4 (rb)	4	g ∝ ms Alexa 488 / g ∝ rb Cy5

Paraformaldehyde (PFA), mouse (ms), rabbit (rb), goat (g)

Antibodies

Table 3.3 gives a summary of the antibodies used in the present study. Details for the antibodies used against the C-terminal binding protein 2 (CtBP2), gephyrin and glutamate receptor subunit 4 (GluR4) are outlined in Section 2.2 (page 43).

An antibody against the carbohydrate epitope (CD15) was used at a dilution of 1:6. This antibody is a mouse monoclonal IgM antibody derived from hybridoma cell lines (MMA, ATCC HB78), which reacts with the 3-fucosyl-N-acetyl-lactosamine antigen. The CD15 antibody has been characterised in retinas of various species (Andressen and Mai, 1997) and in marmoset has been shown to label flat midget bipolar and diffuse bipolar type 6 (DB6) cells (Chan et al., 2001).

Analysis

Image acquisition

Image acquisition processes and parameters are as described in Section 2.2 (page 43).

Ganglion cell eccentricity and quantification of dendritic parameters

Ganglion cell eccentricity was determined in the same way as outlined in Section 2.2 (page 43). For all large sparse and broad thorny ganglion cells, measurements of dendritic field diameter, stratification and branch density were made in the same way as outlined in Section 2.2 (page 43).

For a few cells, image stacks were also analysed using Imaris software (Version 7.0, Bitplane, Zurich, Switzerland). A three-dimensional representation of the dendritic tree was made using semi-automatic tracing routines (Filament Tracer module). The [X, Y, Z] coordinates of dendritic branch and terminal points were measured together with threshold-segmented locations of all immunoreactive (IR) puncta in the dendritic field. The dendritic stratification was extracted from these data using custom software written in MatLAB, available on request from the authors. For two cells, the total dendritic surface area, dendritic length and branch number were determined from the filament trace.

Synaptic input

The density and distribution of synaptic input was determined in the same way as outlined in Section 2.2 (page 43).

One large sparse ganglion cell was analysed manually as the label in the dendrites was too weak to run the semi-automated analysis. The number of co-localized IR puncta found for this cell was in the same range as determined for the other cells (see also Jusuf et al., 2007).

For large sparse ganglion cells, analyses were run on the entire dendritic field, however results may exclude small portions of dendrite where processes were either obscured by somas of other labelled ganglion cells, or obscured by the bright labelling from the soma of the cell under analysis. At times, small portions of dendrites could not be outlined from intensity contour maps without overestimation of the dendritic area, and, as such were excluded from the analysis. For the same reasons, small portions of dendrite within the 30 µm by 30 µm regions analysed from broad thorny ganglion cells were excluded from the analysis.

Relationship between amacrine and bipolar input

Amacrine cell processes may form synapses in a feedforward and/or feedback manner. In a feedforward synapse, an amacrine cell process postsynaptic at a bipolar dyad provides a synapse onto a ganglion cell dendrite also present at the same dyad. In the case of a feedback or reciprocal synapse the amacrine cell process provides input back onto the bipolar cell from which it receives input (e.g., Kolb and Dekorver, 1991). Reciprocal synapses cannot be detected with the antibodies used here, as gephyrin immunoreactivity is absent at synapses between amacrine and bipolar terminals (Grünert and Wässle, 1993; Pourcho and Owczarzak, 1991; Sassoè-Pognetto et al., 1995; Zucker, 1998).

Putative feedforward synapses were identified by first identifying all (gephyrin and GluR4) IR puncta located within 0.1 μm of the dendrite surface (derived using the surfaces tool and spots tool in the surpass module of Imaris). From those colocalised puncta, colocalised gephyrin puncta that were within 1 μm of a colocalised GluR4 puncta were quantified.

Cone convergence

Cone convergence and cone density were estimated as described in Section 2.2 (page 43). The number of short wavelength sensitive (S) cones encompassed by the dendritic field was also estimated in the same way as in Section 2.2 (page 43). This was only done for the sample of large sparse ganglion cells, as preliminary results have suggested that large sparse cells may receive S cone input.

DB6 overlap

The overlap between axon terminal processes of diffuse bipolar type 6 (DB6) cells and dendrites of sparse cells was quantified in two ways. Firstly, the dendritic tree of the sparse cell, and the overlying DB6 axon terminals were traced onto separate acetate sheets. By overlaying the drawings, 2-dimensional regions of overlap between DB6 axon terminals and ganglion cell dendrites were identified (Jusuf et al., 2006b). A z-stack of images at each putative overlap point was then examined to confirm or negate 3-dimensional colocalisation.

In the second method, image stacks were analysed directly using Imaris (Colocalisation module). A threshold was set for each of two image channels (ganglion cell dendrites and axon terminals) and the number of colocalised supra-threshold image voxels was counted.

Correlation between the brightness of colocalised pixels in the two image channels is expressed as a Pearson's correlation coefficient, where a coefficient of + 1 means that all colocalised pixels have identical brightness in each channel, and a coefficient of – 1 indicates a perfect inverse relationship where bright pixels in one image channel correspond to dark pixels in the other image channel and vice versa. The colocalisation of CD15 labelled DB6 axonal processes with retrogradely sparse ganglion cell dendrites were compared to pseudo-random colocalisation obtained by flipping the DB6 image channel along the y-axis.

3.3 *Results*

A total of thirteen retrogradely labelled and photofilled cells (nine large sparse and four broad thorny cells) were analysed. The quality of dendritic filling in these cells is poorer compared to labelling obtained by intracellular injections (see Figure 3.1 and Ghosh et al., 1996) but is adequate to enough to allow full analysis of morphology, stratification and synaptic input.

Large sparse ganglion cells

Large sparse ganglion cells have fine dendrites, which are largely free of hooks or spines, which form a sparsely branched dendritic tree. The morphology of large sparse cells analysed in the present study are consistent with previous descriptions in marmoset (Ghosh et al., 1996; Szmajda et al., 2008) and macaque (Dacey and Packer, 2003; Yamada et al., 2005) retinas. The sample of large sparse ganglion cells is from eccentricities ranging from 0.34 mm to 8.47 mm, corresponding to an eccentricity range of approximately 2 to 73 degrees of visual angle. Examples are shown in Figure 3.2A and Figure 3.3. The majority of their dendrites stratify at 60 to 80 % depth of the inner plexiform layer. A histogram representing the depth levels of dendritic processes for one large sparse cell is shown in Figure 3.4A.

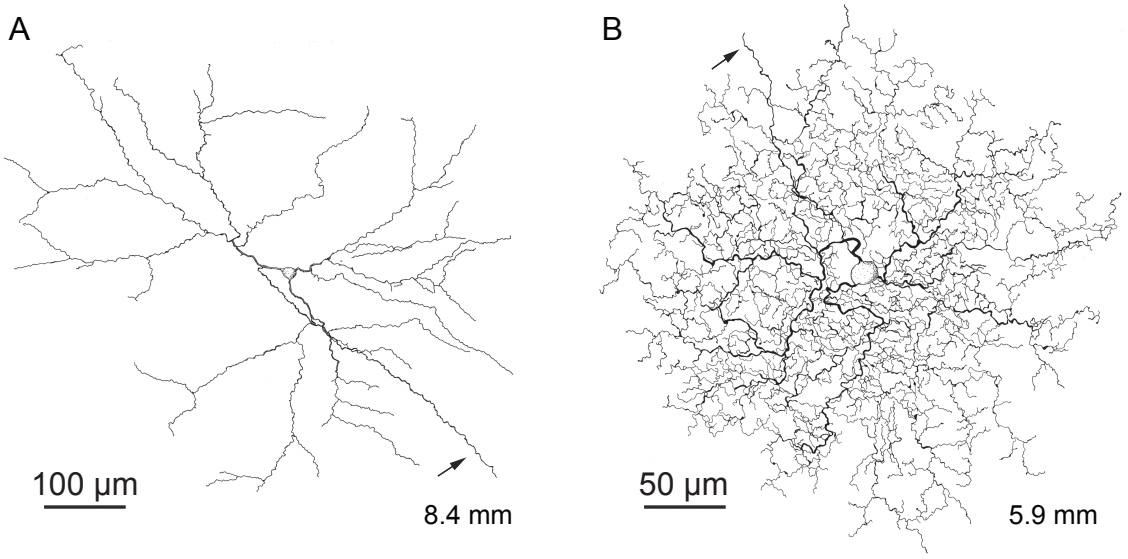


Figure 3.1 Camera lucida drawings of intracellularly injected ganglion cells in marmoset retina. Injections and drawings by Krishna Ghosh (for details see Ghosh et al., 1996). **A**: Sparse cell. **B**: Broad thorny cell. Eccentricities are indicated beneath each cell. Arrows indicate axons.

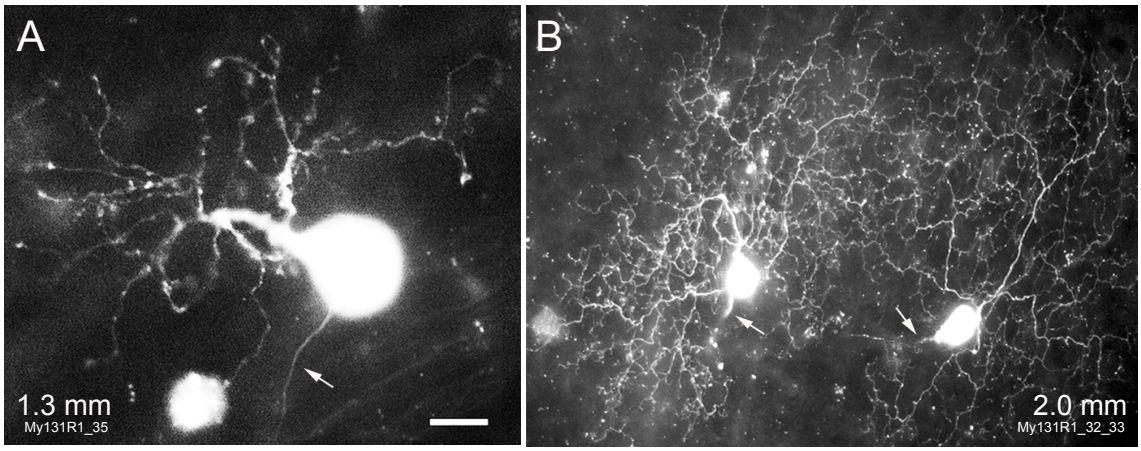


Figure 3.2 Micrographs of retrogradely labelled and photofilled ganglion cells in marmoset retina. **A**: Large sparse cell. **B**: Two adjacent broad thorny cells with overlapping dendritic fields. Eccentricities are indicated beneath each cell. Arrows indicate axons. Scale bar applies to both panels but = 10 μm in A and 20 μm in B.

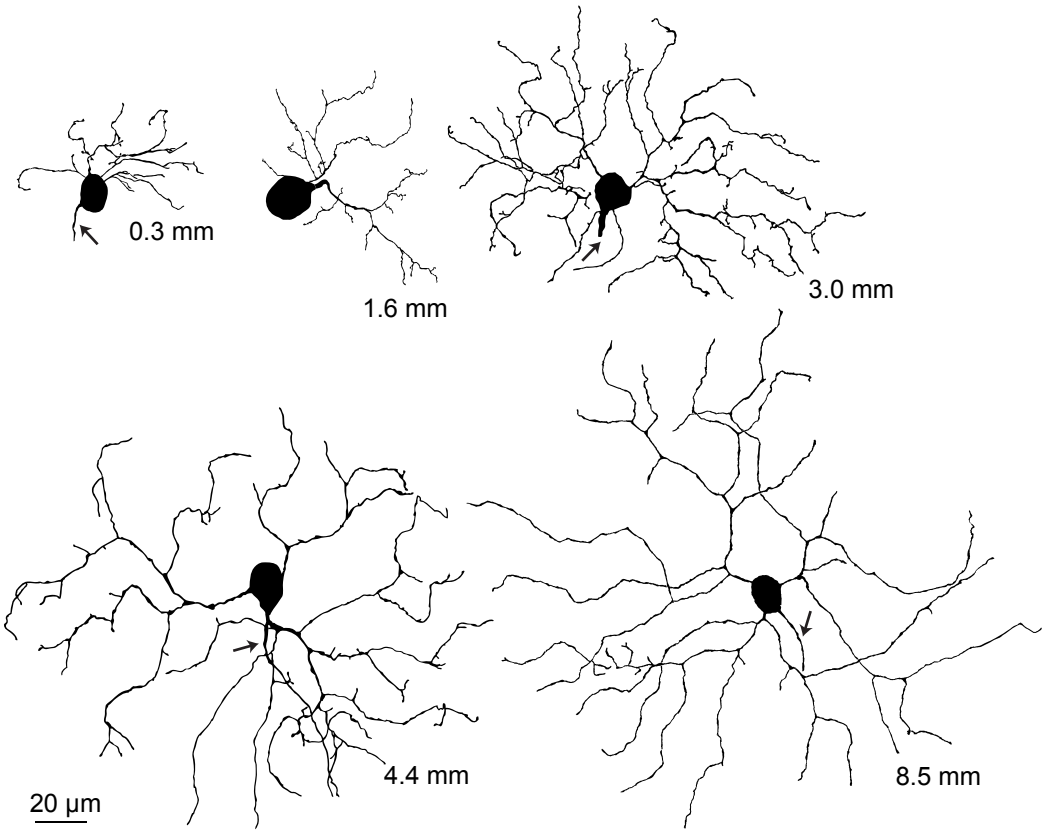


Figure 3.3 Drawings of retrogradely labelled large sparse ganglion cells. Eccentricities are indicated beneath each cell. Arrows indicate axons.

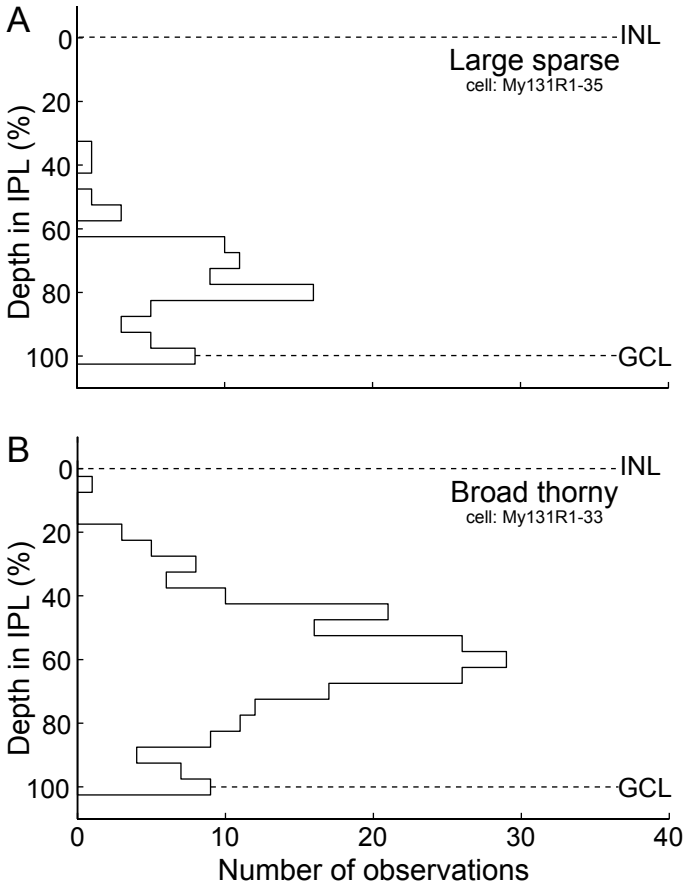


Figure 3.4 Histograms representing dendritic stratification for one large sparse (**A**), and one broad thorny ganglion cell (**B**). Micrographs of these cells are shown in Figure 2A, B.

Broad thorny ganglion cells

As described previously in marmoset (Ghosh et al., 1996; Szmajda et al., 2008) and macaque (Dacey and Packer, 2003; Yamada et al., 2005) retina, broad thorny ganglion cells have fine, densely branching dendrites with thorn-like protrusions at irregular intervals (Figures 3.1B, 3.2B). Analysed cells are from eccentricities between 2.00 - 4.89 mm, which corresponds to approximately 16 to 39 degrees of visual angle. Dendrites of broad thorny cells are broadly stratified in the inner plexiform layer with a stratification range of approximately 30 to 85%. Dendritic stratification levels are illustrated for one broad thorny cell in Figure 3.4B. It was found that for two adjacent broad thorny cells, the dendritic fields showed some degree of overlap (Figure 3.5). The degree of overlap for the two broad thorny cells shown in Figure 3.5 is 11.089 and 10.155 % for the cell to the left and right respectively. In their study of wide-field ganglion cells in macaque monkey, Dacey et al. (2010) have estimated the proportion of broad thorny ganglion cells to be approximately 1.5 % of all ganglion cells. Assuming the proportion of broad thorny ganglion cells in marmoset is similar to that in macaque, the coverage factor (or the number of ganglion cells of a specific type which samples a given point on the retina) is approximately 3.6 (determined using an approximated ganglion cell density of ~15,000 cells / mm^2 for eccentricities of 2 mm in temporal marmoset retina from Wilder et al. (1996)) compared to 1.2 in macaque (Dacey et al., 2010).

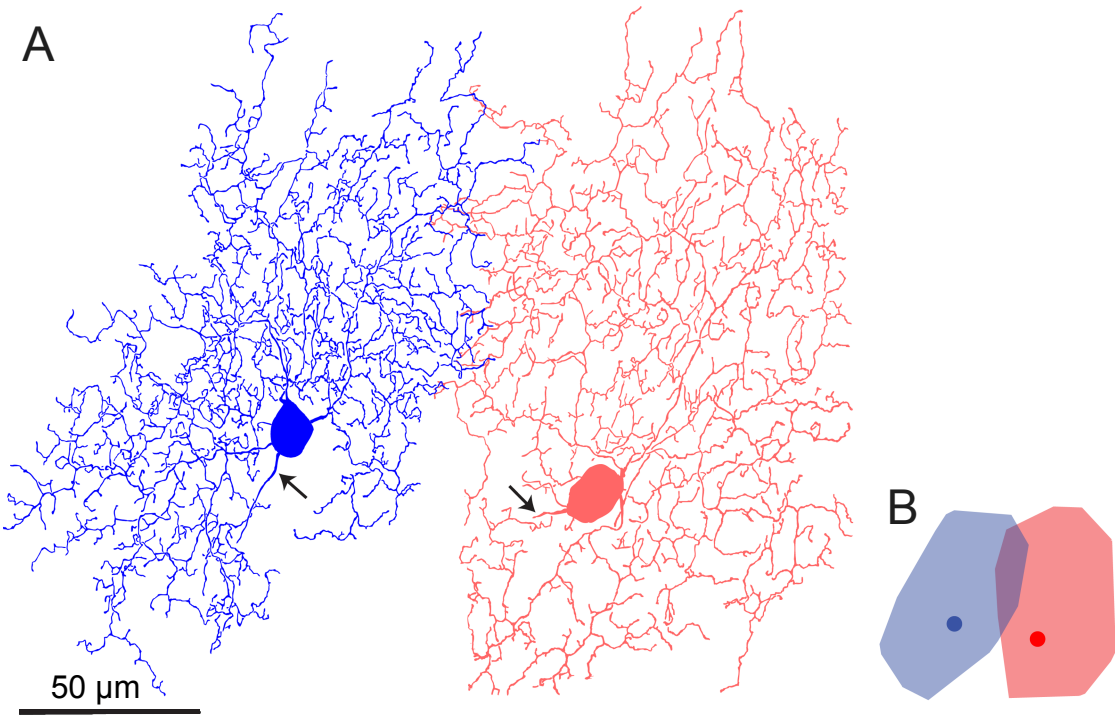


Figure 3.5 Dendritic overlap of broad thorny cells. **A**: Drawing of two adjacent broad thorny cells from 2 mm eccentricity (see also Figure 3.2 B). Arrows indicate axons. **B**: Outlines of the overlapping dendritic fields of the two cells. Degree of overlap for the cell on the left is 11.089 % and for the cell on the right is 10.155 %.

Quantitative comparison of morphology and cone convergence

Large sparse and broad thorny cells have comparable dendritic field diameters, which, as found for other ganglion cell types in primate retina, increase with increasing eccentricities (Figure 3.6A, B). As shown for macaque (see Figure 4 by Dacey and Packer, 2003) and marmoset (see Figure 7A by Szmajda et al., 2008) both cell types have dendritic fields that are larger than that of parasol cells. The number of dendritic branch points was determined for one large sparse cell and one broad thorny cell with similar dendritic field diameter (125 µm and 141 µm respectively). The large sparse cell had 36 branch points, a total dendritic length of approximately 920 µm and a dendritic surface area of approximately 1155 μm^2. The broad thorny cell on the other hand had 399 branch points, a total dendritic length of approximately 3487 µm and a dendritic surface area of approximately 3883 μm^2. Broad thorny cells can therefore have dendritic surface areas three times that of large sparse cells at similar eccentricities despite having similar dendritic field sizes.

In order to estimate the number of cones, which could potentially provide input to large sparse and broad thorny cells, the number of cones lying within the dendritic field was determined. The number of cones located in the dendritic field was correlated with the dendritic field diameter as shown in Figure 3.6B. As large sparse cells have been associated with blue-OFF pathways (Dacey et al., 2003; Szmajda et al., 2008) the number of S-cones in the dendritic field of these cells was estimated for the nine cells studied here. The number of S-cones in the dendritic field increases with eccentricity, and ranges from 5 to 22 S-cones. Thus, these cells could potentially derive substantial S-cone input, but the circuitry connecting S-cones to large sparse cells is yet to be determined.

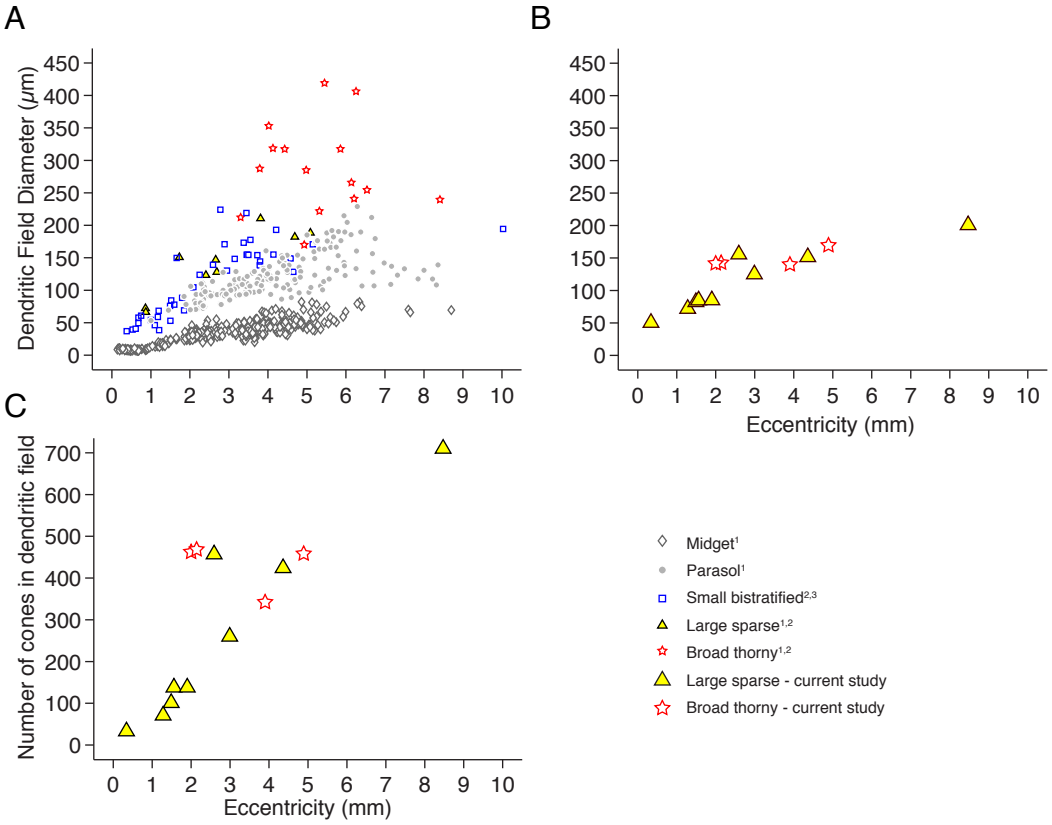


Figure 3.6 A: Dendritic field diameters of ganglion cells from previous studies in marmoset retina (Ghosh et al., 1996; Szmajda et al., 2008; Percival et al., 2009). **B**: Dendritic field diameters of large sparse and broad thorny cells from the current study. **C**: Number of cones in the dendritic fields of large sparse and broad thorny cells from the present study.

Synaptic input to large sparse and broad thorny cells: Qualitative results

As shown previously, antibodies against gephyrin, the glutamate receptor subunit 4 (GluR4), and C-terminal binding proterin 2 (CtBP2) show punctate labelling throughout the inner plexiform layer (gephyrin: Grünert and Wässle, 1993) (GluR4: Grünert et al., 2002) (CtBP2: Jusuf et al., 2006a). Presumed bipolar and/or amacrine input was studied by determining the number of CtBP2 or GluR4 (bipolar input) and/or gephyrin (amacrine input) immunoreactive (IR) puncta that overlapped with dendritic processes. Examples of IR puncta that are colocalised with dendritic processes are seen in Figure 3.7.

All cells show presumed synaptic input throughout the dendritic tree (Figure 3.8 and Figure 3.9), and both presumed amacrine and presumed bipolar synapses were distributed relatively evenly. The spatial relationships between the two kinds of inputs however were not analysed. No obvious changes in the density of IR puncta were observed with increasing dendritic distances from the soma. In the case of broad thorny ganglion cells, presumed input is observed on, but is not restricted to, dendritic thorns. A similar distribution of synaptic inputs onto dendritic thorns as well as remaining dendrites has been reported for alpha ganglion cells in the cat retina (Freed and Sterling, 1988). The functional importance of input to thorns versus other dendritic surfaces in retinal neurons is not clear.

Presumed synapses on both cell types sometimes form clusters, leaving regions of the dendritic tree apparently free of synaptic input. Clusters do not coincide with branch points or with dendritic distance from the soma nor are there any obvious patterns to the regions where inputs were presumably lacking. Similar patterns have been observed in previous studies of melanopsin-containing (Jusuf et al., 2007), parasol (Eriköz et al., 2008; Lin et al., 2002), and small bistratified (see Chapter 2; Percival et al., 2009) ganglion cells. The presence of clusters of bipolar input is most likely correlated with the overlapping regions between ganglion cell dendrites and bipolar axon terminal processes.

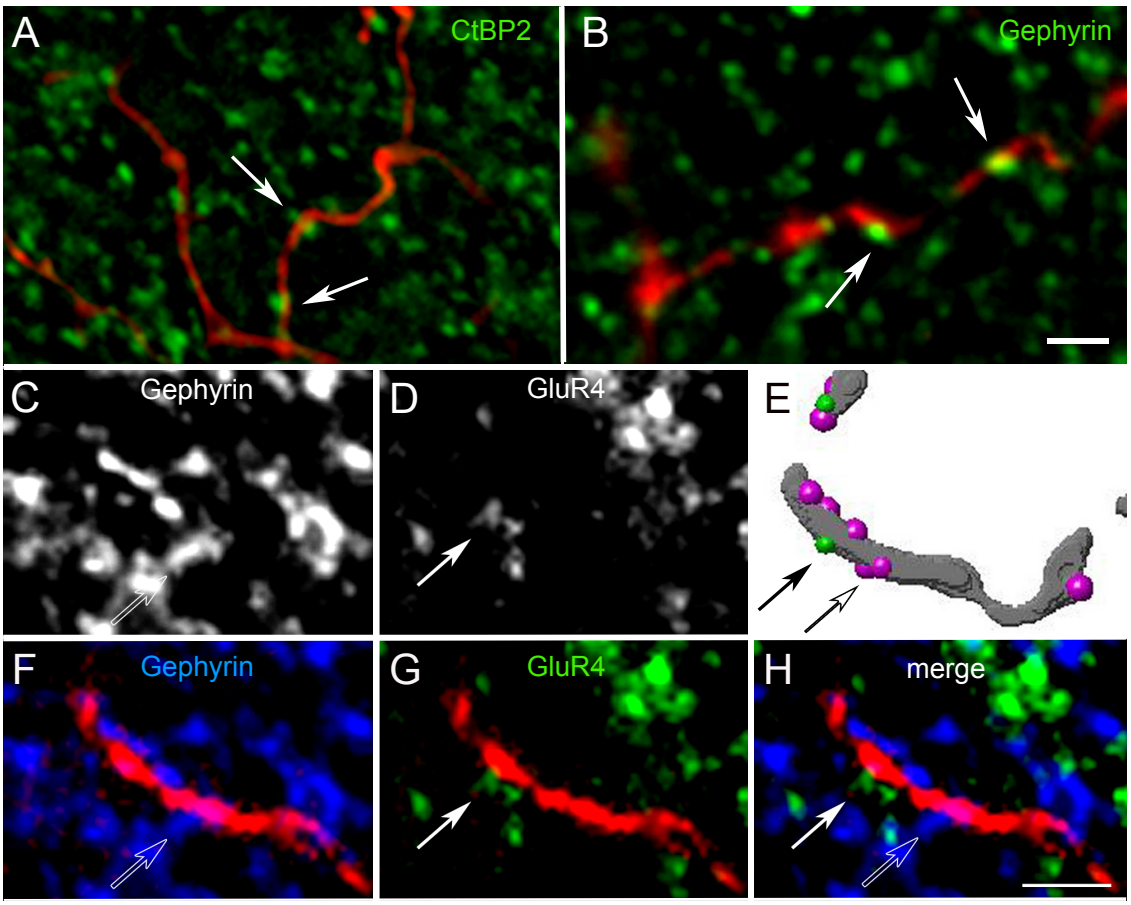


Figure 3.7 Micrographs of double and triple labelled preparations showing excitatory and inhibitory input to retrogradely labelled ganglion cells. Only images representing a single plane of focus are shown. **A**: Dendrites of a broad thorny cell together with C-terminal binding protein (CtBP2) immunoreactive puncta (IR, bipolar input). **B**: Dendrites of a large sparse cell together with gephyrin IR puncta (amacrine input). Arrows point to colocalised IR puncta. Scale bar shown in A = 2 µm (also valid for B). **C**, **D** and **F** - **H**: Dendrites of a broad thorny cell together with IR puncta representing presumed bipolar (AMPA receptor subunit GluR4) and amacrine (gephyrin) input. Open arrows point to colocalised gephyrin IR puncta; filled arrows point to GluR4 IR puncta. In some cases, labelling of IR puncta may be seen to lie largely outside of the dendrite; this may be due to the amplification of the synaptic marker signal particularly on the extracellular side, or due to the level of focus shown. Scale bar shown in H = 2 µm (also valid for C, D, F, G). **E**: Reconstruction of a single dendrite from the dendritic tree of a broad thorny cell (grey). Colocalised gephyrin IR puncta are shown in purple, colocalised GluR4 IR puncta are shown in green.

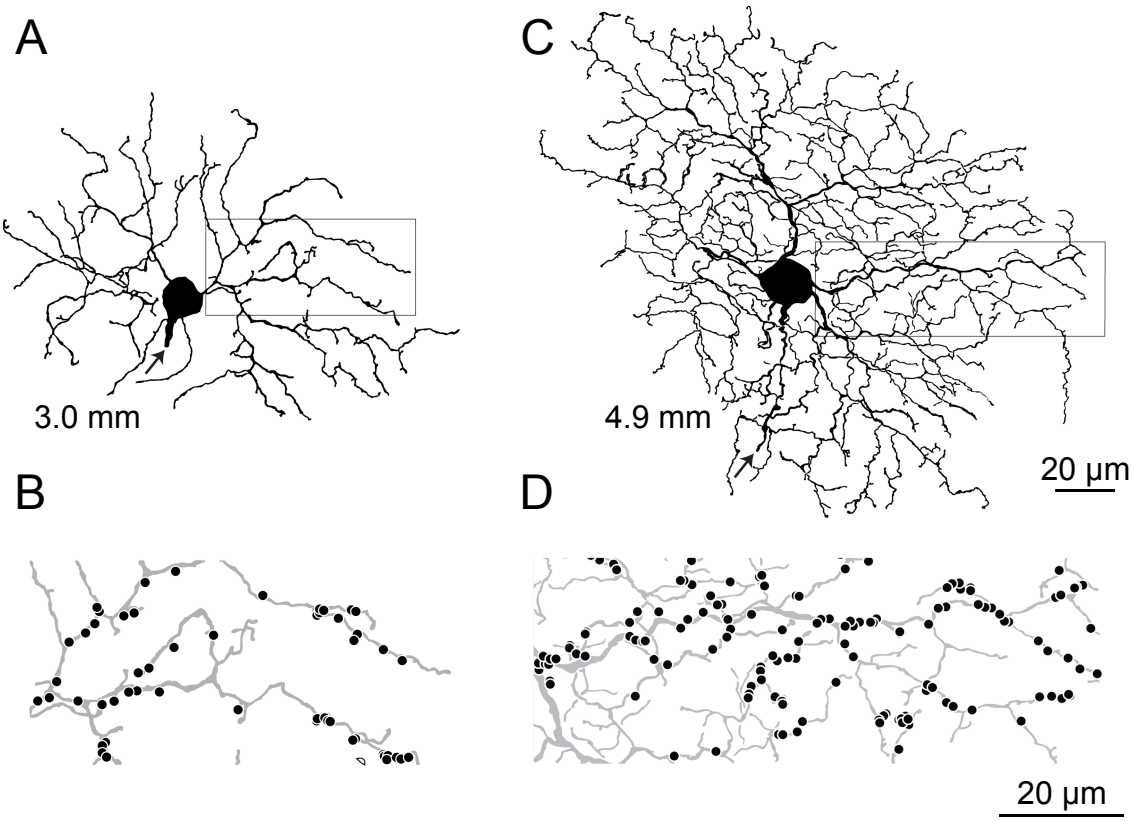


Figure 3.8 Distribution of presumed bipolar (excitatory) inputs across the dendritic field. Tracings of a large sparse (**A**, **B**) and a broad thorny ganglion cell (**C**, **D**) together with colocalised C-terminal binding protein 2 (CtBP2) immunoreactive (IR) puncta are shown. The rectangles in A and C indicate the regions shown in B and D. Scale bar shown in C is also valid for A. Scale bar shown in D is also valid for B. Eccentricities are indicated beneath each cell. Arrows indicate axons.

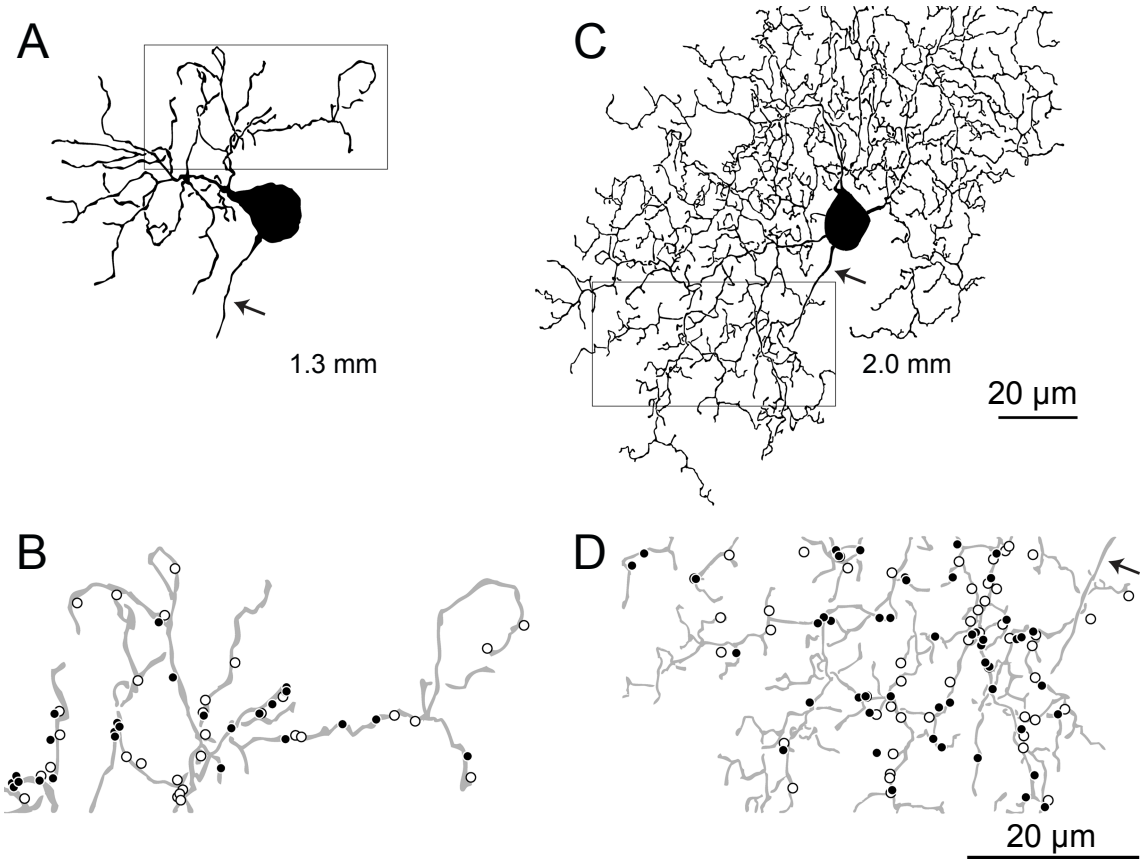


Figure 3.9 Distribution of presumed bipolar and amacrine inputs across the dendritic field. Tracings of a large sparse (**A**, **B**) and a broad thorny ganglion cell (**C**, **D**) together with colocalised GluR4 (filled circles) and gephyrin (open circles) immunoreactive (IR) puncta (B) are shown. A drawing of the entire cell in C is shown in Figure 3.5 A. The rectangles in A and C indicate the regions shown in B and D. Scale bar shown in C is also valid for A. Scale bar shown in D is also valid for B. Eccentricities are indicated beneath each cell. Arrows indicate axons.

Synaptic input: Quantitative results

Large sparse ganglion cells

The quantitative data are summarised in Table 3.4. The total number of presumed bipolar input to large sparse ganglion cells increases with increasing dendritic field size. To allow for comparisons between cells of different sizes, densities of presumed bipolar inputs were obtained with respect to dendritic surface area. Average densities (± SD) were calculated across all sampled regions. An average density of 3.0 ± 1.5 IR puncta per 100 μm^2 for GluR4 and 4.5 ± 2.2 IR puncta per 100 μm^2 for CtBP2 was found. The lower density obtained for GluR4 IR puncta with comparison to CtPB2 IR puncta may be explained by the fact that the antibody against CtBP2 labels ribbons at all bipolar cell synapses, whereas the antibody against GluR4 recognizes a single glutamate receptor subunit type.

The estimated total number of presumed amacrine cell input to large sparse cells at eccentricities between 0.3 mm and 1.9 mm (five cells) ranges from 22 to 63. For these cells an average of 3.5 ± 2.0 gephyrin IR puncta per 100 μm^2 was found. For three cells from eccentricities of 0.3, 1.3 and 1.5 mm labelling for both GluR4 and gephyrin allowed direct within-cell comparisons of presumed bipolar and amacrine cell inputs. In these three cells, an average ratio of bipolar to amacrine cell input of about 1:1 was obtained (Table 3.4). This proportion of presumed bipolar input changes from approximately 46 % to 56 % when the average density results for CtBP2 IR puncta are taken into account (see Table 3.4).

Table 3.4 Synaptic input onto large sparse and broad thorny ganglion cells

				Presumed bipolar cell input (CtBP2 or GluR4)				Presumed amacrine cell input (Gephyrin)			
Cell number	Cell type	Eccentri-city (mm)	Dendritic field diameter (µm)	Total number	Per 100 µm^2 of dendritic surface area (Av. ± SD)	Number of regions analysed	Proportion of total input (%)	Total number	Per 100 µm^2 of dendritic surface area (Av. ± SD)	Number of regions analysed	Proportion of total input (%)
My131R1-29	Large sparse	0.34	50.3	16 (GluR4)	2.3 ± 0.6	3	42.0	22	2.3 ± 2.1	3	58.0
My131R1-35	Large sparse	1.28	71.8	57 (GluR4)	3.2 ± 1.7	5	47.5	63	3.8 ± 2.0	5	52.5
My131R1-18	Large sparse	1.49	82.2	52 (GluR4)	3.1 ± 1.7	8	57.1	39	2.7 ± 1.6	8	42.9
My124R1-04	Large sparse	1.56	84.8	n.d.	n.d.	n.d.	n.d.	45	5.4 ± 1.6	7	n.d.
My124R1-05	Large sparse	1.90	85.1	n.d.	n.d.	n.d.	n.d.	56	n.d.	n.d.	n.d.
My115L1-F03	Large sparse	2.99	125.0	317* (CtBP2)	4.5 ± 2.2	15	n.d.	n.d.	n.d.	n.d.	n.d.
Average	**Large sparse**			**GluR4**	**3.0 ± 1.5**	**16**	**46.2**	**Gephyrin**	**3.5 ± 2.0**	**23**	**53.8**
Average	**Large sparse**			**CtBP2**	**4.5 ± 2.2**	**15**	**56.2**				**43.8**
Average	**Large sparse**			**GluR4 + CtBP2**	**3.7 ± 2.0**	**31**	**51.4**				**48.6**
My131R1-32	Broad thorny	2.00	142.8	110* (GluR4)	2.4 ± 0.3	6	50.0	110*	2.3 ± 0.8	6	50.0
My131R1-33	Broad thorny	2.14	143.7	125* (GluR4)	3.1 ± 0.8	6	57.9	91*	2.3 ± 0.9	6	42.1
My115R1A-12	Broad thorny	3.90	141.1	237* (CtBP2)	5.6 ± 2.3	6	n.d.	n.d.	n.d.	n.d.	n.d.
My115R1A-20	Broad thorny	4.89	170.7	199* (CtBP2)	5.1 ± 1.9	6	n.d.	n.d.	n.d.	n.d.	n.d.
Average	**Broad thorny**			**GluR4**	**2.8 ± 0.7**	**12**	**54.9**	**Gephyrin**	**2.3 ± 0.8**	**12**	**45.1**
Average	**Broad thorny**			**CtBP2**	**5.4 ± 2.0**	**12**	**70.1**				**29.9**
Average	**Broad thorny**			**GluR4 + CtBP2**	**4.1 ± 2.0**	**24**	**63.5**				**36.5**

* Approximately a third of the dendritic field was analysed.

Average (Av.), standard deviation (SD), not determined (n.d.)

Broad thorny ganglion cells

Analyses of four broad thorny ganglion cells were run on six adjacent regions of the dendritic tree for each cell. The average density (± SD) of presumed bipolar input is 2.8 ± 0.7 IR puncta per 100 μm^2 for GluR4 and 5.4 ± 2.0 IR puncta per 100 μm^2 for CtBP2 (Table 3.4). Thus, as was for the sparse cells, the density of colocalised GluR4 IR puncta is lower than that of CtBP2. At this stage the possibility that, with the antibody against GluR4 some bipolar synapses are missed (see above) cannot be ruled out, however this is the only antibody that currently allows for the simultaneous localisation of excitatory and inhibitory synapses. The average density for presumed amacrine input is 2.3 ± 0.8 gephyrin IR puncta per 100 μm^2. For two cells where the presumed amacrine and bipolar input was compared directly, the proportion of presumed bipolar input is approximately 55% (Table 3.4), when the averages for the CtBP2 IR puncta are used the proportion increases to 70% (Table 3.4).

Feedforward synapses

The percentage of potential feedforward synapses for three large sparse cells and 12 dendritic regions from two broad thorny cells was determined (see methods). For the large sparse cells, 7, 12 and 15% of the colocalised gephyrin IR puncta was found to be located within 1 μm of a colocalised GluR4 IR punctum. Similar numbers were found for dendritic regions from two broad thorny ganglion cells, where 10 and 16 % of the colocalised gephyrin IR puncta was located within 1 μm of a colocalised GluR4 IR punctum. Thus, for both cell types approximately 10 to 15 % of amacrine cell synapses may provide feedforward synapses onto the ganglion cell.

Relationship between large sparse ganglion cells and DB6 cells

The possible relationship between large sparse ganglion cells and diffuse bipolar type 6 (DB6) cells has been suggested in a previous study where it was shown that processes from the two cell types have some points of intersection (Szmajda et al., 2008). In the present study these regions of overlap were analysed in detail using retinal preparations containing retrogradely labelled large sparse ganglion cells which were processed with the antibody against the carbohydrate epitope (CD15). Consistent with

previous studies, in marmoset retina, the CD15 antibody labels two types of bipolar cells - namely flat midget bipolar and DB6 cells (Chan et al., 2001; Jusuf et al., 2004). The two bipolar cell types can be distinguished by their axon terminal stratification. Axon terminals of flat midget bipolar cells stratify in the OFF sublamina of the inner plexiform layer whereas the axon terminals of DB6 cells stratify close to the ganglion cell layer. Figure 3.10A-C show labelling of dendritic processes of large sparse ganglion cells together with axon terminal processes of DB6 cells.

The number of DB6 axon terminals lying within the dendritic field, and the number of DB6 axon terminals that overlap with the dendrites were determined for three large sparse cells. The quantitative results are summarised in Table 3.5. On average, 81 % of DB6 cell axon terminals lying within the dendritic fields of large sparse ganglion cells overlap with dendritic processes and all of these axon terminals also show three-dimensional colocalisation as determined by focusing through image stacks. For example the cell shown in Figure 3.10D, E has 26 DB6 axon terminals in its dendritic field. Of these 26 axon terminals, all 22 terminals with processes that overlap with the dendritic tree in two-dimensional view also form presumed contact areas (or three-dimensional colocalisations).

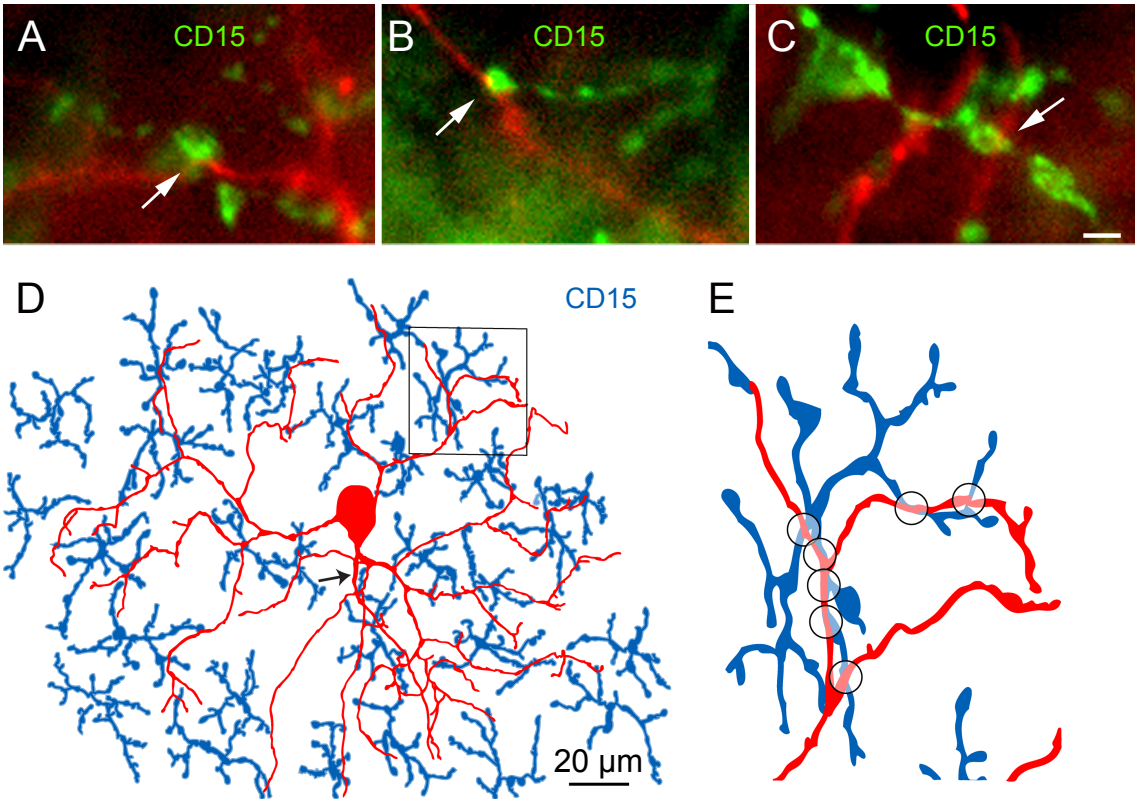


Figure 3.10 Relationship between dendrites of a large sparse ganglion cell and axons terminals of DB6 cells. **A** - **C**: Dendrites of a large sparse cell together with CD15 labelled axon terminals of DB6 bipolar cells. Arrows indicate presumed contact areas. Scale bar shown in C = 2 µm also valid for A and B. **D**: Tracings of a large sparse cell at 4.4 mm eccentricity together with the axon terminals of CD15 labeled DB6 bipolar cells. In total 26 DB6 axon terminals are located within the dendritic field of this large sparse cell and 22 axon terminals overlap with its dendrites. **E**: Potential areas of contact, as detected in three-dimensional space, are indicated by circles, for the region outlined in D.

The total number of presumed contact areas formed by DB6 axons onto large sparse cells is lower than the total presumed bipolar input as determined by using synaptic markers. For example, for a large sparse cell from approximately 3 mm eccentricity there are 317 CtBP2 IR puncta located close to its dendrites (Table 3.4), whereas a cell from 2.6 mm eccentricity with a similar dendritic field size has only 30 potential contact areas with DB6 axons (Table 3.5). Each contact area probably involves multiple synaptic sites, and thus the number of contact areas most likely is an underestimate of the bipolar input to sparse cells. Furthermore, it is possible that other yet to be determined bipolar types provide input to large sparse ganglion cells. The average number of presumed contact areas made by individual DB6 axon terminals with a single large sparse cell increases slightly with eccentricity (Table 3.5) but this number is lower than the number of presumed DB6 output synapses (~40 per DB6 axon terminal) estimated in central retina (Grünert et al., 2003). This finding is consistent with the idea that DB6 cells contact amacrine cells as well as other ganglion cell types (Grünert et al.; Jusuf et al., 2004; Jusuf et al., 2007).

Table 3.5 - Presumed synaptic sites between large sparse ganglion cells and DB6 bipolar cells

			Number of DB6 axon terminals		Presumed contact areas	
Cell number	Eccentricity (mm)	Dendritic field diameter (µm)	within dendritic field	overlapping dendrites	per ganglion cell	per DB6 axon terminal (Av. ± SD)
My103L1-F03	2.59	155.7	15	12	30	1.8 ± 1.8
My109L2-F16	4.36	151.4	26	22	70	2.5 ± 2.0
My104L2-F06	8.47	200.7	28	22	67	2.8 ± 2.0

Average (Av.), standard deviation (SD)

As a further test for DB6 inputs onto large sparse ganglion cells, the percentage colocalisation between pixels from image channels representing dendritic labelling of large sparse cells and DB6 axon terminal processes was determined in Imaris (see Methods). In the veridical image orientation, 15 – 25 % of pixels representing the dendrites of large sparse ganglion cells (n = 3 cells) are colocalised with those from the image channel representing DB6 labelling. In the flip control, only 3 – 13 % of pixels representing large sparse dendrites are colocalised with those from the image channel representing DB6 labelling. The mean Pearson's correlation coefficient was 0.23 ± 0.12

for veridical orientations and -0.05 ± 0.08 for flipped image orientations. The higher colocalisation values for veridical image orientations compared to control values provide support for DB6 axon terminal processes providing at least some of the input onto large sparse ganglion cells.

Taken together results here indicate that DB6 cells may be responsible for some but not all of the bipolar input to large sparse ganglion cells. However, triple labelling involving a synaptic marker and/or electron microscopy will be necessary to confirm this conclusion.

3.4 *Discussion*

Here it is shown that the large sparse and the broad thorny cell type in marmoset retina, despite showing contrasting dendritic morphology and stratification, have similar densities of bipolar and amacrine inputs. The current findings are consistent with light microscopic (rabbit: Jakobs et al., 2008; Jeon et al., 2002; mouse: Morgan et al., 2008; guinea pig: Xu et al., 2008) and electron microscopic studies (macaque: Bordt et al., 2006; rabbit: Famiglietti, 2005; cat: Freed and Sterling, 1988; Kier et al., 1995; Owczarzak and Pourcho, 1999) showing that different types of retinal ganglion cells across mammalian species to have comparable densities of bipolar input. The finding that the two cell types investigated here differ with respect to their dendritic surface area but receive synaptic input with a similar density is in support of the view that the amount of dendritic surface area available may govern the number of synaptic inputs made onto a ganglion cell (Xu et al., 2008).

Because broad thorny cells have a larger dendritic surface area, they receive more total synaptic input than do large sparse cells. Xu et al. (2008) have previously postulated functional implications of overall differences in the number of bipolar inputs between ganglion cell types. The authors suggest that a higher number of bipolar inputs onto a ganglion cell may provide this cell with an increased sensitivity to visual stimuli. This hypothesis would predict that broad thorny cells show high luminance sensitivity. However, physiological recordings addressing this hypothesis are still lacking.

Differences between ganglion cell types

The density of the bipolar input to different ganglion cell types described previously ranged from 8 to 45 synapses per 100 μm dendritic length or between 13 and 30 per 100 μm^2 dendritic membrane area (primate: Bordt et al., 2006; Eriköz et al., 2008; rabbit: Famiglietti, 2005; cat: Freed and Sterling, 1988; Jakobs et al., 2008; Jeon et al., 2002; Kier et al., 1995; Lin et al., 2002; mouse: Morgan et al., 2008; Owczarzak and Pourcho, 1999; guinea pig: Xu et al., 2008).

The estimates of bipolar input density obtained in the present study were compared with previous measurements obtained for midget, parasol (Eriköz et al., 2008) and small bistratified cells (Chapter 2; Percival et al., 2009) using the same methods. Figure 3.11 shows, for cells processed with the C-terminal binding protein (CtBP2; ribbon marker) antibody that the density varies by a factor of approximately twofold across six cell types compared. Although this difference is overall significant ($p < 0.01$, Kruskal-Wallis non-parametric analysis of variance), post-hoc comparison showed this is because small bistratified cells have lower synaptic density than midget cells ($p < 0.05$, f statistic); no significant differences are present between other cell groups. In other words, variation in synaptic input density *between* cell types is close to the variation *within* a single type. In summary, the current results are consistent with general mechanisms governing synaptic density across ganglion cell populations, rather than specific mechanisms linking synaptic density to functional properties such as contrast sensitivity.

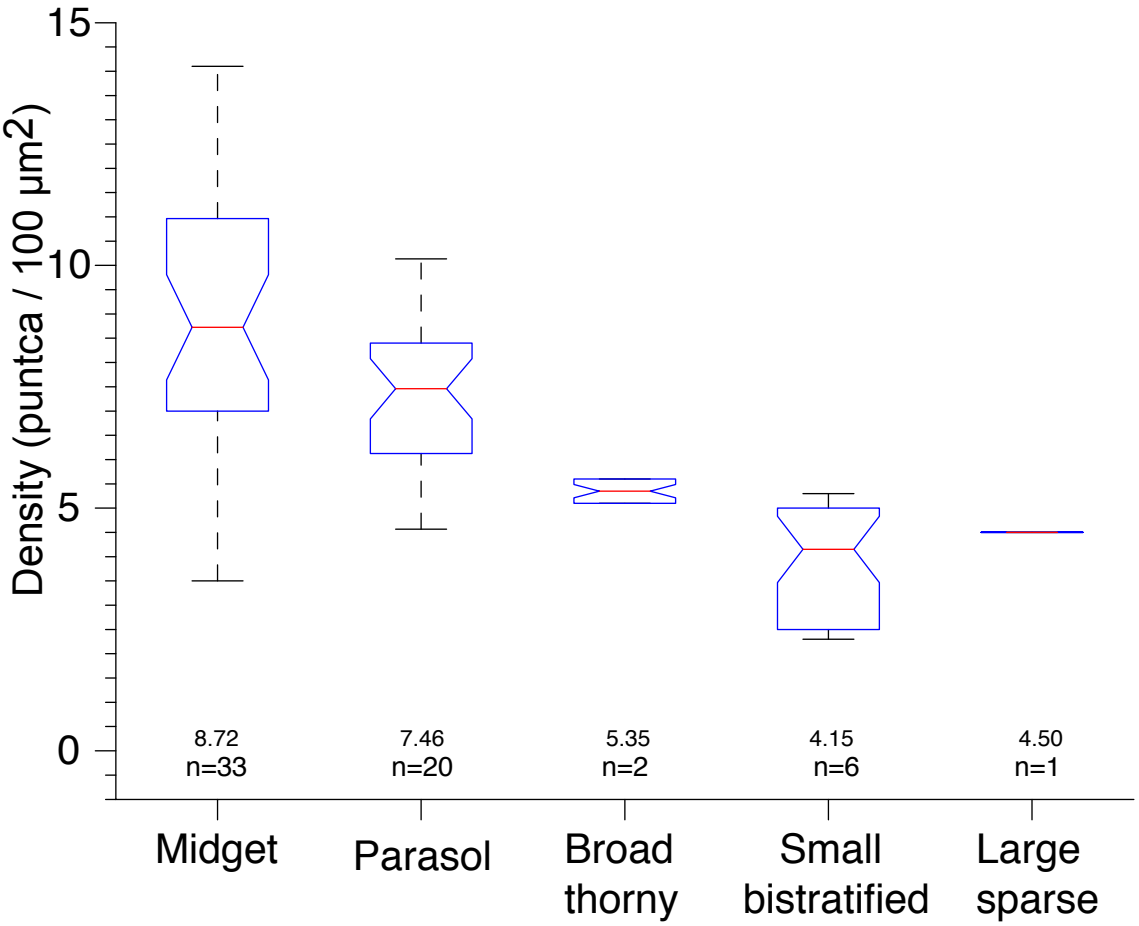


Figure 3.11 Box plot comparing bipolar input density across two ganglion cell types (broad thorny and large sparse) measured in the current study, and three types (midget, parasol, and small bistratified or SBS) measured in our previous studies using the same techniques (Eriköz et al., 2008; Percival et al., 2009). Cell types are sorted in descending order of median synaptic density. For each type the central mark shows the median, the edges of the box are the 25th and 75th percentiles, and the dotted lines show the data range. Median density and number of cells measured (n) are shown for each type.

Relationship between bipolar and amacrine input

In the present study the presumed amacrine and bipolar input was compared directly for three large sparse and two broad thorny cells, all of which showed similar densities of bipolar and amacrine cell inputs. Assuming equal weighting of each synapse, large sparse and broad thorny ganglion cells can be thought to receive balanced excitation and inhibition. In this respect the two cell types are comparable to a number of fully reconstructed foveal midget ganglion cells in human and macaque retinas (Calkins et al., 1994; Kolb and Dekorver, 1991) using electron microscopy. They are also similar to one midget ganglion cell (Eriköz et al., 2008) and five small bistratified cells (Chapter 2;Percival et al., 2009) from central retina in marmoset retina analysed using the same methods as in the present study. The method used here may have resulted in the underestimation of inputs as these ganglion cells may express glutamate receptors that do not contain the glutamate receptor subunit 4 (GluR4) or GABA/glycine receptors that are not anchored by gephyrin. It has been shown previously, however, that the large majority of puncta immunolabelled with the antibody against GluR4 are also labelled with antibodies against ribbon proteins (Jusuf et al., 2006a) and thus antibodies against GluR4 are thought to be suitable markers for most bipolar synapses (Hoshi et al., 2009). Gephyrin is considered to be associated with the large majority of glycine and $GABA_A$ receptors (Sassoè-Pognetto et al., 1995). In conclusion, it can be assumed that markers used here are a valid (but not perfect) estimate of the excitatory and inhibitory inputs.

For primate midget, parasol and small bistratified cells it has been suggested that there may be eccentricity related differences in the ratio of amacrine to bipolar input (reviewed by Bordt et al., 2006; Eriköz et al., 2008). No eccentricity related differences were seen in the sample of large sparse and broad thorny cells analysed (Table 3.4).

The proportion of bipolar input varied for different ganglion cell types in EM studies of foveal macaque retina. One small bistratified cell (Calkins et al., 1998) and one OFF parasol cell (Calkins and Sterling, 2007) received the majority (60 and 70%, respectively) of their input from bipolar cells, whereas one garland cell (Calkins and Sterling, 2007) received only 30% of its input from bipolar cells. In peripheral retina, low percentages of bipolar input (about 20%) were found for five partially reconstructed ON parasol cells in baboon (Jacoby et al., 1996), two small bistratified cells in marmoset

(Ghosh and Grünert, 1999) and one OFF parasol cell in macaque (Bordt et al., 2006). In cat retina, differences in the proportion of bipolar and amacrine inputs have been reported for ganglion cells of the same type. For alpha cells bipolar inputs have been reported to make up 50% (Watanabe et al., 1985), 14%, 33% (Freed and Sterling, 1988), 20% (Kolb and Nelson, 1993), 38% (Weber and Stanford, 1994), and 11% (Owczarzak and Pourcho, 1999) or synaptic inputs. For cat beta cells, the proportion of bipolar input has been reported at 36 to 38% (Watanabe et al., 1985), 38% (Kolb and Nelson, 1993) and 51% (Weber and Stanford, 1994) of the total synaptic input.

These differences in ratios may partially be explained by differences in the criteria used to define synapses and problems in identifying postsynaptic densities in the labelled ganglion cell dendrites. However, taken together data from primate and cat ganglion cells seem to indicate that there is no consistent pattern with respect to the ratio of amacrine to bipolar input for different ganglion cell types. Thus, one may conclude that the percentage of bipolar input does not play a crucial role for the distinct functional properties of different ganglion cell types.

Feedforward synapses

A previous study using electron microscopy found that in the midget pathway of macaque retina, just over half (58%) of the amacrine synapses to midget ganglion cells are feedforward synapses, i.e. they are formed by processes that are postsynaptic to the same midget bipolar cell that contacts the midget ganglion cell (Calkins and Sterling, 1996). In contrast, small bistratified cells (Calkins et al., 1998) and parasol cells (Marshak et al., 2002) only rarely receive feedforward synapses.

In the present study it was estimated that for broad thorny and large sparse cells, 10 to 15% of amacrine synapses are feedforward synapses. It was assumed that gephyrin and GluR4 immonureactive (IR) puncta that are colocalised with the labelled ganglion cell dendrite and are located close (less than 1 μm) to each other, may represent feedforward synapses. These proportions may be overestimates as counts may include gephyrin IR puncta that are postsynaptic to small amacrine cell processes which are not postsynaptic to the same bipolar terminal.

Cell types providing input to large sparse cells

In vitro recordings in macaque retina have suggested that large sparse ganglion cells possess a blue-OFF/yellow-ON response (Dacey and Packer, 2003; Dacey et al., 2003) however, the underlying retinal circuitry giving rise to the response pattern observed is still unknown. The yellow-ON component of the response may arise from diffuse bipolar type 6 (DB6) cells whose dendrites receive the large majority of their input from long (L) and medium (M) wavelength sensitive cones (Lee and Grünert, 2007) and whose axon terminals have been shown to co-stratify with dendrites of large sparse ganglion cells in stratum 5 (S5) of the inner plexiform layer (Szmajda et al., 2008). In the current study, sites of potential synaptic contact between axonal processes of DB6 cells and dendritic processes of large sparse ganglion cells, were found at a percentage higher than chance. Similar areas of overlap have been observed between DB6 axon terminals and inner stratifying melanopsin labelled ganglion cells in the presence of a synaptic marker (Grünert et al.). Taken together, the results of the present study indicate that DB6 cells provide at least some of the bipolar input to large sparse cells.

In macaque and human retina at least 24 amacrine cell types have been described in Golgi preparations (Kolb et al., 1992; Mariani, 1990). Amacrine types with processes in S5 include the A5 (or knotty type 3), A13, A14 (or wavy multistratified), A17 (or spidery), the semilunar type3 and the wooly type (Kolb et al., 1992). Nothing is known about the connectivity of these amacrine cell types in primates. In cat retina, the A13 and A17 types have been shown to not make output synapses onto ganglion cells in the ON sublamina (Kolb and Nelson, 1983; 1996) which make them unlikely candidates for providing inputs onto large sparse cells. Whether or not, the other amacrine cell types listed provide inputs to large sparse cells remains to be determined.

Bipolar types providing input to broad thorny cells

For the sample of broad thorny ganglion cells analysed, inputs were not segregated to any particular sublamina of the inner plexiform layer, but rather found on dendrites of all depths. Given this, it seems highly likely that broad thorny ganglion cells receive inputs from both ON and OFF type bipolar cells stratifying close to the center of the inner plexiform layer. Consistently, transient ON-OFF responses of broad thorny cells have

been reported in "initial recordings" from these cells in macaque retina (Dacey, 2004). Bipolar types stratifying at the level of broad thorny cell dendrites include ON and OFF midget bipolar cells and diffuse bipolar (DB) types DB2, DB3, DB4, and DB5 (Boycott and Wässle, 1991; Chan et al., 2001). Midget bipolar cells exclusively contact midget ganglion cells (Calkins et al., 1994; Jusuf et al., 2006a; Jusuf et al., 2006b; Kolb and Dekorver, 1991) and can therefore be ruled out as sources of bipolar input onto broad thorny cells. DB2 and DB3 cells contact OFF parasol cells (Jacoby and Marshak, 2000; Jacoby et al., 2000) as well as small bistratified cells (Calkins et al., 1998; Ghosh et al., 1997) however, since they have rather extensive axon terminal systems they could potentially also provide OFF input to broad thorny cells. The ON input may derive from DB4 and/or DB5 cells, both of which have been suggested to contact ON parasol cells (Wässle, 1999).

Conclusion

Results of the current study are consistent with the idea that the differences in the physiological properties of different ganglion cell types are likely to be shaped from the properties of the presynaptic cells rather than a unique "fingerprint" of receptor expression by each functional class of ganglion cell (DeVries, 2000; Freed, 2000).

Chapter 4 Wide-field ganglion cells in foveal retina

4.1 *Introduction*

This chapter investigates the anatomical basis for the contributions of non-midget, non-parasol pathways to vision at the fovea. As outlined in Section 1.7 (page 35), the fovea is characterised by gross anatomical features such as the close packing of cones at the foveola, the lateral displacement of postreceptoral neurons and the absence of inner retinal blood vessels. The following section will discuss some aspects of what is currently known about the retinal circuitry within the fovea, and how these findings may point to the possible involvement of wide-field ganglion cell pathways in foveal vision.

Our current knowledge on ganglion cells within the fovea, support the potential involvement of wide-field ganglion cells in foveal vision. Midget and parasol ganglion cells have been estimated to make up 73 - 80 % (Calkins et al., 1992; Perry et al., 1984) and 5.8 % (Grünert et al., 1993) of all ganglion cells within the fovea respectively. Based on these figures, there are potentially 21.1 - 14.2 % of ganglion cells which are wide-field type ganglion cells. Consistently, a number of previous anatomical (Perry and Cowey, 1984; Stone and Johnston, 1981) and physiological (de Monasterio and Gouras, 1975; Gouras, 1969; Schiller and Malpeli, 1978) studies have reported the presence of ganglion cells that are morphologically and physiologically unrelated to midget and parasol ganglion cells.

A further point to consider in the contribution of non-midget pathways to foveal vision is the outputs of cones residing in the fovea. While cone to bipolar cell divergence is lowest at the fovea, previous studies have reported the presence of at least 2.5 - 3 bipolar cells per cone (Ahmad et al., 2003; Krebs and Krebs, 1989; Martin and Grünert, 1992; Missotten, 1974). This leaves room for cones to connect to bipolar cell types other than the flat and invaginating midget bipolar cells, namely the diffuse cone bipolar cells. The diffuse bipolar type 2 (DB2) and DB3 cells have been shown to connect to the outer tiers of small bistratified ganglion cells (Calkins et al., 1998), in addition to providing inputs onto OFF type parasol cells (Bordt et al., 2006; Calkins and Sterling, 2007; Jacoby and Marshak, 2000; Jacoby et al., 2000). In addition, light microscopy studies have

suggested that the large sparse and giant sparse / melanopsin-containing wide-field ganglion cell types receive inputs from the DB6 type diffuse bipolar cell type (see Chapter 2; Grünert et al., 2011; Szmajda et al., 2008). Thus, if the third post-synaptic partner at a foveal cone is a diffuse bipolar cell type, it may be possible that that particular diffuse bipolar cell provides input to a wide-field ganglion cell in the inner plexiform layer, thereby completing the circuit for the involvement of wide-field ganglion cells to foveal vision. As further support for the involvement of diffuse bipolar cells in the retinal circuitry subserving foveal vision, densities of approximately 10,000 and 23,000 cells / mm^2 have been reported for ON and OFF type diffuse bipolar cells at eccentricities of 480 - 640 μm in macaque retina (Ahmad et al., 2003).

The present study aimed to build on the current understanding of the possible contributions of wide-field ganglion cells to foveal vision. The involvement of a subset of diffuse bipolar cell types, thought to provide inputs onto wide-field ganglion cells, was confirmed by the use of immunohistochemical markers in marmoset and macaque foveal retina. Three types of previously described wide-field ganglion cells were identified from a sample of retrogradely labelled wide-field ganglion cells lying within 1 mm of the foveal center in marmoset retina. Three examples of a potentially novel type of wide-field ganglion cell were identified in addition to twenty-one wide-field ganglion cells showing a range of different morphological characteristics.

4.2 *Materials and methods*

Animals

Tracer injections for the labelling of ganglion cells were carried out on eight adult marrmosets (*Callithrix jacchus*), obtained from the Australian National Health and Medical Research Council (NHMRC) combined breeding facility (see Table 4.1). Tissue for the analysis of bipolar cells was obtained from one adult marmoset, and one adult macaque monkey (*Macaca fascicularis*). All procedures were carried out according to the provisions of the NHMRC code of practice for the care and use of animals and were approved by the University of Melbourne ethics committee.

Table 4.1: Experimental parameters - Animals and anaesthesia for tracer injections and photofilling

Animal number	Species	Sex	Weight (g)	Anaesthesia for surgery
My88	*Callithrix jacchus*	Male	286	Alcuronium chloride
My101	*Callithrix jacchus*	Female	442	Ketamine / Zylazine
My108	*Callithrix jacchus*	Male	330	Ketamine / Zylazine
My124	*Callithrix jacchus*	Male	460	Ketamine / Zylazine
My131	*Callithrix jacchus*	Female	386	Alfaxalone
My132	*Callithrix jacchus*	Female	374	Alfaxalone
My134	*Callithrix jacchus*	Male	438	Alfaxalone
My137	*Callithrix jacchus*	Male	390	Alfaxalone

Table 4.2: Experimental parameters - Animals and anaesthesia for bipolar cell analysis

Animal number	Species	Sex	Weight (g)	Anaesthesia for surgery
My130	*Callithrix jacchus*	Female	330	Alfaxalone / Zylazine
Mk39	*Macaca fascicularis*	Male	3400	Sufentanil / Vercuronium

Analysis of ganglion cells

Tracer injections and photo-filling

Dye injections, photofilling and immunohistochemical processing of retinal pieces were carried out as described in Section 2.2 (page 43) using the following experimental parameters shown in Table 4.3 and 4.4. In some cases, two injections were made into the dorsal lateral geniculate nucleus (LGN) at different depths along a single track.

Table 4.3: Experimental parameters - Tracer injections and photofilling

Animal number	Injection tip size (µm)	Microruby concentration (%)	Duration of first injection (min) / duration of second injection (min)	Transport time for first injection (hours) / transport time for second injection (hours)
My88	n.d.	5	30 / 30	73.1 / 72.5
My101	25	10	45 / NA	86.3 / NA
My108	25	5	65 / NA	n.d.
My124	70	5	120 / NA	66.0 / NA
My131	50	5	120 / NA	88.5 / NA
My132	30	5	120 / NA	87.9 / NA
My134	40	5	30 / 120	67.9 / 67.3
My137	30	5	30 / 125	67.7 / 67.1

Not determined (n.d.), not applicable (NA)

Table 4.4: Experimental parameters - Immunohistochemical processing of retinal wholemounts

Retinal piece	Concentration / duration of immersion fix	Primary antibodies used	Duration of primary antibody incubation (days)	Secondary antibodies used
My88R2	4 % PFA / 120 min	NA	NA	NA
My101R1	4 % PFA / 120 min	NA	NA	NA
My108R1	4 % PFA / 120 min	CD15 (ms)	14	g ∝ ms Alexa 488
My124R1	4 % PFA / 30 min	Gephyrin (ms) / GluR4 (rb)	9	g ∝ ms Cy5 / g ∝ rb Alexa 488
My124L1	4 % PFA / 30 min	Gephyrin (ms) / GluR4 (rb)	9	g ∝ ms Alexa 488 / g ∝ rb Cy5
My131R1	4 % PFA / 30 min	Gephyrin (ms) / GluR4 (rb)	4	g ∝ ms Alexa 488 / g ∝ rb Cy5
My132 R1	4 % PFA / 30 min	NA	NA	NA
My132 L1	4 % PFA / 30 min	Gephyrin (ms) / GluR4 (rb)	4	g ∝ ms Alexa 488 / g ∝ rb Cy5
My134 L1	4 % PFA / 30 min	CD15 (ms) / GluR4 (rb)	9	g ∝ ms Alexa 488 / g ∝ rb Cy5
My137 R1	4 % PFA / 30 min	CtBP2 (ms) / PKC (rb)	9	g ∝ ms Cy5 / g ∝ rb Alexa 488

Paraformaldehyde (PFA), mouse (ms), rabbit (rb), goat (g), not applicable (NA)

Antibodies

Table 4.4 gives a summary of the fixation times and antibodies used in the present study. Details for the antibodies used against the C-terminal binding protein 2 (CtBP2), gephyrin and the glutamate receptor subunit 4 (GluR4) are outlined in Section 2.2 (page 43). Details for the antibody against the carbohydrate epitope (CD15) are given in Section 3.2 (page 76).

In one preparation, a rabbit antiserum against protein kinase Cα (PKCα) was used at a concentration of 1:50,000 to label rod bipolar and diffuse bipolar type 4 (DB4) cells in both macaque and marmoset tissue. This antiserum has been characterised by immunoblotting by the manufacturer (Sigma, St Louis, MO). It produces the same staining pattern as monoclonal antibodies against PKCα. Antibodies against PKCα are well established markers for rod bipolar and DB4 cells in primate retinas (Grünert et al., 1994; Mills and Massey, 1999).

Image acquisition

Image acquisition processes and parameters are as described in Section 2.2 (page 43).

Ganglion cell eccentricity and quantification of dendritic parameters

Ganglion cell eccentricities, dendritic field diameter, dendritic stratification and dendritic branch densities were determined in the same way as outlined in Section 2.2 (page 43).

In the current analysis, ganglion cells from eccentricities of up to 1.0 mm from the foveal center were included. The primary reason for this was to gain a better understanding of the systematic changes in ganglion cell morphology within foveal and central retina, where previous means of ganglion cell labelling by methods of intracellular injection have proven difficult due to the thickening of the nerve fiber layer.

A second factor considered in the inclusion of ganglion cells up to 1.0 mm in eccentricity is the fact that, due to lateral displacements, peak ganglion cell density in marmoset retina is often reached within 0.8 - 1.0 mm from the foveal center (Wilder et al., 1996). This accumulation of ganglion cell bodies corresponds to the borders of the fovea and the end of the foveal slope, where ganglion cells receiving inputs from cones

adjacent to the foveola are most likely included. Consistently, functions which estimate lateral shifts between cones and ganglion cells for marmoset retina show that ganglion cells at eccentricities between 0.80 to 1.00 mm may be connected to cones lying between 0.57 and 0.81 mm from the foveal center.

Analysis of bipolar cells

Immunohistochemical processing of vertical sections

Two eyes were obtained from one adult macaque (*Macaca fascicularis*) and marmoset (*Callithrix jacchus*) from unrelated physiological experiments after an overdose of sodium pentobarbitone. The eyes were perfused with saline prior to perfusion fixation with 4 % paraformaldehyde (PFA) in 0.1 M phosphate buffer (PB; pH 7.4) for ten minutes. The eyes were removed and cut open and the posterior eye cup was immersion fixed in 4 % PFA in 0.1 M PB for 20 minutes for the marmoset tissue and 30 minutes for the macaque tissue at 4 °C. After fixation, the eye cup was rinsed in 0.1 M PB and the retina was dissected, cryo-protected in 30 % sucrose in 0.1 M PB overnight, frozen, and stored at -70 °C until use.

Retinal pieces were cut using a scalpel blade, under observation with a dissection microscope in preparation for cryostat sectioning. Pieces where the fovea was nicely intact were selected for sectioning, and cut so that the fovea lied roughly at the center of the piece.

For the macaque tissue, the dimensions of the retinal piece were roughly 4.5 - 5.5 × 4.0 mm. The optic disc was located at the corner of the piece; as such, the axis of the horizontal meridian ran diagonally through the piece. The dimensions of the piece covered eccentricities ranging from approximately 0 - 3 mm on the nasal as well as the temporal sides of the fovea, along the horizontal meridian.

For the marmoset tissue, the horizontal meridian lay along the width of the piece, with approximately 2 mm on either side of the foveal center. The side of the piece furthest from the optic disc was squared off with a length of approximately 5 mm. On the opposite side of the piece, the edges of the tissue converged at the optic disc, starting approximately half way along the piece.

Prepared pieces were sectioned vertically, along the length of the piece, at an angle of roughly 45 degrees from the horizontal meridian for the macaque tissue, and parallel to the horizontal meridian for the marmoset tissue. Sections were cut at a thickness of 12 μm and collected onto gelatinised slides. Sequential sections were picked up on to four alternating slides, with six sections per slide, to maximise the number of slides containing sections through the foveal slope. Five slides of the macaque tissue, and four slides for marmoset tissue was selected for immunohistochemical processing, based on the clear presence of sections through the foveal slope.

Antibodies

Antibodies were used to label subpopulations of bipolar cells or synaptic ribbons in vertical sections. Details for all antibodies used are listed in Table 4.5 and antibody combinations used are listed in Table 4.6. Details from previous studies on the staining patterns of antibodies used against CtBP2, CD15 and PKCα are outlined in Section 2.2 (page 43), Section 3.2 (page 76) and in the previous section respectively.

Table 4.5 - Antibodies

Anibody name	Immunogen	Supplier	Catalogue number / Antibody type	Dilution
C-terminal binding protein 2 (CtBP2)	Amino acids 361 - 445 of mouse CtBP2	BD Biosciences, Heidelberg, Germany	612044 / Mouse monoclonal	1:10,000
CD15	Membrane preparation of the human histiocytic cell line U-937	J. Mai, University of Düsseldorf, Germany	NA / Mouse monoclonal	1:6
Protein kinase C α (PKCα)	Amino acids 659 - 672 of rat PKCα	Sigma, St. Louis, MO	P4334 / Rabbit antiserum	1:50,000
Calbindin (CaBP)	Calbindin-D purified from chicken gut	Sigma, St. Louis, MO	C8666 / Mouse monoclonal	1:20,000
Calbindin (CaBP)	Recombinant rat calbindin	Swant Swiss Antibodies, Bellinzona, Switzerland	CB-38 / Rabbit antiserum	1:20,000
Recoverin	Recombinant human recoverin	Millipore, Billerica, MA	AB5585 / Rabbit polyclonal	1:5,000
Vesicular glutamate transporter-1 (vGlut-1)	Synthetic peptide from rat vGlut-1 protein	Millipore, Billerica, MA	AB5905 / Guinea pig polyclonal	1:50,000

Not applicable (NA)

The mouse monoclonal antibody against the calcium binding protein calbindin (CaBP) has been characterised by the manufacturer and stains the ^{45}Ca binding spot of calbindin-D in a two dimensional immuno-blot. A more recent batch of the rabbit antiserum against CaBP has been characterised by the manufacturer by immunoblotting, and by immunohistochemistry in the cerebellum of CaBP knock out mice. Antibodies against CaBP have been shown to label DB3 type bipolar cells in both macaque (Grünert et al., 1994; Martin and Grünert, 1992) and marmoset (Chan et al., 2001; Luo et al., 1999) and have been used to study DB3 bipolar cells (Cuenca and Kolb, 1998; Ghosh et al., 1997; Hanna and Calkins, 2007; Jacoby and Marshak, 2000; Jusuf et al., 2005).

The rabbit polyclonal antibody against recoverin used here has been characterised by the manufacturer by western blot where it recognises a band of 26kDa. Antibodies against recoverin have been shown to label flat midget bipolar cells in macaque retina (Milam et al., 1993) and have been used previously to study flat midget bipolar cells (Grünert, 1997; Jusuf et al., 2005; Jusuf et al., 2006a; Wässle et al., 1994).

The guinea pig polyclonal antibody against the vesicular glutamate transporter 1 (vGlut-1) was tested by the manufacturer on tissue sections from rat central nervous system and found to mainly label nerve fibers and terminals. Antibodies against vGlut-1 have previously been shown to label bipolar cell axons in macaque (Jusuf et al., 2005) cat (Fyk-Kolodziej et al., 2004) and mouse (Haverkamp et al., 2003; Johnson et al., 2003; Sherry et al., 2003) retina.

Secondary antibodies were used in combinations of three per slide as indicated in Table 4.6. Secondary antibodies were goat anti-mouse or goat anti-rabbit immunoglobulin G (IgG) coupled to either Alexa 594 (Molecular Probes, Eugene, OR) or Cy5 (Jackson ImmunoResearch, West Grove, PA), and goat anti-guinea pig IgG coupled to Alexa 488 (Molecular Probes, Eugene, OR). The anti-rabbit Cy5 was used at a dilution of 1:100, the anti-mouse Cy5 at a dilution of 1:200, the anti-guinea pig Alexa 488 at a dilution of 1:250 and finally, both anti-rabbit and anti-mouse Alexa 594 were used at a dilution of 1:500.

Table 4.6: Experimental parameters - Immunohistochemical processing of vertical sections

Section number	Primary antibodies	Secondary antibodies	Labeling in IPL
vMy130R1A_33	CtBP2 (ms)	g ∝ ms Alexa 594	Ribbon synapses
	PKCα (rb)	g ∝ rb Cy5	DB4 and RB
	vGlut-1 (gp)	g ∝ gp Alexa 488	All bipolar axons
vMy130R1A_34	CD15 (ms)	g ∝ ms Alexa 594	FMB and DB6
	CaBP (rb)	g ∝ rb Cy5	DB3
	vGlut-1 (gp)	g ∝ gp Alexa 488	All bipolar axons
vMy130R1A_35	CD15 (ms)	g ∝ ms Alexa 594	FMB and DB6
	PKCα (rb)	g ∝ rb Cy5	DB4 and RB
	vGlut-1 (gp)	g ∝ gp Alexa 488	All bipolar axons
vMy130R1A_36	CtBP2 (ms)	g ∝ ms Alexa 594	Ribbon synapses
	CaBP (rb)	g ∝ rb Cy5	DB3
	vGlut-1 (gp)	g ∝ gp Alexa 488	All bipolar axons
vMk39L1A_33	CaBP (ms)	g ∝ ms Alexa 594	DB3
	Recoverin (rb)	g ∝ rb Cy5	FMB
	vGlut-1 (gp)	g ∝ gp Alexa 488	All bipolar axons
vMk39L1A_34	CD15 (ms)	g ∝ ms Alexa 594	DB6
	PKCα (rb)	g ∝ rb Cy5	DB4 and RB
	vGlut-1 (gp)	g ∝ gp Alexa 488	All bipolar axons
vMk39L1A_35	CtBP2 (ms)	g ∝ ms Cy5	Ribbon synapses
	CaBP (rb)	g ∝ rb Alexa 594	DB3
	vGlut-1 (gp)	g ∝ gp Alexa 488	All bipolar axons
vMk39L1A_36	CtBP2 (ms)	g ∝ ms Cy5	Ribbon synapses
	Recoverin (rb)	g ∝ rb Alexa 594	FMB
	vGlut-1 (gp)	g ∝ gp Alexa 488	All bipolar axons
vMk39L1A_37	CtBP2 (ms)	g ∝ ms Cy5	Ribbon synapses
	PKCα (rb)	g ∝ rb Alexa 594	DB4 and RB
	vGlut-1 (gp)	g ∝ gp Alexa 488	All bipolar axons

Inner plexiform layer (IPL), mouse (ms), rabbit (rb), guinea pig (gp), goat (g), diffuse bipolar cell (DB), flat midget bipolar cell (FMB), rod bipolar cell (RB)

Immunohistochemical processing of vertical sections

Sections were rinsed in phosphate buffered saline (PBS), and preincubated in PBS containing 5 % bovine serum albumin (BSA) and 0.5 % Triton X-100 for 30 minutes. Sections were then incubated in one of the primary antibodies (see Table 4.6) diluted in PBS containing 1 % BSA, 0.5 % Triton X-100 and 0.1 % sodium azide overnight. After several rinses in PBS, sections were incubated for 1 hour in the appropriate secondary antibody (see Table 4.6) diluted in PBS containing 1 % BSA and 0.5 % Triton X-100. All secondary antibodies were centrifuged at 1300 g for 6 minutes before being applied to sections. After incubation in the secondary antibody, sections were rinsed in PBS. Incubations and rinses were repeated for each primary and secondary antibody combination, in sequence. Finally, sections were cover slipped in Mowiol (Hoechst, Sydney, Australia) containing 10 % of 1,4-diazobicyclo-[2.2.2]-octane (Harlow and Lane, 1988).

Analysis of immunostained sections

Fluorescent sections were viewed using a Zeiss (Oberkochen, Germany) Axioplan deconvolution microscope. Stacks of images (14 - 30 optical sections) were taken with a digital camera (Axiocam, Zeiss) using a 63× or 40× oil immersion objective at a step size of 0.275 µm. For each section chosen for analysis, one stack of images was taken on the temporal side of the foveal slope, so that the point closest to the middle of the foveal slope was at the edge of the field of view. The second stack of images was taken approximately 1 mm temporal to the first stack of images. In each case, where the quality of the section on the temporal side of the fovea was not ideal, the nasal side of the fovea was taken instead.

Stacks of images were processed using Axiovision deconvolution software, and the brightness and contrast adjusted using Axiovision software or Adobe Photoshop (San Jose, CA; v.7). Analyses of axon terminal stratification patterns, for labelled bipolar cells, were performed using Imaris software package (Bitplane, Zurich, Switzerland).

Image stacks were imported into the surpass module of Imaris (Bitplane, Zurich, Switzerland), in which a three-dimensional perspective of the image stack was rendered.

The measurement points tool was used, along a single focal plane, to measure the distance between bipolar cell axon terminals and the border of the inner plexiform layer with the inner nuclear layer. This value was then calculated as a percentage of the distance between the two borders of the inner plexiform layer (or the total breadth of the inner plexiform layer) at the same x position. The borders of the inner plexiform layer were identified from synaptic ribbon marker labelling, or, where sections were not processed with the ribbon marker, labelling of all bipolar axonal processes with the antibody against vGlut-1 was used. Where axon terminal processes ramified broadly, the breadth of axonal stratification was measured and the midpoint was taken as the stratification value for each measurement point.

Measurements were not made from regions where obvious distortions due to the presence of blood vessels were observed. Measurements were kept at least 3 - 5 μm apart along the plane of the retina, to ensure that no single axon terminal was over represented in the results of the analysis. The total number of measurement points for each bipolar cell type was between 26 and 94. The number of measurement points for each bipolar cell type at each retinal location is summarised in Table 4.7.

For the analysis of bipolar cells, morphological characteristics of bipolar cells lying within the foveal slope (up to approximately 0.14 mm eccentricity for images taken at x40 and up to approximately 0.22 mm eccentricity for images taken at x63) were compared to those at approximately 1 mm from the foveal center. Bipolar cells within the slope were assumed to sample central most cones, and those at 1 mm eccentricity were thought to connect to cones at approximately 0.84 mm, according to functions which estimate the lateral shift between cone inner segments and there pedicles in marmoset retina (Wilder et al., 1996).

Table 4.7: Analysis of vertical sections

Species	Bipolar cell type	Total number of measurement points	Number of measurement points within foveal slope	Number of measurement points at ~1 mm
Callithrix jacchus	FMB	91	45	46
	DB3	94	32	62
	DB4	54	21	33
	DB6	60	18	42
Macaca fascicularis	FMB	77	26	51
	DB3	46	11	35
	DB4	79	28	51
	DB6	26	12	14

Flat midget bipolar cell (FMB), diffuse bipolar cell (DB)

4.3 *Results*

Foveal/central wide-field ganglion cells

A total of thirty-seven retrogradely labelled wide-field ganglion cells were analysed. They were located at 0.31 - 1.00 mm of the fovea, which equates to 2.11 - 8.16 degrees. Figure 4.1 shows examples of these cells. A midget and parasol ganglion cell pair (A) is shown for comparison with an example of a small bistratified cell (B, C), a large sparse cell (D), a ganglion cell with a relatively large and bistratified dendritic tree (E, F) and examples of unclassified wide-field ganglion cells which could not be placed into specific morphological types (G - I).

Figure 4.2 shows drawings of a subset of wide-field ganglion cells from similar eccentricites that were analysed in this study. These ganglion cells were classified as either small bistratified (A); large sparse (B); broad thorny (C) or large bistratified, (D) based on morphological parameters such as dendritic field size, stratification and branching pattern.

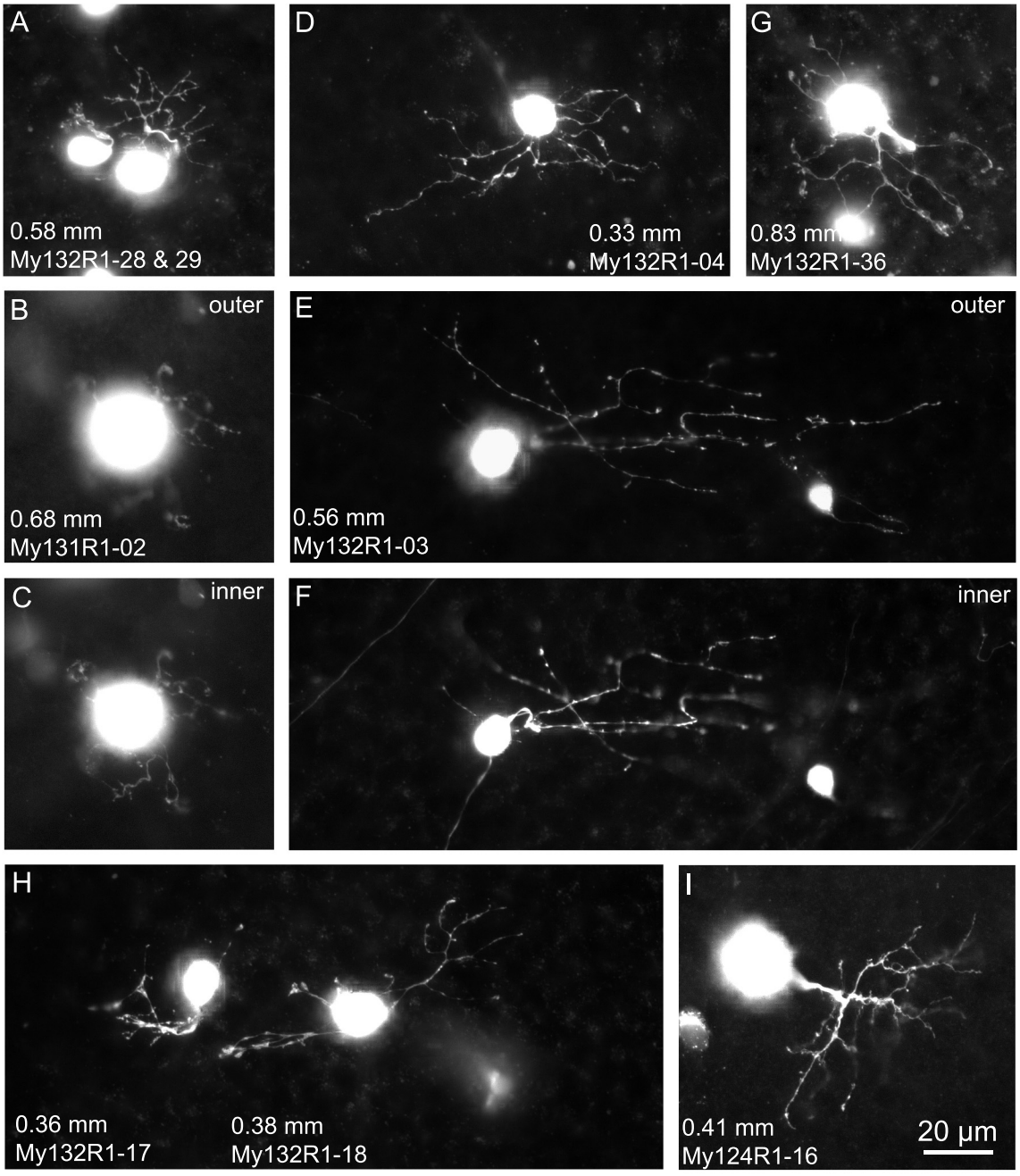


Figure 4.1 Photomicrographs of retrogradely labelled ganglion cells within 1 mm of the foveal center. **A**: Midget (left) and parasol (right) cells. **B**, **C**: Outer (B) and inner (C) dendrites of a small bistratified cell. **D**: Large sparse cell. **E**, **F**: Outer (E) and inner (F) dendrites of a large bistratified cell. Arrowheads indicate a labelled midget cell. **G**, **H**, **I**: Examples of unclassified cells. Eccentricities are indicated beneath each cell. Scale bar in I applies to all panels.

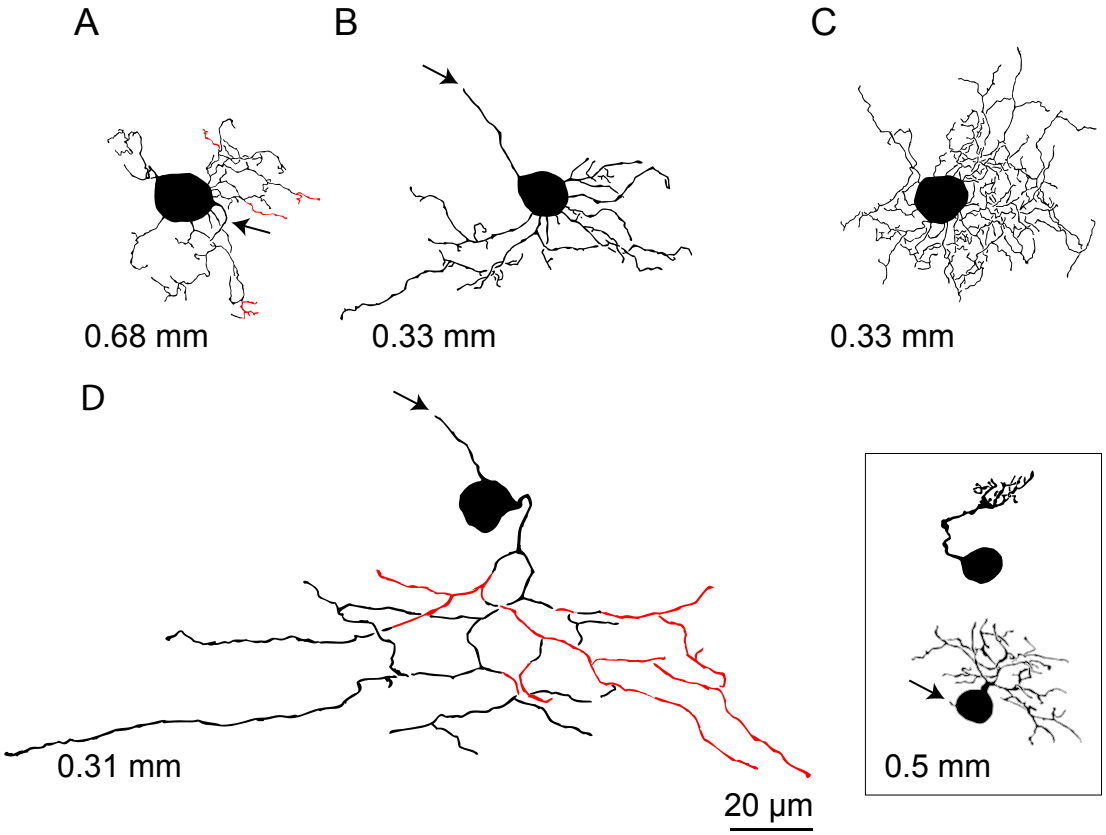


Figure 4.2 Drawings of wide-field ganglion cells from within 1 mm of the center of the fovea. **A**: Small bistratified cell. **B**: Large sparse cell. **C**: Broad thorny cell. **D**: Large bistratified cell. For bistratified cells, outer stratifying dendrites are shown in red. Inset to the lower right shows a midget (top) and parasol (bottom) cell from a similar eccentricity. Eccentricities are indicated beneath each cell. Arrows indicate axons.

Qualitative results

Presumed small bistratified ganglion cells (Figure 4.1 B, C; Figure 4.2 A) from the current study (n = 6 cells) showed morphological characteristics similar to that described previously for small bistratified cells (see results from Chapter2; Dacey, 1993a; Ghosh et al., 1997; Rodieck, 1991; Rodieck and Watanabe, 1993; Silveira et al., 1999). All six cells had bistratified dendritic trees, with a larger and relatively densely branching inner tier and a comparatively smaller outer tier.

Dendrites of presumed large sparse ganglion cells (n = 6; Figure 4.1 D; Figure 4.2 B) are narrowly stratified within the inner plexiform layer, near the border with the ganglion cell layer. Dendrites were relatively sparsely branching and mostly absent of hooks and spines. These morphological parameters are inline with previous reports of large sparse ganglion cells (see results from Chapter 3; Dacey et al., 2003; Peterson and Dacey, 1999; Szmajda et al., 2008; Yamada et al., 2005).

A single example of a presumed broad thorny ganglion cell was found within the sample of ganglion cells from the current study (Figure 4.2 C). Dendrites were seen to stratify broadly across several slices of the image stack. Dendrites of this broad thorny ganglion cell branched repeatedly with many processes frequently crossing over one another. All of the above-mentioned morphological charateristics of this presumed broad thorny cell matches that previously reported for broad thorny cells (see results from Chapter 3; Dacey and Packer, 2003; Yamada et al., 2005).

Three ganglion cells from the current study had large dendritic fields, which were distinctly bistratified. These have provisionally been named large bistratified ganglion cells for their large and distinctly bistratified dendritic tree (Figure 4.1 E, F; Figure 4.2 D). One particularly striking characteristic common to all three examples were their highly elongated and asymmetric dendritic tree. Such distortions of ganglion cell dendritic trees near the fovea have been reported previously. In a study of parasol ganglion cells, it was noted that parasol cells lying within 0.7 mm of the foveal center showed a circumferential bias of their dendritic trees (Grünert et al., 1993). At eccentricities > 0.7 mm however, the dendritic fields adopted a more circular dendritic field (Grünert et al., 1993). Similarly, in a study of giant sparse / melanopsin containing ganglion cells, a distortion of the dendritic tree can be seen for a cell from 0.42 mm,

however in an example from 0.90 mm, this distortion is lost (see Figure 2, Jusuf et al., 2007). For the current sample of large bistratified ganglion cells, there is a chance that the elongation of their dendritic trees is an inherent morphological feature of this particular type, as the large bistratified cell from 0.90 mm also exhibited an elongated dendritic tree - an eccentricity at which both Grünert et al. (1993) and Jusuf et al. (2007) saw the dendritic trees of ganglion cells to assume a circular arrangement. This being said, there is also a possibility that incomplete dendritic filling in the labelling process has resulted in only a small part of the dendritic field being labelled, giving the impression of an elongated dendritic field.

Twenty-one wide-field ganglion cells from the current sample, did not share all morphological properties characteristic of any of the above types. Such unclassified wide-field ganglion cells consisted of cells displaying a wide range of morphological characteristics as seen in Figure 4.3.

Quantitative results

The sample of small bistratified ganglion cells is located between 0.38 to 1.00 mm eccentricity, and dendritic fields of the inner tiers ranged from 36.94 - 60.85 µm in diameter. Dendritic fields are within, or just above the range found for parasol ganglion cells from similar eccentricities (see Figure 4.4). Dendritic branch densities for small bistratified ganglion cells range from 0.112 - 0.207 intercepts / µm using the method described in Section 2.2 (page 43).

The sample of large sparse ganglion cells is from 0.32 - 0.86 mm eccentricity, with dendritic fields ranging in diameter from 34.95 - 70.07 µm. The relationship observed in peripheral retina, between the dendritic field sizes of large sparse ganglion cells and other ganglion cell types, is largely maintained within the eccentricity range investigated (see Figure 4.4). Dendritic branch densities for large sparse ganglion cells ranged from 0.072 - 0.102 intercepts / µm.

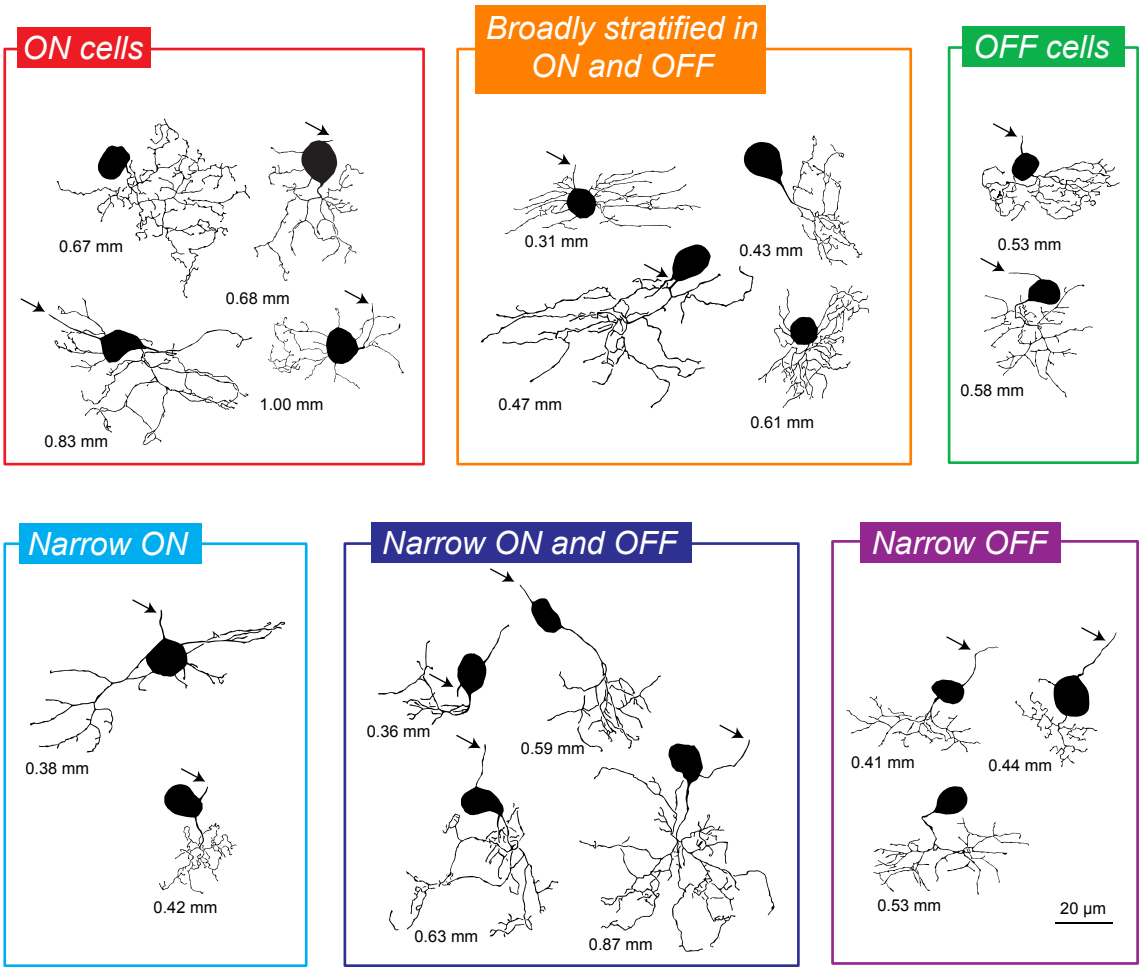


Figure 4.3 Drawings of unclassified wide-field ganglion cells found within 1 mm from the foveal center. Cells are grouped according to the pattern of their dendritic stratification. ON and OFF cells have dendrites stratifying within ON and OFF halves of the inner plexiform layer (IPL). Broadly stratifying cells have dendrites that stratify across more than 50 % of the IPL and straddle both ON and OFF halves. Cells were classified as narrowly stratified where dendrites were restricted to less than 20 % of the IPL. Eccentricities are indicated beneath each cell. Arrows indicate axons.

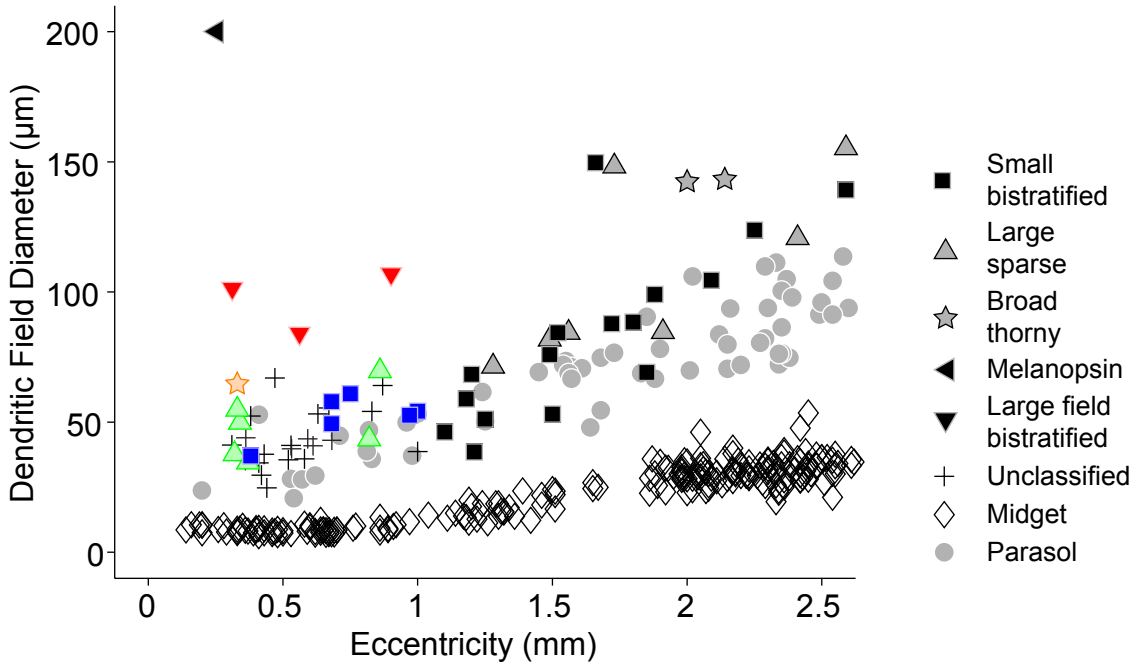


Figure 4.4 Dendritic field sizes of foveal and extra foveal ganglion cell types. Coloured symbols indicate dendritic field diameters of cells from the current study. Symbols in greyscale indicate dendritic field diameters of cells from previous studies (Ghosh et al., 1996; Jusuf et al., 2007; Szmajda et al., 2008).

The broad thorny ganglion cell was found at an eccentricity of 0.33 mm, and the size of the dendritic field was 65.10 µm in diameter. As seen in Figure 4.4, the broad thorny ganglion cell was larger than most ganglion cell types at similar eccentricities, but smaller than the large bistratified ganglion cells discussed below, and melanopsin-containing ganglion cells from previous studies (Jusuf et al., 2007). The dendritic branch density of this broad thorny ganglion cell was relatively high at 0.221 intercepts / µm.

Large bistratified ganglion cells were found at eccentricities ranging from 0.31 - 0.90 mm, and the size of their dendritic fields ranged from 83.25 - 106.00 µm in diameter. The dendritic fields of large field bistratified ganglion cells were larger than all other ganglion cell types at similar eccentricities with the exception of melanopsin containing ganglion cells (see Figure 4.4), which are close to twice the size of large field bistratified ganglion cells (Jusuf et al., 2007). In all examples of this type, dendritic trees were bistratified and highly elongated. The elongation of the dendritic tree was such that, along one axis the dendritic field spanned between 154.22 - 204.61 µm, and at right angles to this axis, the dendritic field reached lengths of 53.32 - 54.97 µm. The two dendritic tiers were segregated to narrow portions of the ON and OFF sublamina. In all three examples, the dendritic tree was extremely sparsely branched with dendritic branch densities ranging from 0.048 - 0.101 intercepts / µm.

Unclassified ganglion cells included those with dendrites largely restricted to the ON (n = 6) and OFF sublamina (n = 5). Of the ON cells, two cells were narrowly stratified within 20% of the inner plexiform layer. Of the OFF cells three were narrowly stratified. Nine of the unclassified ganglion cells had dendrites that stratified across portions of both ON and OFF sublamina. Of these nine cells, four were broadly stratified covering > 50 % of the inner plexiform layer, four were narrowly stratified across < 20 % of the inner plexiform layer and a single cell covered approximately 30 % of the inner plexiform layer. Branching patterns were highly variable with dendritic branch densities ranging from 0.032 - 0.309 intercepts / µm.

In summary, at least three wide-field ganglion cell types previously identified in peripheral retina, are present within 1 mm of the fovea. Following the overall decrease in dendritic field size with decreasing eccentricities for all ganglion cells, small bistratified, large sparse and broad thorny ganglion cells within 1 mm eccentricity were all smaller in

size than their peripheral equivalents. Previously identified wide-field ganglion cell types present in the fovea, maintained overall size relationships with other ganglion cell types observed in peripheral retina. Morphological parameters such as dendritic stratification and branching patterns were similar between small bistratified, large sparse and broad thorny ganglion cells in peripheral and foveal retina.

Bipolar cell axon terminal stratification - qualitative observations

Figure 4.5 shows micrographs of a subset of vertical sections analysed in the current study. Sections are from temporal marmoset retina, and show examples of labelled bipolar cells found approximately 1 mm from the fovea and those closest to the foveal slope. Consistently, a slight rightward displacement of the axonal processes from the dendritic processes can be seen in the micrographs, and this displacement is more pronounced in micrographs from the foveal slope compared to those from 1mm.

From these sets of micrographs it can also be seen that the thickness of the outer nuclear, and inner plexiform layers are dramatically reduced in the examples from the foveal slope compared to those from 1 mm eccentricity.

Axon terminal processes of the labelled bipolar cell types show distinct stratification patterns, such that axonal processes of flat midget bipolar (FMB) cells (Figure 4.5 E, F) stratify near the border of the inner plexiform layer with the inner nuclear layer, followed, in order, by diffuse bipolar type 3 (DB3; Figure 4.5 A, B), DB4 (Figure 4.5 C, D), DB6 (Figure 4.5 E, F) and rod bipolar (Figure 4.5 D) cells. The vertical extent of axon terminal ramification also differs slightly between different bipolar cell types.

Also shown in Figure 4.5 is an example of a section from the foveal slope processed with an antibody that labels axon terminal processes of all bipolar cells (Figure 4.5 G). The dense labelling seen within the inner plexifrom layer indicates that there is a high chance that axonal processes of many bipolar cell types are present within the foveal slope. A section through the foveal slope processed with a marker for synaptic ribbons is shown (Figure 4.5 H). As presynaptic terminal processes of bipolar cells contain synaptic ribbons, the presence of antibody labelling here also supports the presence of bipolar cells within the foveal slope.

Figure 4.5 Photomicrographs of vertical sections through marmoset and retina processed with bipolar cell and synaptic markers. **A** and **B** show diffuse bipolar (DB) type 3 cells within the foveal slope (A) and ~ 1mm eccentricity (B) as labeled with the antibody against CaBP. **C** and **D** show DB4 cells within the foveal slope and both DB4 and rod bipolar (RB) cells from ~ 1mm eccentricity as labeled with the antibody against PKCα. Arrowheads in D point to the upper band of labeling representing DB4 axon terminals. **E** and **F** show flat midget bipolar (FMB) and DB6 cells within the foveal slope and ~ 1mm eccentricity as labeled with the antibody against CD15. Arrowheads point to axon terminal processes of DB6 cells. **G** shows a section from the foveal slope as processed with the antibody against vGlut-1, which labels axon terminals of all bipolar cells (BC). **H** shows a section from the foveal slope as processed with the antibody against CtBP2, which labels synaptic ribbons. All sections are from nasal retina. Scale bar in H applies to all panels. Outer plexiform layer (OPL), outer nuclear layer (ONL), inner plexiform layer (IPL), ganglion cell layer (GCL).

DB3 slope
A
OPL
ONL
IPL
GCL
DB3 ~1 mm
B
ONL
IPL
GCL
DB4 slope
C
OPL
ONL
IPL
GCL
DB4/RB ~1 mm
D
ONL
IPL
FMB/DB6 slope
E
OPL
ONL
IPL
GCL
FMB/DB6 ~1 mm
F
ONL
IPL
GCL
All BC axon terminals
G
OPL
ONL
IPL
GCL
Synaptic ribbons
H
OPL
ONL
IPL
GCL
20 µm

Bipolar cell axon terminal stratification - quantitative results

In order to quantify the patterns of axon terminal stratification noted above, the level of axon terminal ramification was measured with respect to the borders of the inner plexiform layer. These values are expressed as percentages of the inner plexiform layer, with 0 % representing the border of the inner plexiform layer and inner nuclear layer, and 100 % denoting the border of the inner plexiform layer and ganglion cell layer. Where axon terminals ramify broadly, the breadth of stratification was measured and the midpoint taken as the average stratification measure.

Measurements obtained for all image stacks have been summarised in the form of histograms shown in Figure 4.6. Axonal terminal stratification depths for every measurement point are plotted for marmoset and macaque samples at 1 mm and within the foveal slope. It can be seen from the histograms that the pattern of axon terminal stratification observed at 1 mm eccentricity are largely maintained at the foveal slope.

Table 4.8 and 4.9 summarise the average stratification depths and stratification breadth values for the different bipolar cell types analysed in marmoset and macaque retina respectively. Measures of stratification depth was obtained for four bipolar cell types (FMB, DB3, DB4 and DB6) at two sample locations (foveal slope and approximately 1 mm) in both marmoset and macaque tissue. Axon terminal stratification depth at the foveal slope was compared with that at ~1 mm for each bipolar cell type. Of the four bipolar cell types, three (FMB, DB4, DB6) showed comparable depth measurements between the two sample locations in marmoset ($P > 0.2$, *t*-test). For macaque, depth measurements were comparable for DB3 and DB4 cells ($P > 0.4$, *t*-test) but not for the FMB and DB6 types. Thus, for the majority of the bipolar cell types tested, the depth of axon terminal ramification did not change between the foveal slope and at 1 mm eccentricity. It is likely that depth measures for DB3 cells in marmoset and FMB and DB6 cells in macaque were not comparable ($P < 0.05$, *t*-test) between the foveal slope and ~1 mm sample due to the small number of measurement points as shown in Table 4.7.

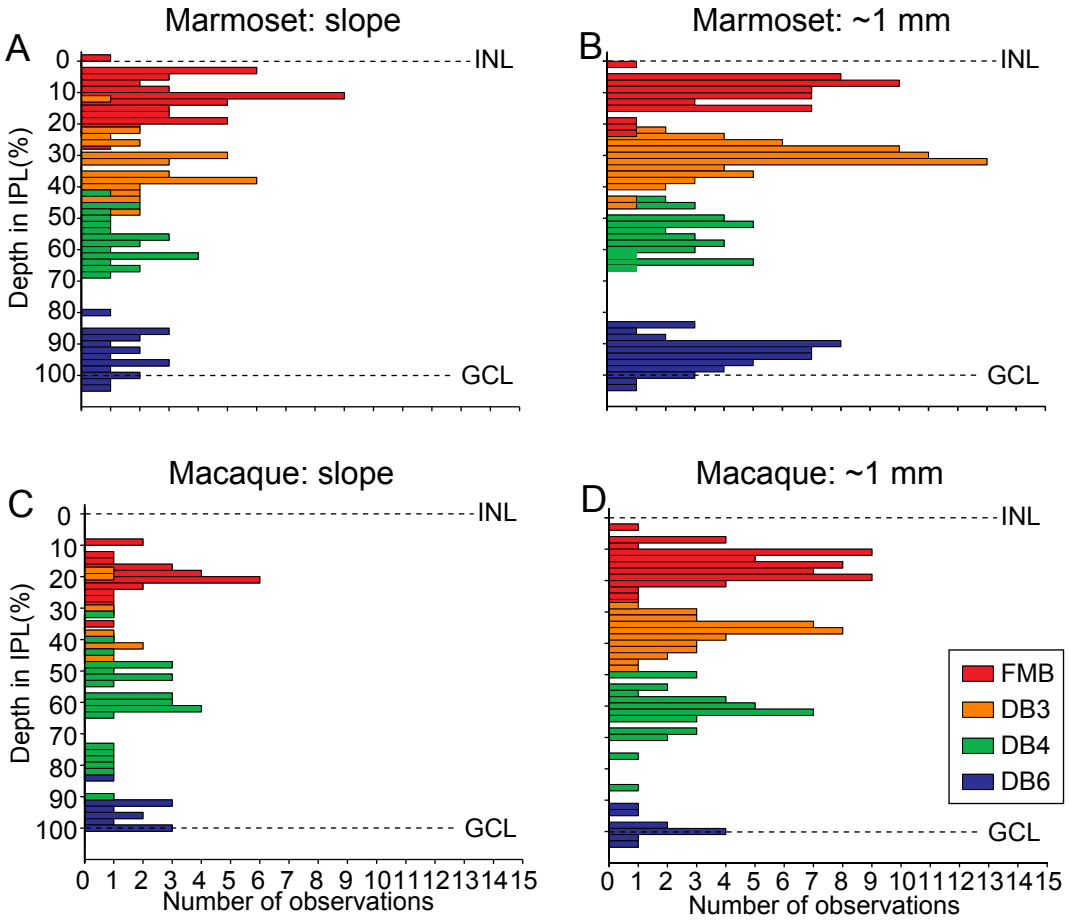


Figure 4.6 Histograms showing stratification patterns of bipolar axon terminals along the foveal slope (A, C) and at approximately 1 mm eccentricity (B, D). **A** and **B** show data from marmoset retina, graphs **C** and **D** are results from macaque retina. Stratification depth is represented as a percentage with 0 % indicating the border of the inner plexiform layer (IPL) with the inner nuclear layer (INL) and 100 % denoting the border with the ganglion cell layer (GCL). Stratification patterns were measured for preparations processed with markers for flat midget bipolar cells (FMB) and diffuse bipolar (DB) types 3, 4 and 6.

Measurements of stratification breadth were obtained for FMB and DB4 cells at the foveal slope and ~1 mm in both marmoset and macaque tissue, and for DB3 cells at ~1 mm in marmoset. In the case of FMB cells "axon tails" (Jusuf et al., 2006a) were usually not included in the measurements. Stratification breadth measures were taken in these cases, as processes within single axon terminals were seen in vertical sections to span a small portion of the vertical extent of the inner plexiform layer. In all other bipolar cell types only a single axon terminal process was observed at most points within the inner plexiform layer. Average values for the vertical extent of the inner plexiform layer covered by each bipolar cell type at the foveal slope and at approximately 1 mm are summarised in Table 4.8 and 4.9 for marmoset and macaque respectively.

For marmoset retina, the breadth of FMB axon terminal stratification is broader for the foveal slope sample than it is at 1mm, but for DB4 cells stratification is broader at 1mm. Axon terminals of DB3 cells from 1 mm in marmoset retina, were seen to stratify somewhat broadly, despite showing narrow stratification in the foveal sample. Thus, the results for marmoset retina suggest that there are no consistent changes that occur between the foveal slope and at ~1 mm eccentricity, in the axon terminal stratification breadths of these bipolar cells. In macaque retina, the breadth of axon terminal stratification for FMB and DB4 cells is narrower for the 1 mm sample compared to the foveal slope sample. This suggests that in macaque retina there may be a tendency for bipolar cell axon terminals to span a broader extent of the inner plexiform layer within the foveal slope than at ~1 mm.

Table 4.8: Axon terminal stratification - Marmoset

Bipolar cell type	Mean stratification depth ± SD at foveal slope (%)	Mean stratification breadth ± SD at foveal slope (%)	Mean stratification depth ± SD at 1 mm (%)	Mean stratification breadth ± SD at 1 mm (%)
FMB	11.56 ± 6.84	17.77 ± 9.76	9.97 ± 4.63	14.75 ± 4.84
DB3	34.42 ± 8.10	n.d.	31.81 ± 4.87	9.36 ± 2.58
DB4	56.87 ± 7.37	19.83 ± 5.45	55.32 ± 6.21	21.68 ± 5.45
DB6	92.91 ± 6.52	n.d.	93.23 ± 4.68	n.d.

Standard deviation (SD), not determined (n.d.)

Table 4.9: Axon terminal stratification - Macaque

Bipolar cell type	Mean stratification depth ± SD at foveal slope (%)	Mean stratification breadth ± SD at foveal slope (%)	Mean stratification depth ± SD at 1 mm (%)	Mean stratification breadth ± SD at 1 mm (%)
FMB	22.20 ± 8.65	33.00 ± 9.17	15.05 ± 4.82	25.34 ± 7.43
DB3	35.69 ± 10.07	n.d.	36.60 ± 4.77	n.d.
DB4	59.56 ± 13.17	18.56 ± 10.51	60.98 ± 7.17	16.05 ± 4.81
DB6	94.53 ± 4.94	n.d.	97.96 ± 3.15	n.d.

Standard deviation (SD), not determined (n.d.)

4.4 *Discussion*

Results from the current study show diffuse bipolar (DB) cell types DB3, DB4 and DB6 to be present in foveal retina. Similarly, the small bistratified, large sparse and broad thorny wide-field ganglion cell types are present within 1 mm of the fovea along with other previously unidentified types. The current findings show that neural components that may be involved in the circuitry of a subset of wide-field ganglion cell types are present at the fovea.

These findings support the view (Wässle and Boycott, 1991) that the same neuronal types interact with the same synaptic partners in the fovea as they do in peripheral retina. Foveal vision therefore, does not seem to reflect the sole contribution of the neurons of the midget pathway, but rather an overall increased density of all cell types seen in the periphery (with the selective exclusion of rods and rod bipolar cells).

Accounting for lateral displacement at the fovea

As outlined in Section 1.7 (page 35), the foveal excavation is primarily formed through the lateral migration of post receptoral elements away from the fovea, and the concurrent movement of the inner components of cone photoreceptors towards the fovea (Hendrickson and Kupfer, 1976; Hendrickson, 1994; Provis et al., 1998; Yuodelis and Hendrickson, 1986). As a result, in the fully developed fovea, the majority of the lateral deviation is apparent between the inner segments and pedicles of cones - connected by fibers of Henle (Perry and Cowey, 1988; Schein, 1988).

Henle fibers belonging to the central most cones have been reported to reach lengths of 125 - 350 μm in human retina (Missotten, 1974) and macaque retina (Wässle et al., 1989; 1990), and reach a maximum of 300 - 600 μm, in cones with inner segments

lying approximately 0.5 mm from the foveal center (Missotten, 1974; Schein, 1988; Sjöstrand et al., 1994; Sjöstrand et al., 1999b).

This lateral deviation results in cone pedicles being absent from the first 100 - 350 μm from the foveal center in human, macaque and marmoset (Ahnelt and Pflug, 1986; Missotten, 1974; Perry and Cowey, 1988; Schein, 1988; Wilder et al., 1996; Yamada, 1969; Yuodelis and Hendrickson, 1986).

Postreceptoral elements can be displaced even further due to lateral deviations between the dendrites and axon terminals of bipolar cells (Polyak, 1941). As seen in the obliquely running axon processes of Figure 4.1, lateral deviations were also observed in samples of bipolar cells in the current study. Perry and Cowey (1988) measured lateral shifts of 66 μm within the length of bipolar cells closest to the fovea, and 12.5 μm for bipolar cells at 1mm eccentricity. Consistently, bipolar cells from preparations within the foveal slope displayed a more pronounced displacement between their dendrites and axon terminals, compared to preparations from 1 mm eccentricity in the current study. There were no obvious differences between bipolar cell types and the magnitude of their lateral displacement.

The combined effects of lateral displacement in the retinal layers described above, result in the absence of ganglion cells from the central 60 - 300 μm from the fovea (Curcio and Allen, 1990; Perry and Cowey, 1988; Schein, 1988; Sjöstrand et al., 1994; Stone and Johnston, 1981). Consistently, the current study did not find ganglion cells within 0.3 μm of the foveal center.

Functions have been described to estimate the total lateral displacement between cone inner segments and ganglion cells (Curcio and Allen, 1990; Perry and Cowey, 1988; Schein, 1988; Sjöstrand et al., 1994; Sjöstrand et al., 1999a; Wilder et al., 1996). These studies show that ganglion cells may be displaced by as much as 300 - 350 μm from the cones providing their input. The samples taken for the current study include bipolar and ganglion cells up to 1 mm, which, according to measurements made in marmoset retina (Wilder et al., 1996), will include those bipolar and ganglion cells which are connected to cones sampling the first 0.8 mm of the retina. As such, the results from the current study are thought to be an accurate representation of the anatomical substrates subserving foveal vision.

Previously identified wide-field ganglion cell types at the fovea

The current study found examples of small bistratified, large sparse and broad thorny ganglion cells within 1 mm from the foveal center. These three wide-field types were identified based on characteristics including the size and general morphology of the dendritic tree and measures of dendritic branching patterns and stratification levels.

General morphological characteristics of the dendrites from presumed small bistratified, large sparse, and broad thorny ganglion cells were similar to previous reports of these types (see Chapters 2 and 3; Dacey, 1993a; Ghosh et al., 1997; Percival et al., 2009; Szmajda et al., 2008; Yamada et al., 2005). Hooks and spines are present on the inner dendritic tiers of presumed small bistratified ganglion cells - the inner tier being much larger and more densely branching than the outer tier. The thin dendrites of presumed large sparse ganglion cells branched in a more or less radial pattern reminiscent of those described in extra-foveal retina. The single example of a presumed broad thorny ganglion cell showed densely branching contorted dendrites as reported previously.

The patterns of dendritic stratification and branching are also consistent with previous reports of the three ganglion cell types, in marmoset (see Chapters 2 and 3; Ghosh et al., 1997; Percival et al., 2009; Szmajda et al., 2008) macaque and human (Dacey, 1993a; Yamada et al., 2005). Owing to the overall decrease in the dendritic fields of ganglion cells with decreasing retinal eccentricity, the dendritic fields of ganglion cells from the current study were smaller than their corresponding types outside the fovea.

Previous studies have reported circumferential distortions or elongations of the dendritic tree in ganglion cells lying within 0.7 mm from the fovea (Grünert and Wässle, 1993). No obvious distortions were observed in the current sample of small bistratified, large sparse and broad thorny ganglion cells, even in examples located at eccentricities < 0.7 mm. This may be due to the fact that the dendritic trees of these cells were relatively small and any distortions that were present are not as pronounced as is seen in ganglion cells with relatively large dendritic fields (see Figure 2 from Jusuf et al., 2007).

A single type of wide-field ganglion cell, which showed extremely large dendritic fields with very sparsely branching dendrites, was found in the current study. These have been provisionally termed these large bistratified ganglion cells on the basis of the characteristics of their dendritic tree, however it is unclear whether these ganglion cells

correspond to the previously described large bistratified ganglion cells as discussed below (Dacey et al., 2003; Peterson and Dacey, 2000; Yamada et al., 2005).

The long, and sparsely branching dendrites of large bistratified ganglion cells from the current study resemble those of the giant sparse / melanopsin containing ganglion cells, which have previously been described in primates including marmoset (Dacey et al., 2005; Hannibal et al., 2004; Jusuf et al., 2007; Szmajda et al., 2008). Unlike the large bistratified ganglion cells of the current study the giant sparse / melanopsin containing type in primate retina, does not possess a bistratified dendritic tree; instead two subtypes exist with dendrities stratifying at either ends of the inner plexiform layer. It should be noted however, that bistratified examples of the giant sparse / melanopsin containing ganglion cells have been reported in mouse retina (Berson et al., 2010). In addition, examples of melanopsin containing ganglion cells have been reported within 1 mm of the fovea in marmoset retina (Jusuf et al., 2007), for which dendritic field sizes are considerably larger than LFB cells (Figure 4.4). Thus, it seems unlikely that LFB cells are simply a foveal variant of melanopsin containing ganglion cells.

The bistratified dendritic tree of foveal large bistratified ganglion cells described here, may also suggest a correspondence with the previously described large bistratified ganglion cell type from peripheral macaque and human retina (Dacey and Packer, 2003; Peterson and Dacey, 2000; Yamada et al., 2005).

Large bistratified ganglion cells from previous studies have dendritic tiers that are restricted to S5 and S3 of the inner plexiform layer. Similarly, dendrites of large bistratified ganglion cells from the current study were narrowly stratified within the ON and OFF halves of the inner plexiform layer. Previous reports of peripheral large bistratified ganglion cells however do not report a highly elongated dendritic tree, as is a prominent feature in the sample of foveal large bistratified ganglion cells analysed here. The difference between the circumferential dendritic trees of previously described large bistratified cells, and the highly elongated dendritic tree of the current large bistratified cells, may be explained by the fact that distortions of the dendritic tree have occured in the current foveal sample due to their close proximity with the foveola. Grünert et al. (1993) reported distortions in the dendritic trees of foveal parasol ganglion cells where dendrites were seen to wrap around the foveola. In the same way, dendrites of foveal

large bistratified ganglion cells found here may wrap around the foveola resulting in the appearance of an elongated dendritic tree. As such, the large bistratified ganglion cells from the current study may simply correspond to a foveal variant of the large bistratified types described in peripheral retina. Another possibility is that the elongated appearance of the current sample of foveal large bistratified ganglion cells has resulted from incomplete labelling of the dendritic tree. This may result in the elongated appearance of an otherwise circular dendritic tree. Given these uncertainties it is not certain as to whether the current sample of foveal large bistratified ganglion cells belong to the same type previously described in peripheral retina.

Bipolar cell types at the fovea

Studies outlined in Section 1.3 (page 8) have shown that different bipolar cell types can be readily distinguished by the nature and number of their cone contacts, the lateral extent and morphology of their dendritic fields and axon terminals, and most notably by the level of axon terminal stratification within the inner plexiform layer. The current study identified diffuse bipolar cell types DB3, DB4 and DB6 within retinal preparations from the foveal slope and at approximately 1 mm eccentricity in macaque and marmoset retina. Bipolar cell types were distinguished by the use of specific immunocytochemical markers, and the pattern of axon terminal ramification of the labelled bipolar cells.

The relative axon terminal positions of the different bipolar cell types, as shown in previous studies (Boycott and Wässle, 1991; Chan et al., 2001), are maintained in both the foveal slope and 1mm samples from the current study. Amongst the bipolar cell types studied here, axon terminals of flat midget bipolar cells stratified near the border of the inner plexiform layer with the inner nuclear layer, followed by DB3, DB4 and DB6 bipolar cells, in increasing distances toward the border with the ganglion cell layer.

Results for the quantification of axon terminal stratification for the bipolar cell types investigated, were consistent with previous studies. Values reported by Boycott and Wässle (1991) for macaque retina were not directly comparable with the current results, as they were expressed as measurements from the cone pedicles to the axon terminal of the bipolar cell, for a retinal piece from 7 mm. The authors, however, also report measurements of 31 μm for the distance between the cone pedicles and the outer border

of the inner plexiform layer, and a total inner plexiform layer thickness of 24 μm for the retinal piece analysed. From these values, percentage estimates for Boycott and Wässle's (1991) data were made of the depth of axon terminal stratification with respect to the borders of the inner plexiform layer. As shown in Table 4.10 and 4.11, axon terminal stratification measures for macaque and marmoset samples were comparable with stratification ranges reported by Boycott and Wässle (1991), Jusuf et al., (2004) and Chan et al. (2001b).

Table 4.10: Axon terminal stratification comparisons - marmoset

Bipolar cell type	Axon terminal stratification range (%) - Marmoset			
	Chan et al. (2001) - 0.25 - 9.24 mm	Jusuf et al. (2004) - ~1.00 - 4.00 mm	Current study - foveal slope	Current study - 1 mm
FMB	14 - 41	6 - 17	5 - 18	5 - 15
DB3	27 - 38	NA	26 - 43	27 - 37
DB4	42 - 74	50 - 69	50 - 64	49 - 62
DB6	84 - 110	89 - 96	86 - 99	89 - 98

Not applicable (NA)

Table 4.11: Axon terminal stratification comparisons - macaque

Bipolar cell type	Axon terminal stratification range (%) - Macaque		
	Boycott and Wässle (1991) - 6 - 7 mm	Current study - foveal slope	Current study - 1 mm
FMB	29	14 - 31	10 - 20
DB3	30 - 37	26 - 46	32 - 41
DB4	54 - 67	46 - 73	54 - 68
DB6	83 - 100	90 - 99	95 - 101

Consistent with findings from previous studies in macaque and marmoset retina, axon terminals of the flat midget and DB4 cells from the current study spanned a small portion of the vertical extent of the inner plexiform layer. Axon terminals of DB4 cells in macaque retina at approximately 7 mm eccentricity were reported to span a band of 3 - 4 μm, which equates to approximately 12.50 - 16.67 % of the inner plexiform layer (Boycott and Wässle, 1991). Mean axon terminal stratification breadths for DB4 cells in the macaque sample were within the same range (at 1 mm, the average breadth of stratification was 16.05 ± 4.81 % and at the foveal slope was 18.56 ± 10.51 %).

Here, three diffuse bipolar cell types have been shown to be present at the foveal slope, with most features consistent with descriptions of these bipolar cell types outside the fovea. As such, it may be assumed that the connectivity of these diffuse bipolar cell

types within the foveal slope does not differ from what has been reported outside of the fovea.

Functional implications for foveal vision

The functional significance of these non-midget, non-parasol pathways are, at present, limited by our knowledge of the properties of the cells involved in this pathway. Of the wide-field types described to date, only responses of small bistratified ganglion cells have been well characterised (Chichilnisky and Baylor, 1999; Crook et al., 2009; Dacey and Lee, 1994; Field et al., 2009; Field et al., 2007; Silveira et al., 1999). Small bistratified ganglion cells show blue-ON/yellow-OFF response properties, thus their presence at the fovea indicates the capacity for such processing to occur in foveal vision.

Nonetheless, when the results of the current study are considered together with previous reports showing anatomical (Perry and Cowey, 1984; Stone and Johnston, 1981) and physiological (de Monasterio and Gouras, 1975; Gouras, 1969; Schiller and Malpeli, 1978) evidence for the presence of non-midget, non-parasol ganglion cells at the fovea, it seems highly likely that wide-field ganglion cells contribute to foveal vision.

Conclusion

Findings of the current study show that at least three types of previously described wide-field ganglion cells, and three types of diffuse bipolar cells are present within the fovea. Thus, a subset of the anatomical components required in the retinal circuitry of wide-field ganglion cell pathways is present at the fovea, providing support for wide-field ganglion cells contributing to foveal vision.

Chapter 5 Conclusion

As points of discussion relating to the results of each specific study have been considered in the discussion section of each project chapter, this section will focus largely on possible improvements to the studies and future directions.

The studies described in this thesis sought to further understand the connectivity of wide-field ganglion cell pathways within the retina. Results from the study described in Chapter 2 found an anatomical basis for the balancing of the blue-ON and yellow-OFF components of the small bistratified cell's chromatic response, in support of a previously proposed model for its retinal circuitry. Findings from Chapter 3 point to potential synaptic partners of the large sparse and broad thorny wide-field ganglion cell types, and show that functional differences between midget, parasol, small bistratified, large sparse and broad thorny ganglion cells do not arise from differences in synaptic input densities. Finally results from Chapter 4 confirm the presence of small bistratified, large sparse and broad thorny ganglion cells, together with potential diffuse bipolar type synaptic partners within the fovea, providing evidence for the potential for wide-field pathways to carry signals from the foveal representation of the visual scene.

While these findings have uncovered important aspects of the connectivity of wide-field ganglion cells, many of their detailed properties still remain unknown. In the case of small bistratified ganglion cells, the role of the rod mediated response of this cell type remains unclear, and for the large sparse and broad thorny types, a detailed study of their physiological responses is still required. Furthermore, the three wide-field ganglion cell types studied here represent a small proportion of the wide-field ganglion cells described to date, and there may be up to thirteen different morphological types which have yet to be studied in detail (Yamada et al., 2005).

The studies described here demonstrate the means by which an investigation of the connectivity of ganglion cells can be achieved by anatomical methods at the level of light microscopy. While it is very difficult to achieve, such methods may be further improved by the combined use of markers for synaptic inputs together with markers for potential synaptic partners. For example in the study of bipolar inputs onto large sparse cells from Chapter 2, a marker for the diffuse bipolar cell type 6 (DB6) together with the

antibody against the glutamate receptor subunit 4 (GluR4) may have been used on a preparation containing labelled large sparse ganglion cells. In the analysis of such a triple labelled preparation, if the location of presumed bipolar inputs (GluR4 immunoreactive puncta) were found to coincide with the regions of overlap between dendritic processes of large sparse ganglion cells and axon terminal processes of DB6 cells, this would provide more definitive proof of DB6 cells as a candidate for providing inputs onto large sparse ganglion cells. In the same way amacrine cell markers may be used in conjunction with the antibody against gephyrin to identify the source of inhibitory inputs onto ganglion cells.

References

Agardh E, Ehinger B, Wu JY. 1987. GABA and GAD-like immunoreactivity in the primate retina. Histochemistry 86(5):485-490.

Ahmad KM, Klug K, Herr S, Sterling P, Schein S. 2003. Cell density ratios in a foveal patch in macaque retina. Vis Neurosci 20(2):189-209.

Ahnelt P, Keri C, Kolb H. 1990. Identification of pedicles of putative blue-sensitive cones in the human retina. J Comp Neurol 293(1):39-53.

Ahnelt PK, Kolb H, Pflug R. 1987. Identification of a subtype of cone photoreceptor, likely to be blue sensitive, in the human retina. J Comp Neurol 255(1):18-34.

Ahnelt PK, Pflug R. 1986. Telodendrial contacts between foveolar cone pedicles in the human retina. Experientia 42(3):298-300.

Amthor FR, Oyster CW, Takahashi ES. 1984. Morphology of on-off direction-selective ganglion cells in the rabbit retina. Brain Res 298(1):187-190.

Amthor FR, Takahashi ES, Oyster CW. 1989. Morphologies of rabbit retinal ganglion cells with complex receptive fields. J Comp Neurol 280(1):97-121.

Andrade da Costa BL, Hokoç JN. 2000. Photoreceptor topography of the retina in the New World monkey Cebus apella. Vision Res 40(18):2395-2409.

Andressen C, Mai JK. 1997. Localization of the CD15 carbohydrate epitope in the vertebrate retina. Vis Neurosci 14(2):253-262.

Baylor D. 1996. How photons start vision. Proc Natl Acad Sci U S A 93(2):560-565.

Berson DM, Castrucci AM, Provencio I. 2010. Morphology and mosaics of melanopsin-expressing retinal ganglion cell types in mice. J Comp Neurol 518(13):2405-2422.

Blessing EM, Solomon SG, Hashemi-Nezhad M, Morris BJ, Martin PR. 2004. Chromatic and spatial properties of parvocellular cells in the lateral geniculate nucleus of the marmoset (Callithrix jacchus). J Physiol 557(Pt 1):229-245.

Bordt AS, Hoshi H, Yamada ES, Perryman-Stout WC, Marshak DW. 2006. Synaptic input to OFF parasol ganglion cells in macaque retina. J Comp Neurol 498(1):46-57.

Borwein B, Borwein D, Medeiros J, McGowan JW. 1980. The ultrastructure of monkey foveal photoreceptors, with special reference to the structure, shape, size, and spacing of the foveal cones. Am J Anat 159(2):125-146.

Boycott BB, Dowling JE, Kolb H. 1969. Organization of the primate retina: light microscopy. Philosophical Transactions of the Royal Society of London Series B, Biological Sciences 255(799):109-184.

Boycott BB, Hopkins JM. 1991. Cone bipolar cells and cone synapses in the primate retina. Vis Neurosci 7(1-2):49-60.

Boycott BB, Wässle H. 1991. Morphological Classification of Bipolar Cells of the Primate Retina. Eur J Neurosci 3(11):1069-1088.

Buzás P, Blessing EM, Szmajda BA, Martin PR. 2006. Specificity of M and L cone inputs to receptive fields in the parvocellular pathway: random wiring with functional bias. J Neurosci 26(43):11148-11161.

Calkins DJ. 1999. Synaptic organization of cone pathways in the primate retina. In: Gegenfurtner KR, Sharpe LT, editors. Color vision: from genes to perception. Cambridge: Cambridge University Press. p 163-179.

Calkins DJ. 2001. Seeing with S cones. Prog Retin Eye Res 20(3):255-287.

Calkins DJ, Schein SJ, Tsukamoto Y, Masarachia P, Sterling P. 1992. Parallel pathways to midget ganglion cells in macaque fovea. Investigative Ophthalmology and Visual Science 33:1173.

Calkins DJ, Schein SJ, Tsukamoto Y, Sterling P. 1994. M and L cones in macaque fovea connect to midget ganglion cells by different numbers of excitatory synapses. Nature 371(6492):70-72.

Calkins DJ, Sterling P. 1996. Absence of spectrally specific lateral inputs to midget ganglion cells in primate retina. Nature 381(6583):613-615.

Calkins DJ, Sterling P. 2007. Microcircuitry for two types of achromatic ganglion cell in primate fovea. J Neurosci 27(10):2646-2653.

Calkins DJ, Tsukamoto Y, Sterling P. 1996. Foveal cones form basal as well as invaginating junctions with diffuse ON bipolar cells. Vision Res 36(21):3373-3381.

Calkins DJ, Tsukamoto Y, Sterling P. 1998. Microcircuitry and mosaic of a blue-yellow ganglion cell in the primate retina. J Neurosci 18(9):3373-3385.

Chan TL, Martin PR, Clunas N, Grünert U. 2001. Bipolar cell diversity in the primate retina: morphologic and immunocytochemical analysis of a new world monkey, the marmoset Callithrix jacchus. J Comp Neurol 437(2):219-239.

Chichilnisky EJ, Baylor DA. 1999. Receptive-field microstructure of blue-yellow ganglion cells in primate retina. Nat Neurosci 2(10):889-893.

Chun MH, Grünert U, Martin PR, Wässle H. 1996. The synaptic complex of cones in the fovea and in the periphery of the macaque monkey retina. Vision Res 36(21):3383-3395.

Conradi N, Sjöstrand J. 1993. A morphometric and stereologic analysis of ganglion cells of the central human retina. Graefes Arch Clin Exp Ophthalmol 231(3):169-174.

Croner LJ, Kaplan E. 1995. Receptive fields of P and M ganglion cells across the primate retina. Vision Res 35(1):7-24.

Crook JD, Davenport CM, Peterson BB, Packer OS, Detwiler PB, Dacey DM. 2009. Parallel ON and OFF cone bipolar inputs establish spatially coextensive receptive field structure of blue-yellow ganglion cells in primate retina. J Neurosci 29(26):8372-8387.

Crook JM, Lange-Malecki B, Lee BB, Valberg A. 1988. Visual resolution of macaque retinal ganglion cells. J Physiol 396:205-224.

Cuenca N, Kolb H. 1998. Circuitry and role of substance P-immunoreactive neurons in the primate retina. J Comp Neurol 393(4):439-456.

Curcio CA, Allen KA. 1990. Topography of ganglion cells in human retina. J Comp Neurol 300(1):5-25.

Curcio CA, Allen KA, Sloan KR, Lerea CL, Hurley JB, Klock IB, Milam AH. 1991. Distribution and morphology of human cone photoreceptors stained with anti-blue opsin. J Comp Neurol 312(4):610-624.

Curcio CA, Sloan KR, Kalina RE, Hendrickson AE. 1990. Human photoreceptor topography. J Comp Neurol 292(4):497-523.

Dacey D, Packer OS, Diller L, Brainard D, Peterson B, Lee B. 2000. Center surround receptive field structure of cone bipolar cells in primate retina. Vision Res 40(14):1801-1811.

Dacey DM. 1993a. Morphology of a small-field bistratified ganglion cell type in the macaque and human retina. Vis Neurosci 10(6):1081-1098.

Dacey DM. 1993b. The mosaic of midget ganglion cells in the human retina. J Neurosci 13(12):5334-5355.

Dacey DM. 1994. Physiology, morphology and spatial densities of identified ganglion cell types in primate retina. Ciba Found Symp 184:12-28; discussion 28-34, 63-70.

Dacey DM. 1999. Primate retina: cell types, circuits and color opponency. Prog Retin Eye Res 18(6):737-763.

Dacey DM. 2000. Parallel pathways for spectral coding in primate retina. Annu Rev Neurosci 23:743-775.

Dacey DM. 2004. Origins of perception: retinal ganglion cell diversity and the parallel visual pathways. In: Gazzaniga MS, editor. The Cognitive Neurosciences. Cambridge: MIT Press. p 281-301.

Dacey DM, Lee BB. 1994. The 'blue-on' opponent pathway in primate retina originates from a distinct bistratified ganglion cell type. Nature 367(6465):731-735.

Dacey DM, Liao HW, Peterson BB, Robinson FR, Smith VC, Pokorny J, Yau KW, Gamlin PD. 2005. Melanopsin-expressing ganglion cells in primate retina signal colour and irradiance and project to the LGN. Nature 433(7027):749-754.

Dacey DM, Packer OS. 2003. Colour coding in the primate retina: diverse cell types and cone-specific circuitry. Curr Opin Neurobiol 13(4):421-427.

Dacey DM, Petersen MR. 1992. Dendritic field size and morphology of midget and parasol ganglion cells of the human retina. Proc Natl Acad Sci U S A 89(20):9666-9670.

Dacey DM, Peterson BB, Robinson FR, Gamlin PD. 2003. Fireworks in the primate retina: in vitro photodynamics reveals diverse LGN-projecting ganglion cell types. Neuron 37(1):15-27.

Dacey DM, Peterson BB, Robinson RF. 2002. Identification of an S-cone opponent OFF pathway in the macaque monkey retina: morphology, physiology and possible circuitry. Investigative Ophthalmology and Visual Science 43:E-abstract 2983.

Davanger S, Ottersen OP, Storm-Mathisen J. 1991. Glutamate, GABA, and glycine in the human retina: an immunocytochemical investigation. J Comp Neurol 311(4):483-494.

de Monasterio FM. 1979. Asymmetry of on- and off-pathways of blue-sensitive cones of the retina of macaques. Brain Res 166(1):39-48.

de Monasterio FM, Gouras P. 1975. Functional properties of ganglion cells of the rhesus monkey retina. J Physiol 251(1):167-195.

de Monasterio FM, Gouras P, Tolhurst DJ. 1975. Trichromatic colour opponency in ganglion cells of the rhesus monkey retina. J Physiol 251(1):197-216.

de Monasterio FM, McCrane EP, Newlander JK, Schein SJ. 1985. Density profile of blue-sensitive cones along the horizontal meridian of macaque retina. Invest Ophthalmol Vis Sci 26(3):289-302.

de Monasterio FM, Schein SJ, McCrane EP. 1981. Staining of blue-sensitive cones of the macaque retina by a fluorescent dye. Science 213(4513):1278-1281.

Derrington AM, Krauskopf J, Lennie P. 1984. Chromatic mechanisms in lateral geniculate nucleus of macaque. J Physiol 357:241-265.

DeVries SH. 2000. Bipolar cells use kainate and AMPA receptors to filter visual information into separate channels. Neuron 28(3):847-856.

DeVries SH, Li W, Saszik S. 2006. Parallel processing in two transmitter microenvironments at the cone photoreceptor synapse. Neuron 50(5):735-748.

Dowling JE. 1965. Foveal Receptors of the Monkey Retina: Fine Structure. Science 147:57-59.

Dowling JE, Boycott BB. 1966. Organization of the primate retina: electron microscopy. Proc R Soc Lond B Biol Sci 166(2):80-111.

Ehinger B. 1972. Uptake of tritiated glycine into neurons of the human retina. Experientia 28(9):1042-1043.

Eriköz B, Jusuf PR, Percival KA, Grünert U. 2008. Distribution of bipolar input to midget and parasol ganglion cells in marmoset retina. Vis Neurosci 25(1):67-76.

Famiglietti EV. 2005. Synaptic organization of complex ganglion cells in rabbit retina: type and arrangement of inputs to directionally selective and local-edge-detector cells. J Comp Neurol 484(4):357-391.

Famiglietti EV, Jr., Kolb H. 1975. A bistratified amacrine cell and synaptic cirucitry in the inner plexiform layer of the retina. Brain Res 84(2):293-300.

Field GD, Greschner M, Gauthier JL, Rangel C, Shlens J, Sher A, Marshak DW, Litke AM, Chichilnisky EJ. 2009. High-sensitivity rod photoreceptor input to the blue-yellow color opponent pathway in macaque retina. Nat Neurosci 12(9):1159-1164.

Field GD, Sher A, Gauthier JL, Greschner M, Shlens J, Litke AM, Chichilnisky EJ. 2007. Spatial properties and functional organization of small bistratified ganglion cells in primate retina. J Neurosci 27(48):13261-13272.

Finlay BL, Franco EC, Yamada ES, Crowley JC, Parsons M, Muniz JA, Silveira LC. 2008. Number and topography of cones, rods and optic nerve axons in New and Old World primates. Vis Neurosci 25(3):289-299.

Fischer F, Kneussel M, Tintrup H, Haverkamp S, Rauen T, Betz H, Wässle H. 2000. Reduced synaptic clustering of GABA and glycine receptors in the retina of the gephyrin null mutant mouse. J Comp Neurol 427(4):634-648.

Franco EC, Finlay BL, Silveira LC, Yamada ES, Crowley JC. 2000. Conservation of absolute foveal area in New World monkeys. A constraint on eye size and conformation. Brain Behav Evol 56(5):276-286.

Frederick JM, Rayborn ME, Hollyfield JG. 1984. Glycinergic neurons in the human retina. J Comp Neurol 227(2):159-172.

Freed MA. 2000. Parallel cone bipolar pathways to a ganglion cell use different rates and amplitudes of quantal excitation. J Neurosci 20(11):3956-3963.

Freed MA, Sterling P. 1988. The ON-alpha ganglion cell of the cat retina and its presynaptic cell types. J Neurosci 8(7):2303-2320.

Fyk-Kolodziej B, Dzhagaryan A, Qin P, Pourcho RG. 2004. Immunocytochemical localization of three vesicular glutamate transporters in the cat retina. J Comp Neurol 475(4):518-530.

Ghosh KK, Goodchild AK, Sefton AE, Martin PR. 1996. Morphology of retinal ganglion cells in a new world monkey, the marmoset Callithrix jacchus. J Comp Neurol 366(1):76-92.

Ghosh KK, Grünert U. 1999. Synaptic input to small bistratified (blue-ON) ganglion cells in the retina of a new world monkey, the marmoset Callithrix jacchus. J Comp Neurol 413(3):417-428.

Ghosh KK, Martin PR, Grünert U. 1997. Morphological analysis of the blue cone pathway in the retina of a New World monkey, the marmoset Callithrix jacchus. J Comp Neurol 379(2):211-225.

Gouras P. 1968. Identification of cone mechanisms in monkey ganglion cells. J Physiol 199(3):533-547.

Gouras P. 1969. Antidromic responses of orthodromically identified ganglion cells in monkey retina. J Physiol 204(2):407-419.

Grünert U. 1997. Anatomical evidence for rod input to the parvocellular pathway in the visual system of the primate. Eur J Neurosci 9(3):617-621.

Grünert U, Greferath U, Boycott BB, Wässle H. 1993. Parasol (P alpha) ganglion-cells of the primate fovea: immunocytochemical staining with antibodies against GABAA-receptors. Vision Res 33(1):1-14.

Grünert U, Haverkamp S, Fletcher EL, Wässle H. 2002. Synaptic distribution of ionotropic glutamate receptors in the inner plexiform layer of the primate retina. J Comp Neurol 447(2):138-151.

Grünert U, Jusuf PR, Lee SC, Nguyen DT. 2011. Bipolar input to melanopsin containing ganglion cells in primate retina. Vis Neurosci 28(1):39-50.

Grünert U, Lin B, Martin PR. 2003. Glutamate receptors at bipolar synapses in the inner plexiform layer of primate retina: light microscopic analysis. J Comp Neurol 466(1):136-147.

Grünert U, Martin PR. 1991. Rod bipolar cells in the macaque monkey retina: immunoreactivity and connectivity. J Neurosci 11(9):2742-2758.

Grünert U, Martin PR, Wässle H. 1994. Immunocytochemical analysis of bipolar cells in the macaque monkey retina. J Comp Neurol 348(4):607-627.

Grünert U, Wässle H. 1990. GABA-like immunoreactivity in the macaque monkey retina: a light and electron microscopic study. J Comp Neurol 297(4):509-524.

Grünert U, Wässle H. 1993. Immunocytochemical localization of glycine receptors in the mammalian retina. J Comp Neurol 335(4):523-537.

Grünert U, Wässle H. 1996. Glycine receptors in the rod pathway of the macaque monkey retina. Vis Neurosci 13(1):101-115.

Hanna MC, Calkins DJ. 2007. Expression of genes encoding glutamate receptors and transporters in rod and cone bipolar cells of the primate retina determined by single-cell polymerase chain reaction. Mol Vis 13:2194-2208.

Hannibal J, Hindersson P, Ostergaard J, Georg B, Heegaard S, Larsen PJ, Fahrenkrug J. 2004. Melanopsin is expressed in PACAP-containing retinal ganglion cells of the human retinohypothalamic tract. Invest Ophthalmol Vis Sci 45(11):4202-4209.

Harlow E, Lane D. 1988. Antibodies: a laboratory manual. New York: Cold Spring Harbor Laboratory Press.

Hashemi-Nezhad M, Blessing EM, Dreher B, Martin PR. 2008. Segregation of short-wavelength sensitive ("blue") cone signals among neurons in the lateral geniculate nucleus and striate cortex of marmosets. Vision Res 48(26):2604-2614.

Haverkamp S, Ghosh KK, Hirano AA, Wassle H. 2003. Immunocytochemical description of five bipolar cell types of the mouse retina. J Comp Neurol 455(4):463-476.

Haverkamp S, Grunert U, Wassle H. 2001. The synaptic architecture of AMPA receptors at the cone pedicle of the primate retina. J Neurosci 21(7):2488-2500.

Haverkamp S, Grünert U, Wässle H. 2000. The cone pedicle, a complex synapse in the retina. Neuron 27(1):85-95.

Hendrickson A, Kupfer C. 1976. The histogenesis of the fovea in the macaque monkey. Invest Ophthalmol Vis Sci 15(9):746-756.

Hendrickson A, Troilo D, Djajadi H, Possin D, Springer A. 2009. Expression of synaptic and phototransduction markers during photoreceptor development in the marmoset monkey Callithrix jacchus. J Comp Neurol 512(2):218-231.

Hendrickson AE. 1994. Primate foveal development: a microcosm of current questions in neurobiology. Invest Ophthalmol Vis Sci 35(8):3129-3133.

Hendrickson AE, Koontz MA, Pourcho RG, Sarthy PV, Goebel DJ. 1988. Localization of glycine-containing neurons in the Macaca monkey retina. J Comp Neurol 273(4):473-487.

Herr S, Klug K, Sterling P, Schein S. 2003. Inner S-cone bipolar cells provide all of the central elements for S cones in macaque retina. J Comp Neurol 457(2):185-201.

Hirsch J, Curcio CA. 1989. The spatial resolution capacity of human foveal retina. Vision Res 29(9):1095-1101.

Hofer H, Carroll J, Neitz J, Neitz M, Williams DR. 2005. Organization of the human trichromatic cone mosaic. J Neurosci 25(42):9669-9679.

Hopkins JM, Boycott BB. 1992. Synaptic contacts of a two-cone flat bipolar cell in a primate retina. Vis Neurosci 8(4):379-384.

Hopkins JM, Boycott BB. 1997. The cone synapses of cone bipolar cells of primate retina. J Neurocytol 26(5):313-325.

Hoshi H, Liu WL, Massey SC, Mills SL. 2009. ON inputs to the OFF layer: bipolar cells that break the stratification rules of the retina. J Neurosci 29(28):8875-8883.

Hubel DH, Wiesel TN. 1960. Receptive fields of optic nerve fibres in the spider monkey. J Physiol 154:572-580.

Jacoby R, Stafford D, Kouyama N, Marshak D. 1996. Synaptic inputs to ON parasol ganglion cells in the primate retina. J Neurosci 16(24):8041-8056.

Jacoby RA, Marshak DW. 2000. Synaptic connections of DB3 diffuse bipolar cell axons in macaque retina. J Comp Neurol 416(1):19-29.

Jacoby RA, Wiechmann AF, Amara SG, Leighton BH, Marshak DW. 2000. Diffuse bipolar cells provide input to OFF parasol ganglion cells in the macaque retina. J Comp Neurol 416(1):6-18.

Jakobs TC, Koizumi A, Masland RH. 2008. The spatial distribution of glutamatergic inputs to dendrites of retinal ganglion cells. J Comp Neurol 510(2):221-236.

Jeon CJ, Kong JH, Strettoi E, Rockhill R, Stasheff SF, Masland RH. 2002. Pattern of synaptic excitation and inhibition upon direction-selective retinal ganglion cells. J Comp Neurol 449(2):195-205.

Johnson J, Tian N, Caywood MS, Reimer RJ, Edwards RH, Copenhagen DR. 2003. Vesicular neurotransmitter transporter expression in developing postnatal rodent retina: GABA and glycine precede glutamate. J Neurosci 23(2):518-529.

Jonas JB, Schneider U, Naumann GO. 1992. Count and density of human retinal photoreceptors. Graefes Arch Clin Exp Ophthalmol 230(6):505-510.

Joo HR, Peterson BB, Haun TJ, Dacey DM. Characterization of a novel large-field cone bipolar cell type in the primate retina: Evidence for selective cone connections. Vis Neurosci 28(1):29-37.

Jusuf PR, Haverkamp S, Grunert U. 2005. Localization of glycine receptor alpha subunits on bipolar and amacrine cells in primate retina. J Comp Neurol 488(2):113-128.

Jusuf PR, Lee SC, Grünert U. 2004. Synaptic connectivity of the diffuse bipolar cell type DB6 in the inner plexiform layer of primate retina. J Comp Neurol 469(4):494-506.

Jusuf PR, Lee SC, Hannibal J, Grünert U. 2007. Characterization and synaptic connectivity of melanopsin-containing ganglion cells in the primate retina. Eur J Neurosci 26(10):2906-2921.

Jusuf PR, Martin PR, Grunert U. 2006a. Synaptic connectivity in the midget-parvocellular pathway of primate central retina. J Comp Neurol 494(2):260-274.

Jusuf PR, Martin PR, Grünert U. 2006b. Random wiring in the midget pathway of primate retina. J Neurosci 26(15):3908-3917.

Kaplan E, Shapley RM. 1986. The primate retina contains two types of ganglion cells, with high and low contrast sensitivity. Proc Natl Acad Sci U S A 83(8):2755-2757.

Kier CK, Buchsbaum G, Sterling P. 1995. How retinal microcircuits scale for ganglion cells of different size. J Neurosci 15(11):7673-7683.

Kneussel M, Betz H. 2000. Receptors, gephyrin and gephyrin-associated proteins: novel insights into the assembly of inhibitory postsynaptic membrane specializations. J Physiol 525 Pt 1:1-9.

Kolb H. 1970. Organization of the outer plexiform layer of the primate retina: electron microscopy of Golgi-impregnated cells. Philosophical Transactions of the Royal Society of London Series B, Biological Sciences 258(823):261-283.

Kolb H, Dekorver L. 1991. Midget ganglion cells of the parafovea of the human retina: a study by electron microscopy and serial section reconstructions. J Comp Neurol 303(4):617-636.

Kolb H, Linberg KA, Fisher SK. 1992. Neurons of the human retina: a Golgi study. J Comp Neurol 318(2):147-187.

Kolb H, Marshak D. 2003. The midget pathways of the primate retina. Doc Ophthalmol 106(1):67-81.

Kolb H, Nelson R. 1983. Rod pathways in the retina of the cat. Vision Res 23(4):301-312.

Kolb H, Nelson R. 1993. OFF-alpha and OFF-beta ganglion cells in cat retina: II. Neural circuitry as revealed by electron microscopy of HRP stains. J Comp Neurol 329(1):85-110.

Kolb H, Nelson R. 1996. Hyperpolarizing, small-field, amacrine cells in cone pathways of cat retina. J Comp Neurol 371(3):415-436.

Kouyama N, Marshak DW. 1992. Bipolar cells specific for blue cones in the macaque retina. J Neurosci 12(4):1233-1252.

Krebs W, Krebs IP. 1989. Quantitative morphology of the central fovea in the primate retina. Am J Anat 184(3):225-236.

Lagnado L. 2003. Ribbon synapses. Curr Biol 13(16):R631.

Lee BB. 1993. Macaque ganglion cells and spatial vision. Prog Brain Res 95:33-43.

Lee BB. 1996. Receptive field structure in the primate retina. Vision Res 36(5):631-644.

Lee SC, Grünert U. 2007. Connections of diffuse bipolar cells in primate retina are biased against S-cones. J Comp Neurol 502(1):126-140.

Lee SC, Telkes I, Grünert U. 2005. S-cones do not contribute to the OFF-midget pathway in the retina of the marmoset, Callithrix jacchus. Eur J Neurosci 22(2):437-447.

Leventhal AG, Rodieck RW, Dreher B. 1981. Retinal ganglion cell classes in the Old World monkey: morphology and central projections. Science 213(4512):1139-1142.

Leventhal AG, Thompson KG, Liu D. 1993. Retinal ganglion cells within the foveola of New World (Saimiri sciureus) and Old World (Macaca fascicularis) monkeys. J Comp Neurol 338(2):242-254.

Lin B, Martin PR, Grunert U. 2002. Expression and distribution of ionotropic glutamate receptor subunits on parasol ganglion cells in the primate retina. Vis Neurosci 19(4):453-465.

Lin B, Martin PR, Solomon SG, Grünert U. 2000. Distribution of glycine receptor subunits on primate retinal ganglion cells: a quantitative analysis. Eur J Neurosci 12(12):4155-4170.

Luo X, Ghosh KK, Martin PR, Grünert U. 1999. Analysis of two types of cone bipolar cells in the retina of a New World monkey, the marmoset, Callithrix jacchus. Vis Neurosci 16(4):707-719.

Macri J, Martin PR, Grünert U. 2000. Distribution of the alpha1 subunit of the GABA(A) receptor on midget and parasol ganglion cells in the retina of the common marmoset Callithrix jacchus. Vis Neurosci 17(3):437-448.

Marc RE, Sperling HG. 1977. Chromatic organization of primate cones. Science 196(4288):454-456.

Mariani AP. 1981. A diffuse, invaginating cone bipolar cell in primate retina. J Comp Neurol 197(4):661-671.

Mariani AP. 1983. Giant bistratified bipolar cells in monkey retina. The Anatomical Record 206:215-220.

Mariani AP. 1984. Bipolar cells in monkey retina selective for the cones likely to be blue-sensitive. Nature 308(5955):184-186.

Mariani AP. 1990. Amacrine cells of the rhesus monkey retina. J Comp Neurol 301(3):382-400.

Marshak DW, Yamada ES, Bordt AS, Perryman WC. 2002. Synaptic input to an ON parasol ganglion cell in the macaque retina: a serial section analysis. Vis Neurosci 19(3):299-305.

Martin PR, Grünert U. 1992. Spatial density and immunoreactivity of bipolar cells in the macaque monkey retina. J Comp Neurol 323(2):269-287.

Martin PR, Grünert U. 1999. Analysis of the short wavelength-sensitive ("blue") cone mosaic in the primate retina: comparison of New World and Old World monkeys. J Comp Neurol 406(1):1-14.

Martin PR, White AJ, Goodchild AK, Wilder HD, Sefton AE. 1997. Evidence that blue-on cells are part of the third geniculocortical pathway in primates. Eur J Neurosci 9(7):1536-1541.

McCrane EP, de Monasterio FM, Schein SJ, Caruso RC. 1983. Non-fluorescent dye staining of primate blue cones. Invest Ophthalmol Vis Sci 24(11):1449-1455.

McGuire BA, Stevens JK, Sterling P. 1986. Microcircuitry of beta ganglion cells in cat retina. J Neurosci 6(4):907-918.

Merigan WH, Maunsell JH. 1993. How parallel are the primate visual pathways? Annu Rev Neurosci 16:369-402.

Milam AH, Dacey DM, Dizhoor AM. 1993. Recoverin immunoreactivity in mammalian cone bipolar cells. Vis Neurosci 10(1):1-12.

Mills SL, Massey SC. 1999. AII amacrine cells limit scotopic acuity in central macaque retina: A confocal analysis of calretinin labeling. J Comp Neurol 411(1):19-34.

Mills SL, O'Brien JJ, Li W, O'Brien J, Massey SC. 2001. Rod pathways in the mammalian retina use connexin 36. J Comp Neurol 436(3):336-350.

Missotten L. 1974. Estimation of the ratio of cones to neurons in the fovea of the human retina. Invest Ophthalmol 13(12):1045-1049.

Mollon JD, Bowmaker JK. 1992. The spatial arrangement of cones in the primate fovea. Nature 360(6405):677-679.

Morgan JL, Schubert T, Wong RO. 2008. Developmental patterning of glutamatergic synapses onto retinal ganglion cells. Neural Dev 3:8.

Nelson R, Kolb H. 1983. Synaptic patterns and response properties of bipolar and ganglion cells in the cat retina. Vision Res 23(10):1183-1195.

Nishimura Y, Schwartz ML, Rakic P. 1985. Localization of gamma-aminobutyric acid and glutamic acid decarboxylase in rhesus monkey retina. Brain Res 359(1-2):351-355.

Owczarzak MT, Pourcho RG. 1999. Transmitter-specific input to OFF-alpha ganglion cells in the cat retina. Anat Rec 255(4):363-373.

Packer O, Hendrickson AE, Curcio CA. 1989. Photoreceptor topography of the retina in the adult pigtail macaque (Macaca nemestrina). J Comp Neurol 288(1):165-183.

Packer O, Verweij J, Schnapf JL, Dacey DM. 2007. Primate S cones have blue-yellow opponent receptive fields. Investigative Ophthalmology and Visual Science 48(E-abstract 2849).

Packer OS, Williams DR, Bensinger DG. 1996. Photopigment transmittance imaging of the primate photoreceptor mosaic. J Neurosci 16(7):2251-2260.

Parsons TD, Sterling P. 2003. Synaptic ribbon. Conveyor belt or safety belt? Neuron 37(3):379-382.

Percival KA, Jusuf PR, Martin PR, Grunert U. 2009. Synaptic inputs onto small bistratified (blue-ON/yellow-OFF) ganglion cells in marmoset retina. J Comp Neurol 517(5):655-669.

Perry VH, Cowey A. 1981. The morphological correlates of X- and Y-like retinal ganglion cells in the retina of monkeys. Exp Brain Res 43(2):226-228.

Perry VH, Cowey A. 1984. Retinal ganglion cells that project to the superior colliculus and pretectum in the macaque monkey. Neuroscience 12(4):1125-1137.

Perry VH, Cowey A. 1985. The ganglion cell and cone distributions in the monkey's retina: implications for central magnification factors. Vision Res 25(12):1795-1810.

Perry VH, Cowey A. 1988. The lengths of the fibres of Henle in the retina of macaque monkeys: implications for vision. Neuroscience 25(1):225-236.

Perry VH, Oehler R, Cowey A. 1984. Retinal ganglion cells that project to the dorsal lateral geniculate nucleus in the macaque monkey. Neuroscience 12(4):1101-1123.

Peterson BB, Dacey DM. 1999. Morphology of wide-field, monostratified ganglion cells of the human retina. Vis Neurosci 16(1):107-120.

Peterson BB, Dacey DM. 2000. Morphology of wide-field bistratified and diffuse human retinal ganglion cells. Vis Neurosci 17(4):567-578.

Pfeiffer F, Simler R, Grenningloh G, Betz H. 1984. Monoclonal antibodies and peptide mapping reveal structural similarities between the subunits of the glycine receptor of rat spinal cord. Proc Natl Acad Sci U S A 81(22):7224-7227.

Polyak SL. 1935. Structure of the Retina in Primates. Acta Ophthalmologica 13:52.

Polyak SL. 1941. The Retina. Chicago: University of Chicago Press.

Pourcho RG, Owczarzak MT. 1991. Glycine receptor immunoreactivity is localized at amacrine synapses in cat retina. Vis Neurosci 7(6):611-618.

Prescott ED, Zenisek D. 2005. Recent progress towards understanding the synaptic ribbon. Curr Opin Neurobiol 15(4):431-436.

Provis JM, Diaz CM, Dreher B. 1998. Ontogeny of the primate fovea: a central issue in retinal development. Prog Neurobiol 54(5):549-580.

Qin P, Pourcho RG. 1999. AMPA-selective glutamate receptor subunits GluR2 and GluR4 in the cat retina: an immunocytochemical study. Vis Neurosci 16(6):1105-1114.

Rodieck RW. 1988. The primate retina. In: Steklis HD, Erwin J, editors. Comparative Primate Biology, Volume 4: Neurosciences. New York: Alan R. Liss. p 203-278.

Rodieck RW. 1991. Which cells code for color? In: Valberg A, Lee BB, editors. From Pigments to Perception. New York: Plenum Press.

Rodieck RW, Binmoeller KF, Dineen J. 1985. Parasol and midget ganglion cells of the human retina. J Comp Neurol 233(1):115-132.

Rodieck RW, Watanabe M. 1993. Survey of the morphology of macaque retinal ganglion cells that project to the pretectum, superior colliculus, and parvicellular laminae of the lateral geniculate nucleus. J Comp Neurol 338(2):289-303.

Rolls ET, Cowey A. 1970. Topography of the retina and striate cortex and its relationship to visual acuity in rhesus monkeys and squirrel monkeys. Exp Brain Res 10(3):298-310.

Roorda A, Metha AB, Lennie P, Williams DR. 2001. Packing arrangement of the three cone classes in primate retina. Vision Res 41(10-11):1291-1306.

Roorda A, Williams DR. 1999. The arrangement of the three cone classes in the living human eye. Nature 397(6719):520-522.

Sassoe-Pognetto M, Fritschy JM. 2000. Mini-review: gephyrin, a major postsynaptic protein of GABAergic synapses. Eur J Neurosci 12(7):2205-2210.

Sassoè-Pognetto M, Kirsch J, Grünert U, Greferath U, Fritschy JM, Mohler H, Betz H, Wässle H. 1995. Colocalization of gephyrin and GABAA-receptor subunits in the rat retina. J Comp Neurol 357(1):1-14.

Sassoè-Pognetto M, Wässle H, Grünert U. 1994. Glycinergic synapses in the rod pathway of the rat retina: cone bipolar cells express the alpha 1 subunit of the glycine receptor. J Neurosci 14(8):5131-5146.

Schein S, Sterling P, Ngo IT, Huang TM, Herr S. 2004. Evidence that each S cone in macaque fovea drives one narrow-field and several wide-field blue-yellow ganglion cells. J Neurosci 24(38):8366-8378.

Schein SJ. 1988. Anatomy of macaque fovea and spatial densities of neurons in foveal representation. J Comp Neurol 269(4):479-505.

Schiller PH, Logothetis NK, Charles ER. 1990. Functions of the colour-opponent and broad-band channels of the visual system. Nature 343(6253):68-70.

Schiller PH, Malpeli JG. 1977. Properties and tectal projections of monkey retinal ganglion cells. J Neurophysiol 40(2):428-445.

Schiller PH, Malpeli JG. 1978. Functional specificity of lateral geniculate nucleus laminae of the rhesus monkey. J Neurophysiol 41(3):788-797.

Schmitt B, Knaus P, Becker CM, Betz H. 1987. The Mr 93,000 polypeptide of the postsynaptic glycine receptor complex is a peripheral membrane protein. Biochemistry 26(3):805-811.

Schmitz F, Königstorfer A, Südhof TC. 2000. RIBEYE, a component of synaptic ribbons: a protein's journey through evolution provides insight into synaptic ribbon function. Neuron 28(3):857-872.

Shapiro MB, Schein SJ, de Monasterio FM. 1985. Regularity and structure of the spatial pattern of blue cones of macaque retina. Journal of the American Statistical Association 80(392):803-812.

Sherry DM, Wang MM, Bates J, Frishman LJ. 2003. Expression of vesicular glutamate transporter 1 in the mouse retina reveals temporal ordering in development of rod vs. cone and ON vs. OFF circuits. J Comp Neurol 465(4):480-498.

Silveira LC, Lee BB, Yamada ES, Kremers J, Hunt DM, Martin PR, Gomes FL. 1999. Ganglion cells of a short-wavelength-sensitive cone pathway in New World monkeys: morphology and physiology. Vis Neurosci 16(2):333-343.

Silveira LC, Perry VH. 1991. The topography of magnocellular projecting ganglion cells (M-ganglion cells) in the primate retina. Neuroscience 40(1):217-237.

Sjöstrand J, Conradi N, Klaren L. 1994. How many ganglion cells are there to a foveal cone? A stereologic analysis of the quantitative relationship between cone and ganglion cells in one normal human fovea. Graefes Arch Clin Exp Ophthalmol 232(7):432-437.

Sjöstrand J, Olsson V, Popovic Z, Conradi N. 1999a. Quantitative estimations of foveal and extra-foveal retinal circuitry in humans. Vision Res 39(18):2987-2998.

Sjöstrand J, Popovic Z, Conradi N, Marshall J. 1999b. Morphometric study of the displacement of retinal ganglion cells subserving cones within the human fovea. Graefes Arch Clin Exp Ophthalmol 237(12):1014-1023.

Slonaker JR. 1897. A comparative study of the area of acute vision in vertebrates. Journal of Morphology 13:445-503.

Solomon SG, Lee BB, White AJ, Ruttiger L, Martin PR. 2005. Chromatic organization of ganglion cell receptive fields in the peripheral retina. J Neurosci 25(18):4527-4539.

Sterling P, Matthews G. 2005. Structure and function of ribbon synapses. Trends Neurosci 28(1):20-29.

Stone J, Johnston E. 1981. The topography of primate retina: a study of the human, bushbaby, and new- and old-world monkeys. J Comp Neurol 196(2):205-223.

Szél A, Diamantstein T, Röhlich P. 1988. Identification of the blue-sensitive cones in the mammalian retina by anti-visual pigment antibody. J Comp Neurol 273(4):593-602.

Szmajda BA, Buzas P, Fitzgibbon T, Martin PR. 2006. Geniculocortical relay of blue-off signals in the primate visual system. Proc Natl Acad Sci U S A 103(51):19512-19517.

Szmajda BA, Grünert U, Martin PR. 2005. Mosaic properties of midget and parasol ganglion cells in the marmoset retina. Vis Neurosci 22(4):395-404.

Szmajda BA, Grünert U, Martin PR. 2008. Retinal ganglion cell inputs to the koniocellular pathway. J Comp Neurol 510(3):251-268.

Tailby C, Solomon SG, Lennie P. 2008a. Functional asymmetries in visual pathways carrying S-cone signals in macaque. J Neurosci 28(15):4078-4087.

Tailby C, Szmajda BA, Buzas P, Lee BB, Martin PR. 2008b. Transmission of blue (S) cone signals through the primate lateral geniculate nucleus. J Physiol 586(Pt 24):5947-5967.

Telkes I, Lee SC, Jusuf PR, Grünert U. 2008. The midget-parvocellular pathway of marmoset retina: a quantitative light microscopic study. J Comp Neurol 510(5):539-549.

tom Dieck S, Altrock WD, Kessels MM, Qualmann B, Regus H, Brauner D, Fejtova A, Bracko O, Gundelfinger ED, Brandstätter JH. 2005. Molecular dissection of the photoreceptor ribbon synapse: physical interaction of Bassoon and RIBEYE is essential for the assembly of the ribbon complex. J Cell Biol 168(5):825-836.

tom Dieck S, Brandstätter JH. 2006. Ribbon synapses of the retina. Cell Tissue Res 326(2):339-346.

Troilo D, Howland HC, Judge SJ. 1993. Visual optics and retinal cone topography in the common marmoset (Callithrix jacchus). Vision Res 33(10):1301-1310.

Tse YC, Lai CH, Lai SK, Liu JX, Yung KK, Shum DK, Chan YS. 2008. Developmental expression of NMDA and AMPA receptor subunits in vestibular nuclear neurons that encode gravity-related horizontal orientations. J Comp Neurol 508(2):343-364.

Valberg A, Lee BB, Tigwell DA. 1986. Neurones with strong inhibitory S-cone inputs in the macaque lateral geniculate nucleus. Vision Res 26(7):1061-1064.

Vardi N, Duvoisin R, Wu G, Sterling P. 2000. Localization of mGluR6 to dendrites of ON bipolar cells in primate retina. J Comp Neurol 423(3):402-412.

Wässle H. 1999. Colour vision. A patchwork of cones. Nature 397(6719):473, 475.

Wässle H, Boycott BB. 1991. Functional architecture of the mammalian retina. Physiol Rev 71(2):447-480.

Wässle H, Grünert U, Martin PR, Boycott BB. 1994. Immunocytochemical characterization and spatial distribution of midget bipolar cells in the macaque monkey retina. Vision Res 34(5):561-579.

Wässle H, Grünert U, Rohrenbeck J, Boycott BB. 1989. Cortical magnification factor and the ganglion cell density of the primate retina. Nature 341(6243):643-646.

Wässle H, Grünert U, Rohrenbeck J, Boycott BB. 1990. Retinal ganglion cell density and cortical magnification factor in the primate. Vision Res 30(11):1897-1911.

Watanabe M, Fukuda Y, Hsiao CF, Ito H. 1985. Electron microscopic analysis of amacrine and bipolar cell inputs on Y-, X-, and W-cells in the cat retina. Brain Res 358(1-2):229-240.

Watanabe M, Rodieck RW. 1989. Parasol and midget ganglion cells of the primate retina. J Comp Neurol 289(3):434-454.

Weale RA. 1966. Why does the human retina possess a fovea? Nature 212(5059):255-256.

Weber AJ, Stanford LR. 1994. Synaptology of physiologically identified ganglion cells in the cat retina: a comparison of retinal X- and Y-cells. J Comp Neurol 343(3):483-499.

White AJ, Wilder HD, Goodchild AK, Sefton AJ, Martin PR. 1998. Segregation of receptive field properties in the lateral geniculate nucleus of a New-World monkey, the marmoset Callithrix jacchus. J Neurophysiol 80(4):2063-2076.

Wiesel TN, Hubel DH. 1966. Spatial and chromatic interactions in the lateral geniculate body of the rhesus monkey. J Neurophysiol 29(6):1115-1156.

Wikler KC, Rakic P. 1990. Distribution of photoreceptor subtypes in the retina of diurnal and nocturnal primates. J Neurosci 10(10):3390-3401.

Wikler KC, Williams RW, Rakic P. 1990. Photoreceptor mosaic: number and distribution of rods and cones in the rhesus monkey retina. J Comp Neurol 297(4):499-508.

Wilder HD, Grünert U, Lee BB, Martin PR. 1996. Topography of ganglion cells and photoreceptors in the retina of a New World monkey: the marmoset Callithrix jacchus. Vis Neurosci 13(2):335-352.

Woollard HH. 1927. The differentiation of the retina in primates. Proceedings of the Zoological Society of London 1:1-17.

Xu Y, Vasudeva V, Vardi N, Sterling P, Freed MA. 2008. Different types of ganglion cell share a synaptic pattern. J Comp Neurol 507(6):1871-1878.

Yamada E. 1969. Some structural features of the fovea centralis in the human retina. Arch Ophthalmol 82(2):151-159.

Yamada ES, Bordt AS, Marshak DW. 2005. Wide-field ganglion cells in macaque retinas. Vis Neurosci 22(4):383-393.

Yamada ES, Silveira LC, Gomes FL, Lee BB. 1996. The retinal ganglion cell classes of New World primates. Rev Bras Biol 56 Su 1 Pt 2:381-396.

Yeh T, Lee BB, Kremers J. 1995a. Temporal response of ganglion cells of the macaque retina to cone-specific modulation. J Opt Soc Am A Opt Image Sci Vis 12(3):456-464.

Yeh T, Lee BB, Kremers J, Cowing JA, Hunt DM, Martin PR, Troy JB. 1995b. Visual responses in the lateral geniculate nucleus of dichromatic and trichromatic marmosets (Callithrix jacchus). J Neurosci 15(12):7892-7904.

Yin L, Smith RG, Sterling P, Brainard DH. 2009. Physiology and morphology of color-opponent ganglion cells in a retina expressing a dual gradient of S and M opsins. J Neurosci 29(9):2706-2724.

Yuodelis C, Hendrickson A. 1986. A qualitative and quantitative analysis of the human fovea during development. Vision Res 26(6):847-855.

Zhang J, Li W, Trexler EB, Massey SC. 2002. Confocal analysis of reciprocal feedback at rod bipolar terminals in the rabbit retina. J Neurosci 22(24):10871-10882.

Zrenner E. 1983. Neurophysiological aspects of color vision in primates. Heidelberg: Springer.

Zrenner E, Gouras P. 1981. Characteristics of the blue sensitive cone mechanism in primate retinal ganglion cells. Vision Res 21(11):1605-1609.

Zucker CL. 1998. Localization of gephyrin and glycine receptor subunit immunoreactivity in the rabbit retina. Vis Neurosci 15(2):389-395.

Appendix

Table 1.1 – Previous literature on small bistratified ganglion cells

Reference	Name	Species	Main finding
Polyak (1941)	Shrub	Macaque, chimpanzee & human	Identified as a morphologically distinct type with a bistratified dendritic tree
Gouras (1968)	Blue sensitive cells	Macaque	Recorded from blue sensitive ganglion cells
Boycott & Dowling (1969)	Diffuse	Macaque	Re-named Polyak's shrub type according to their 'diffusely' stratifying dendrites
de Monasterio et al. (1975)	Blue-yellow	Macaque	Showed that both M and L cone mechanisms oppose S cone mechanisms in blue-yellow ganglion cells
de Monasterio & Gouras (1975)	Colour-opponent/non-concentric	Macaque	Recorded from blue-ON/yellow-OFF ganglion cells with non-concentric receptive fields
de Monasterio (1979)	Blue-ON	Macaque	Attempted to identify the morphological correlate of the blue-ON type
Zrenner & Gouras (1981)	Blue-ON	Macaque	Described characteristic responses of blue-ON ganglion cells, including their poor temporal and spatial resolution
Rodieck (1991)	Bistratified	Macaque	Suggested a correspondence between type II blue-ON cells and bistratified cells
Kolb et al. (1992)	G11	Human	Described ganglion cells in human which resemble rabbit ON-OFF direction selective cells and cat G11 cells with a bistratified dendritic tree
Dacey (1993)	Small-field bistratified	Human & macaque	Described detailed morphology of small-field bistratified cells and estimated their overall density
Rodieck & Watanabe (1993)	Parvicellular bistratified	Macaque	Showed that a bistratified ganglion cell type is labelled from retrograde tracer injections into the parvocellular layers of the LGN
Dacey & Lee (1994)	Small bistratified	Macaque	Showed the morphological correlate of blue-ON cells to be the small bistratified type
Ghosh et al. (1996)	Small bistratified	Marmoset	Identified small bistratified cells in marmoset with morphological features similar to those in macaque
Yamada et al. (1996)	Small-field bistratified	Capuchin	Identified the presence of small-field bistratified cells in capuchin, and their absence in owl monkey
Ghosh et al. (1997)	Small bistratified	Marmoset	Showed that axon terminals of blue cone bipolar cells costraify with inner dendrites of small bistratified cells
Calkins et al. (1998)	Blue-yellow	Macaque	Showed that the inner tier receives inputs from blue-cone bipolar cells and the outer tier receives inputs from DB2 and DB3 cells

Table 1.1 continued – Previous literature on small bistratified ganglion cells

Reference	Name	Species	Main finding
Silveira et al. (1999)	Small-field bistratified	Capuchin	Showed that physiological characteristics of blue-ON cells in capuchin were similar to those in macaque
Ghosh and Grünert (1999)	Small bistratified (blue-ON)	Marmoset	Showed that peripheral small bistratified cells receive the majority of their inputs from amacrine cells
Chichilnisky & Baylor (1999)	Blue-yellow	Macaque	Showed that small bistratified cells pool inputs from many s-cones within its dendritic field
Dacey et al. (2003)	Small bistratified	Macaque	Showed that small bistratified cells are labelled from retrograde tracer injections to the LGN
Yamada et al. (2005)	Small bistratified	Macaque	Showed that dendrites of small bistratified cells are mostly restricted to S2 and S5 of the IPL
Field et al. (2007)	Small bistratified	Macaque	Suggest that the yellow OFF component of small bistratified cell responses arise from horizontal cell feedback onto S-cones
Szmajda et al. (2008)	Small bistratified	Marmoset	Showed that axons of small bistratified cells project to the koniocellular layers of the LGN
Crook et al. (2009)	Small bistratified	Macaque	Showed that the yellow-OFF component of small bistratified cells arise from OFF diffuse bipolar input
Field et al. (2009)	Small bistratified	Macaque	Showed that small bistratified cells receive rod input via gap junctions between AII amacrine cells and blue cone bipolar cells
Percival et al. (2009)	Small bistratified	Marmoset	Measured the density of synapses on the dendrites of small bistratified cells

Table 1.2 – Previous literature on large sparse ganglion cells

Reference	Name	Species	Main finding
Polyak (1941)	Small diffuse	Macaque, chimpanzee & human	Identified as a morphologically distinct type with few thin smooth dendrites which run close to the ganglion cell layer
Boycott & Dowling (1969)	Unistratified	Macaque	Described a group of ganglion cells with unistratified dendritic trees, including some with dendrites stratifying near the ganglion cell layer
Leventhal et al. (1981)	C	Macaque	Found that ganglion cells with sparsely branching dendrites are labelled from tracer injections to the superior colliculus and pretectum
Perry & Cowey (1984)	Pγ	Macaque	Found that cells morphologically resembling γ cells of the cat are labelled from retrograde tracer injections to the superior colliculus
Yamada et al. (1996)	γ-like	Cebus, owl monkey & marmoset	Described γ-like cells in New World monkeys exhibiting sparesely branching dendritic trees
Peterson & Dacey (1999)	Large sparse	Human	Measured dendritic field sizes of large sparse cells across the retina and distinguished them from 5 other monostratified wide-field groups
Dacey et al. (2002)	Sparse-monostratified	Macaque	Showed that sparse-monostratified cells show blue-OFF/yellow-ON response properties
Dacey et al. (2003)	Large sparse	Macaque	Showed that large sparse cells are labelled from retrograde tracer injections to the LGN
Yamada et al. (2005)	Large sparse	Macaque	Showed that dendrites of large sparse cells are mostly restricted to S4 of the IPL
Szmajda et al. (2008)	Large sparse	Marmoset	Showed that large sparse cells are labelled from retrograde tracer injections into the koniocellular layers of the LGN
Percival et al. (in press)	Large sparse	Marmoset	Measured the density of synapses on dendrites of large sparse cells

Table 1.3 – Previous literature on broad thorny ganglion cells

Reference	Name	Species	Main finding
Polyak (1941)	Garland	Macaque, chimpanzee & human	Described cells with dendrites 'thickly covered with countless minute contorted branchlets and thorny or hook shaped appendages'
Boycott & Dowling (1969)	Unistratified	Macaque	Described a group of ganglion cells with unistratified dendritic trees, including some which spanned a large extent of the IPL
Leventhal et al. (1981)	-	Macaque	Noted that cells resembling Polyak's garland cells are labelled from retrograde tracer injections to the superior colliculus and pretectum
Rodieck & Watanabe (1993)	T group	Macaque	Described a group of cells labelled from retrograde tracer injections to the superior colliculus with densely branching dendrites
Ghosh et al. (1996)	Hedge (Group C)	Marmoset	Described ganglion cells in marmoset retina with large, densely branching dendritic trees, which stratify broadly thoughtout the IPL
Peterson & Dacey (2000)	Thorny diffuse	Human	Described ganglion cells with very densely branched dendritic trees with many 'twig-like thorny branchlets' terminating throughout the IPL
Dacey et al. (2003)	Broad thorny	Macaque	Showed that a densly branching, broadly stratifiied ganglion cell type is labelled from retrograde tracer injections to the LGN
Dacey (2004)	Broad thorny	Macaque	Suggested that broad thorny ganglion cells may display transient ON-OFF responses without direction selectivity
Yamada et al. (2005)	Broad thorny	Macaque	Showed that the breadth of dendritic stratification for broad thorny cells spans S2 - S4 of the IPL
Percival et al. (in press)	Broad thorny	Marmoset	Measured the density of synaptic inputs on dendrites of broad thorny cells